REPORT 1188

CONTENTS

REPORT 1188

ON THE USE OF THE INDICIAL FUNCTION CONCEPT IN THE ANALYSIS OF UNSTEADY MOTIONS OF WINGS AND WING-TAIL COMBINATIONS

By MURRAY TOBAK

SUMMARY

The concept of indicial aerodynamic functions is applied to the analysis of the short-period pitching mode of aircraft. By the use of simple physical relationships associated with the indicial-function concept, qualitative studies are made of the separate effects on the damping in pitch of changes in Mach number, aspect ratio, plan-form shape, and frequency. The concept is further shown to be of value in depicting physically the induced effects on a tail surface which follows in the wake of a starting forward surface. Considerable effort is devoted to the development of theoretical techniques whereby the transient response in lift at the tail to the wing wake may be estimated. Numerical results for several representative cases are presented, and these are analyzed to reassess the importance of the contribution to the rotary damping moment of the interference lift at the tail.

INTRODUCTION

In the classical study of the longitudinal motion of an aircraft, it is usually found that the motion resulting from a small equilibrium-destroying disturbance consists of two modes: one, a lightly damped, low-frequency motion at essentially constant attitude, called the phugoid oscillation; the other, a rotary-pitching and plunging oscillation of high frequency (relative to the phugoid frequency) called the short-period oscillation. The phugoid oscillation has generally been described as resulting from a slow interchange of potential and kinetic energy as the aircraft experiences periodic variations in airspeed and altitude. The character of the phugoid motion as influenced by airspeed, altitude, and aircraft geometry has been well understood for some time (see, e. g., ref. 1). The short-period motion, on the other hand, having in the past been found to be highly damped and of short duration, has been the cause of no concern. Its characteristics therefore have not been as fully investigated as those of the phugoid oscillation. As flight speeds have progressed to the transonic and supersonic domains, however, the loss of rotary damping occurring in practically all aircraft at speeds near the sonic speed has caused renewed interest in the short-period pitching mode. Unlike the easily controlled phugoid oscillation, the deterioration of damping in the short-period mode is of serious concern to the pilot, since the period of oscillation can be of the same order of magnitude as the pilot's reaction time. The oscillation may therefore be difficult or even impossible for the pilot to control manually. Furthermore, the additional load imposed upon the airframe due to a rapid growth of the amplitude of a negatively damped oscillation makes possible the occurrence of structural failure. It is therefore of considerable interest to obtain an understanding of the nature of the short-period mode, parallel to that which has been gained of the phugoid mode.

One means of viewing the aerodynamic phenomena occurring during the short-period oscillation from a fundamental standpoint is through application of the concept of indicial functions. In this approach, the variations with time of the aircraft angle of attack and angular velocity are replaced by a large number of small instantaneous or step changes. The transient aerodynamic reactions to these step changes are termed "indicial functions" and have been calculated for several classes of isolated wings (refs. 2 to 6). By suitable superposition of these results (refs. 7 to 9) the aerodynamic forces and moments caused by the given maneuver can be studied. It will be the primary purpose of this report to make such a study for the simplified case of an aircraft performing single-degree-of-freedom rotary oscillations, a maneuver which corresponds to the short-period oscillation when the plunging velocity of the aircraft is zero. To effect this end systematically the report is organized in two main categories: First the motion of a tailless aircraft is studied, and here existing theoretical information and the use of simple physical relationships associated with the indicial-function concept enables qualitative studies to be made of the separate effects on the aerodynamic forces and moments of changes in Mach number, aspect ratio, plan form, and frequency. In the second part, the motion of a tailled aircraft is studied, again by use of the indicial-function concept. Here, however, additional theoretical information is required to account for the interference effect of the wing and its wake on the transient lift at the tail, and several sections are devoted to the development of theoretical techniques whereby this effect may be estimated. Results of computations based on these techniques are analyzed, and the importance of the contribution of the interference lift at the tail to the rotary damping moment is re-established. In all of the above work, the aerodynamic forces and moments are those derived from analyses of the linearized equations of potential flow. Thus, the usual limitations imposed by the linear theory on the applicability of the results are in force here as well. However, in a somewhat different vein of inquiry, a final section is devoted to consideration of a problem in aircraft dynamics involving forces of nonlinear character.

The effect on the rotary damping moment of an aerodynamic restoring moment containing a common type of nonlinearity is studied, and conditions are pointed out under which the development of a self-sustained rotary oscillation may be possible.

NOTATION

A aspect ratio, $\frac{b^2}{S}$

C_L lift coefficient, $\frac{\text{lift}}{q_o S}$

C_m pitching-moment coefficient, $\frac{\text{pitching moment}}{q_o S \bar{c}}$

I moment of inertia

$I.P.$ imaginary part

M_o free-stream Mach number, $\frac{V_o}{a_o}$

$R.P.$ real part

S wing (or tail) area

V_o flight speed

a_o speed of sound in free stream

b wing (or tail) span

c local chord

c_o wing (or tail) root chord

$\bar{c}$ forward wing mean aerodynamic chord, $\frac{2}{S}\int_o^{b/2} (\text{local chord})^2\, dy$

c_l two-dimensional lift coefficient, $\frac{\text{lift}}{q_o c}$

e base of natural logarithms

i $\sqrt{-1}$

k reduced frequency parameter, $\frac{\omega \bar{c}}{2V_o}$

l distance between moving vortex and leading edge of tail

m slope of wing (or tail) leading edge

Δp local loading (pressure on lower surface minus pressure on upper surface)

q angular velocity due to pitching

q_o free-stream dynamic pressure, $\frac{1}{2}\rho_o V_o^2$

t $a_o t'$

t' time

t'_a time required following an instantaneous change in angle of attack or angular velocity for the transient lift or moment to attain steady state

w perturbation normal velocity in plane of wing or tail

$\bar{w}_\alpha$ averaged downwash in the plane of the tail due to steady angle of attack of forward wing

$\bar{w}_q$ averaged downwash in the plane of the tail due to steady pitching velocity of forward wing

x,y,z Cartesian coordinates

$x_{a.c.}$ distance from leading edge of M.A.C. to aerodynamic center

x_o distance from leading edge of M.A.C. to axis of rotation

Δx_o $x_{a.c.}-x_o$

α angle of attack of wing center line with respect to free-stream direction (fig. 1)

β $\sqrt{|M_o^2-1|}$

φ distance traveled, measured in half M.A.C. lengths, subsequent to an instantaneous change in angle of attack or angular velocity, $\frac{2V_o t'}{\bar{c}}$

Φ perturbation velocity potential

$\Delta\Phi$ jump in perturbation velocity potential in plane of wing or tail

θ angle of wing center line with respect to horizontal axis (fig. 1)

ν acute angle between wing plane of symmetry and trailing edge (fig. 15)

ρ_o free-stream density

ω angular frequency of oscillation

σ_a distance traveled, measured in half M.A.C. lengths, in the time interval t'_a, $2V_o t'_a/\bar{c}$

When α, $\dot{\alpha}$, and q are used as subscripts, a nondimensional derivative is indicated, and this derivative is evaluated as the independent variable (α, $\dot{\alpha}$, or q) approaches zero. For example,

$$C_{m_\alpha}=\left(\frac{\partial C_m}{\partial \alpha}\right)_{\alpha\to 0} \qquad C_{m_{\dot{\alpha}}}=\left[\frac{\partial C_m}{\partial\left(\frac{\dot{\alpha}\bar{c}}{2V_o}\right)}\right]_{\dot{\alpha}\to 0}$$

$$C_{m_q}=\left[\frac{\partial C_m}{\partial\left(\frac{q\bar{c}}{2V_o}\right)}\right]_{q\to 0}$$

PART I—ISOLATED WINGS

APPLICATION OF INDICIAL FUNCTIONS TO THE AERODYNAMIC THEORY OF UNSTEADY FLOWS

One of the most useful tools in the study of unsteady flows is the concept of indicial aerodynamic functions, which may be defined briefly as the aerodynamic response of the airfoil as a function of time to an instantaneous change in one of the conditions determining the aerodynamic properties of the airfoil in a steady flow. Theoretical aerodynamic indicial functions were first derived by Wagner (ref. 2) for the two-dimensional wing in incompressible flow. More recently, these results have been extended to cover the compressible case for both subsonic and supersonic speeds (refs. 3 and 4). In addition, theoretical indicial functions have now been obtained for both wide and slender triangular wings and rectangular wings, all for supersonic speeds (refs. 4 to 6).

The indicial function derives its usefulness primarily through the ease with which it lends itself to the powerful and well-established methods of the operational calculus (refs. 7 to 9). With the use of these methods, the aerodynamic forces and moments caused by arbitrary motions of the airframe can be studied from a fundamental standpoint. Because of the wide range of applicability of this means of approach in unsteady flow analyses, a considerable portion of the succeeding discussion is devoted to the fundamentals involved.

DEFINITION OF COORDINATE SYSTEM

In the succeeding analysis the stability system of axes is used. The origin of the coordinate system is placed in the airfoil so that the y axis which is perpendicular to the vertical plane of symmetry is coincident with the axis of rotation of the airfoil; the positive branch of the x axis is pointed in the direction of flight; and the z axis lies in the vertical plane of symmetry, positive downward. The angle of attack α is measured as the angle between the chord plane of the airfoil and the xy plane, and is shown as positive in figure 1. The

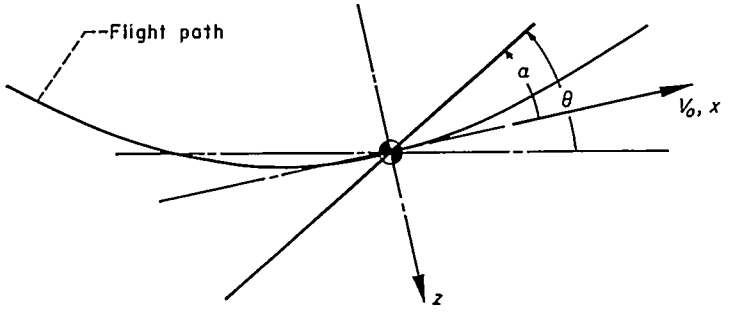

FIGURE 1.—Definition of coordinate system.

Here α and θ are equal, so that the maneuver is defined by one variable, the time history of either α or θ. Let the angle of attack be α and the angular velocity be q ($q \equiv d\theta/dt' = d\alpha/dt'$). At any instant, the normal velocity at any point on the airfoil surface is composed of two parts, one due to the instantaneous angle of attack αV_o, the other due to the angular velocity at the same instant $-qx$ (see fig. 3). These are two of the instantaneous boundary conditions of the unsteady flow.

Solutions for the aerodynamic forces and moments which correspond to these boundary conditions may be derived by a number of methods involving various degrees of approximation. In succeeding sections, the use of the concept of indicial functions and the principle of superposition for this purpose will be illustrated and compared with other current widely used methods.

CONCEPT OF INDICIAL FUNCTIONS

In order to illustrate this concept, assume that the airfoil under consideration has been flying a level path at zero angle of attack. At some time, which is designated time zero, the wing is caused to attain simultaneously a constant angle of

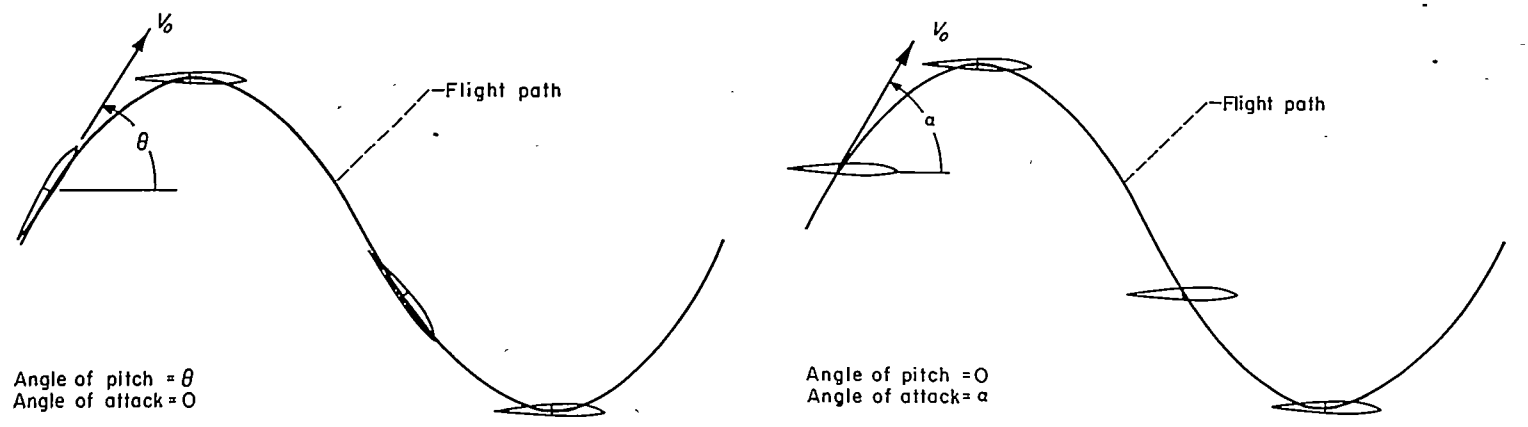

FIGURE 2.—Maneuvers corresponding to purely (a) angle of pitch and (b) angle of attack variations.

angle of pitch θ is the angle between the chord plane of the airfoil and the horizontal plane (an arbitrary reference) and is also shown positive in figure 1. Forces are measured as positive upward, whereas pitching moments are positive when tending to increase the angle of pitch in the positive direction. When the airspeed V_o is constant, which corresponds to the condition under study, the translatory and angular motions of the airfoil with respect to any system of coordinates are defined if the time histories of the angle of attack α and the angle of pitch θ and their derivatives are known. For purposes of clarity, two different harmonic motions of the aircraft are shown in figure 2, illustrating the difference between a flight path which involves a constant angle of attack and a varying angle of pitch and one which involves a constant angle of pitch and a varying angle of attack.

Now consider the case of a wing executing harmonic rotary oscillations about the y axis while the origin of the coordinate system traverses a level path at constant velocity V_o. This case corresponds to that of a wind-tunnel model mounted to permit single-degree-of-freedom rotary oscillations, or to the short-period mode of an aircraft in flight when the plunging velocity of the center of gravity is zero.

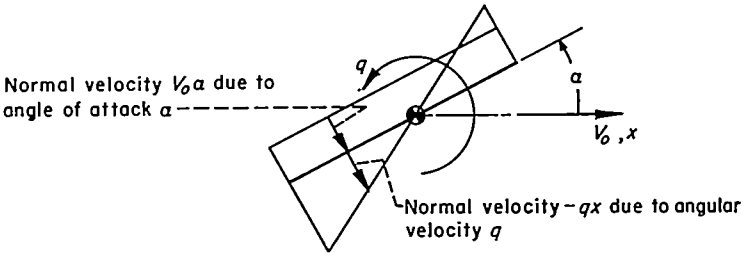

FIGURE 3.—Unsteady flow boundary conditions at airfoil surface.

attack α and angular velocity q. The normal velocity of the flow next to the surface of the airfoil therefore changes discontinuously from zero to a pattern that is constant with time and identical in shape to the pattern shown previously in figure 3. The lift and pitching moment that result are of a transient character and attain their steady-state values corresponding to these new boundary conditions only after a significant interval of time has passed. It should be noted there exists an essential difference between the length of this time interval at subsonic and supersonic speeds. At supersonic speeds, the vorticity shed into the airfoil wake cannot influence the flow about the airfoil but at subsonic speeds this

influence exists for all time. The result is that the lift and moment reach steady-state values in a finite time at supersonic speeds but approach these values asymptotically at subsonic speeds. In either case, however, the time responses in lift and moment to the step changes in α and q are termed "indicial functions." Figure 4 illustrates typical subsonic and supersonic indicial lift responses to a step change in the angle of attack.

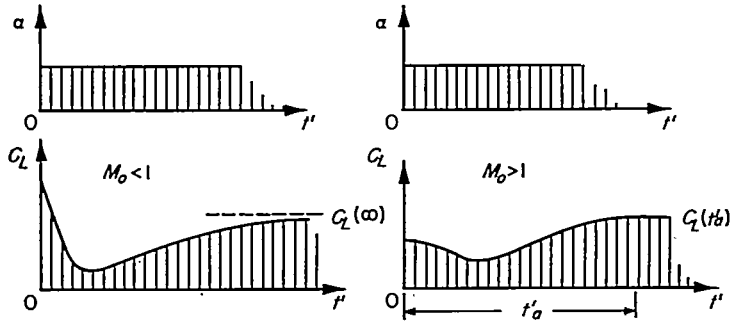

FIGURE 4.—Typical indicial lift responses to step changes in angle of attack.

It is obvious that the time history of the wing motion during a short-period oscillation may be broken down into an infinite number of infinitesimally small step changes in the angle of attack and step changes in the angular velocity. The summation of the indicial lift and moment for these steps then yields the total lift and moment at any prescribed time. In figure 5, the mechanics of the procedure are illustrated for an arbitrary angle-of-attack variation. Here, the given angle-of-attack variation is replaced by a number of small step changes. Within each step the corresponding response in lift is shown plotted for convenience. It is then apparent that the total lift at time t' is equal to the sum of the increments of lift in each step at time t'. As indicated by the leaders, however, it is clear that the increments of lift for the various steps at time t' are equivalent to increments in the first step at time $t'-t'_1$. Alternatively, then, the total lift at time t' can be written as

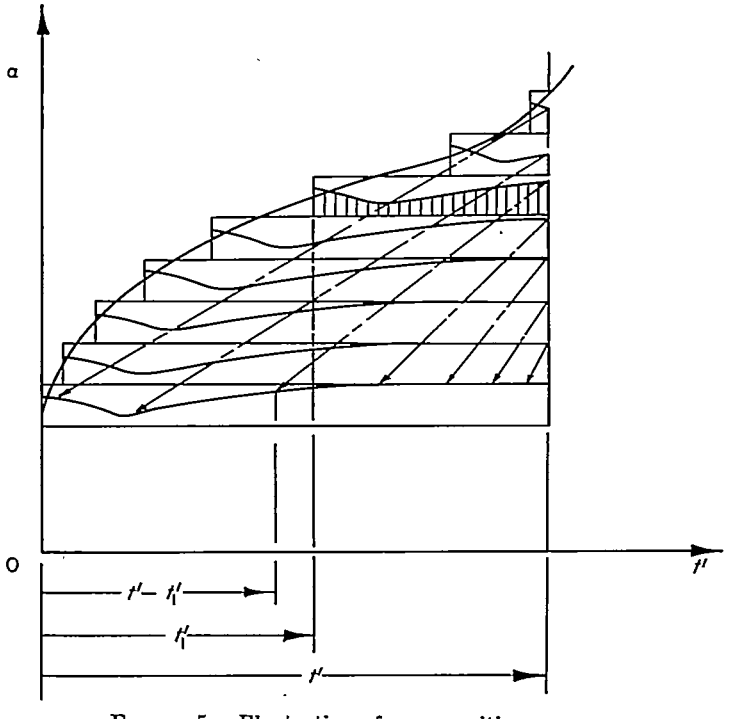

FIGURE 5.—Illustration of superposition process.

$$C_L(t')=C_{L_\alpha}(t')\alpha(0)+\sum_0^{t'}C_{L_\alpha}(t'-t'_1)\frac{\Delta\alpha}{\Delta t'}(t'_1)\Delta t'_1 \qquad (1)$$

After a transformation of variables, $t'-t'_1=\tau$ and letting the increment of time approach zero, equation (1) can be rewritten in a form of Duhamel's integral (see, e. g., ref. 9)

$$C_L(t')=\frac{d}{dt'}\int_0^{t'}C_{L_\alpha}(\tau)\alpha(t'-\tau)d\tau \qquad (2)$$

A similar procedure is carried out for the angular velocity variation, whereupon the total lift coefficient at the prescribed time t' becomes

$$C_L(t')=\frac{d}{dt'}\int_0^{t'}C_{L_\alpha}(\tau)\alpha(t'-\tau)d\tau+\frac{d}{dt'}\int_0^{t'}C_{L_q}(\tau)\frac{\bar{c}}{2V_o}q(t'-\tau)d\tau \qquad (3)$$

It should be pointed out that in this form equation (3) is applicable to the analysis of arbitrary motions, the only restriction being that the flight speed is constant. In the following sections, however, the application of equation (3) is restricted to harmonic motions having a single degree of freedom. The reasons for this restriction are two-fold: first, the motions of a statically stable aircraft in response to a disturbance are most generally of a harmonic nature; and second, such a restriction permits an assessment of the influence of the time rate of the airfoil motions on the aerodynamic forces and moments.

APPLICATION OF INDICIAL FUNCTIONS TO HARMONIC PITCHING OSCILLATIONS

Consider first a pure sinusoidal pitching oscillation, the angle of attack being zero throughout the motion. The flight path for such a motion has been illustrated in figure 2 (a). In this case, the angle of pitch is given by

$$\theta(t')=\theta_o e^{i\omega t'}$$

where θ_o is the maximum amplitude of oscillation and ω is the angular frequency. The angular velocity is, of course, $q(t')=\dot{\theta}=i\omega\theta_o e^{i\omega t'}=i\omega\theta(t')$. Inserting the value for $q(t')$ in equation (3) and performing the indicated operations, there results

$$C_L(t')=-\frac{\omega^2\bar{c}}{2V_0}\theta(t')\int_o^{t'}C_{L_q}(\tau)e^{-i\omega\tau}d\tau+\frac{i\omega\bar{c}}{2V_0}\theta_o C_{L_q}(t') \qquad (4)$$

Note in figure 6 that $C_{L_q}(\tau)$ is equal to $C_{L_q}(t')-F_2(\tau)$, and that $F_2(\tau)$ approaches zero as τ approaches t'. Replacing $C_{L_q}(\tau)$ in equation (4) by this equality,

$$\frac{C_L(t')}{\theta(t')}=\frac{i\omega\bar{c}}{2V_o}C_{L_q}(t')+\frac{\omega^2\bar{c}}{2V_o}\int_o^{t'}F_2(\tau)e^{-i\omega\tau}d\tau \qquad (5)$$

For subsonic speeds, let t' approach infinity. With this substitution, equation (5) thereby represents the lift coefficient due to the harmonic pitching motion after the transient loading subsequent to the start of the motion has reached a steady periodic variation. Then separating equation (5) into components in phase (real part) and out of phase

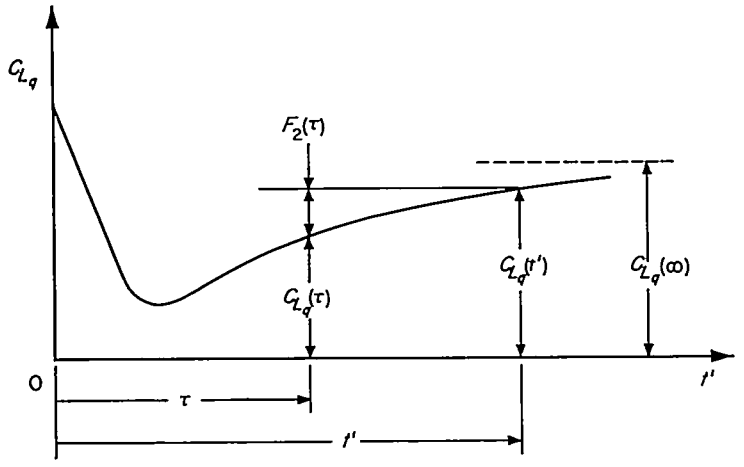

FIGURE 6.—Definition of the function $F_2(\tau)$.

(imaginary part) with θ, there is obtained

$$\left.\begin{aligned} R.P.\left(\frac{C_L}{\theta}\right)&=\frac{\omega^2\bar{c}}{2V_o}\int_o^\infty F_2(\tau)\cos\omega\tau d\tau \\ I.P.\left(\frac{C_L}{\theta}\right)&=\frac{\omega\bar{c}}{2V_o}\left[C_{L_q}(\infty)-\omega\int_o^\infty F_2(\tau)\sin\omega\tau d\tau\right] \end{aligned}\right\} \quad (6)$$

Introduce the nondimensional parameters,

$\varphi=\frac{2V_o}{\bar{c}}\tau$ number of half M. A. C. lengths traveled in time τ

$k=\frac{\omega\bar{c}}{2V_o}$ reduced frequency.

In terms of these parameters, equation (6) becomes, for $M_o<1$,

$$\left.\begin{aligned} R.P.\left(\frac{C_L}{\theta}\right)&=k^2\int_o^\infty F_2(\varphi)\cos k\varphi d\varphi \\ I.P.\left(\frac{C_L}{\theta}\right)&=k\left[C_{L_q}(\infty)-k\int_o^\infty F_2(\varphi)\sin k\varphi d\varphi\right] \end{aligned}\right\} \quad (7)$$

At supersonic speeds, equations (7) may be simplified somewhat since the build-up in lift is completed in a finite number of half M. A. C. lengths of travel σ_a. In equations (7), therefore, the upper limits of the integrals may be replaced by σ_a, since beyond that point $F_2(\varphi)$ is identically zero.

$$\left.\begin{aligned} R.P.\left(\frac{C_L}{\theta}\right)&=k^2\int_o^{\sigma_a}F_2(\varphi)\cos k\varphi d\varphi \\ &\qquad\qquad\qquad\qquad \varphi\geq\sigma_a \\ &\qquad\qquad\qquad\qquad M_o>1 \\ I.P.\left(\frac{C_L}{\theta}\right)&=k\left[C_{L_q}(\sigma_a)-k\int_o^{\sigma_a}F_2(\varphi)\sin k\varphi d\varphi\right] \end{aligned}\right\} \quad (8)$$

Thus it appears from equations (7) and (8) that there are both in-phase and out-of-phase lift forces associated with the harmonic pitching oscillation. Notice, however, in equations (8) that if the trigonometric terms are expanded and the reduced frequency is required to be small compared to unity (corresponding to the frequencies encountered in dynamic stability work), terms containing second and higher powers of k will be small compared to first-order terms. Thus, for low frequencies, the only force of consequence during the pitching oscillation is the first order in frequency out-of-phase lift force, $ik\theta C_{L_q}(\sigma_a)$.[1] The phase relationships for the harmonic pitching oscillation are indicated in figure 7. It is evident that the total lift leads the angle of pitch by nearly 90°.

APPLICATION OF INDICIAL FUNCTIONS TO HARMONIC PLUNGING OSCILLATIONS

Next, consider a purely sinusoidal variation of the angle of attack, the angle of pitch being zero throughout the motion. The flight path for this motion has been illustrated in figure 2 (b). Here, α equals $\alpha_o e^{i\omega t'}$, where, as previously, α_o and ω are the maximum amplitude and angular frequency, respectively. Applying equation (3) again,

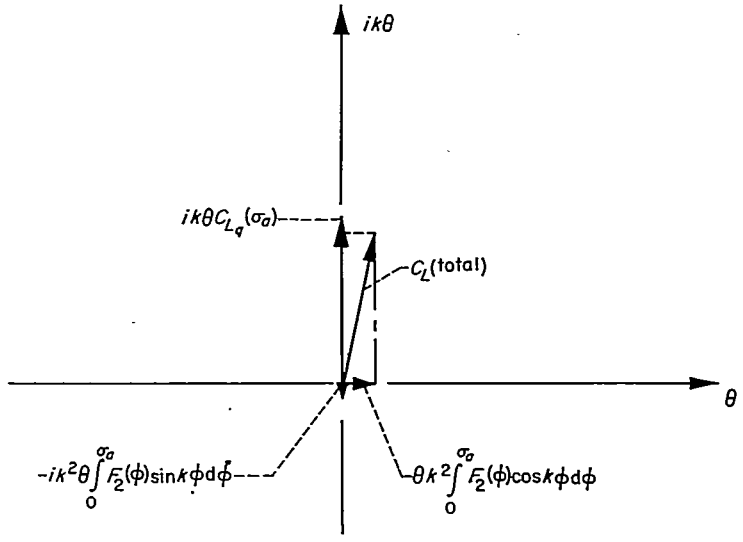

FIGURE 7.—Phase relationships for harmonic pitching oscillation.

$$\begin{aligned} C_L(t')&=\alpha_o\frac{d}{dt'}\int_o^{t'}C_{L_\alpha}(\tau)e^{i\omega(t'-\tau)}d\tau \\ &=i\omega\alpha(t')\int_o^{t'}C_{L_\alpha}(\tau)e^{-i\omega\tau}d\tau+\alpha_o C_{L_\alpha}(t') \end{aligned} \quad (9)$$

Now, as in the previous example, let $C_{L_\alpha}(\tau)=C_{L_\alpha}(t')-F_1(\tau)$ so that equation (9) becomes

$$C_L(t')=\alpha(t')C_{L_\alpha}(t')-i\omega\alpha(t')\int_o^{t'}F_1(\tau)e^{-i\omega\tau}d\tau \quad (10)$$

Again, introduce the nondimensional parameters φ and k, separate equation (10) into its real and imaginary parts, and let φ approach infinity for subsonic speeds and σ_a for supersonic speeds. There results,

$$\left.\begin{aligned} R.P.\left(\frac{C_L}{\alpha}\right)&=C_{L_\alpha}(\lambda)-k\int_o^\lambda F_1(\varphi)\sin k\varphi d\varphi \\ &\qquad\qquad\qquad\qquad \lambda=\infty,\ M_o<1 \\ &\qquad\qquad\qquad\qquad \lambda=\sigma_a,\ M_o>1 \\ I.P.\left(\frac{C_L}{\alpha}\right)&=-k\int_o^\lambda F_1(\varphi)\cos k\varphi d\varphi \end{aligned}\right\} \quad (11)$$

[1] This quantity is, of course, the same lift force in phase with the pitching velocity which would occur alone had the wing been executing a steady turn (q constant). One of the chief advantages of the indicial response method, at least for supersonic speeds, is the ease with which the relative importance of the various terms contributing to the total lift and moment can be assessed and the sources of the important contributions identified.

Notice in equations (11) for supersonic speeds that when the trigonometric terms are expanded for the low frequency case, as was done in the previous example, there appears an in-phase term of zero order in k, $\alpha C_{L_\alpha}(\sigma_a)$, and an out-of-phase term of first order in k, $-ik\alpha\int_o^{\sigma_a} F_1(\varphi)d\varphi$. These, then, are the principal contributions to the lift forces for the low-frequency angle-of-attack variation. The phase relationships for this motion are shown graphically in figure 8. For this case, it is evident that the total-lift force can lag behind the angle of attack because of the negative out-of-phase contribution, $-ik\alpha\int_o^{\sigma_a} F_1(\varphi)\cos k\varphi d\varphi$.

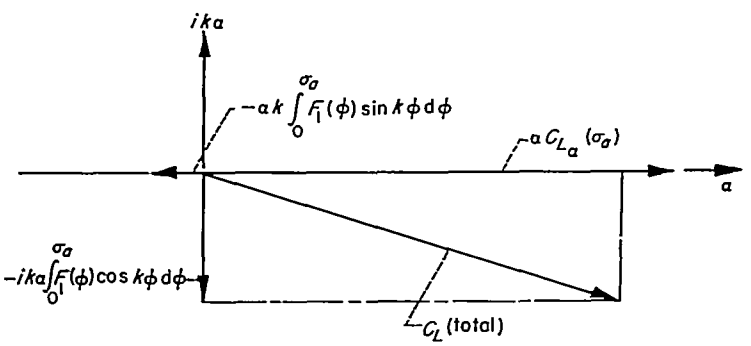

FIGURE 8.—Phase relationships for harmonic plunging oscillation.

APPLICATION OF INDICIAL FUNCTIONS TO HARMONIC ROTARY OSCILLATIONS

Finally, consider the case of harmonic rotary oscillations. Here, as previously mentioned, the normal velocity over the wing surface is composed of contributions from both the angular velocity and the instantaneous angle of attack, so that the complete expression in equation (3) must be employed to obtain the total lift. However, for single-degree-of-freedom rotary oscillations, α equals θ and $\dot{\alpha}$ equals q, so that in this case the separate expressions given for the harmonically pitching wing (eqs. (7) and (8)) and the harmonically plunging wing (eq. (11)) can be combined to give the total lift for a wing executing harmonic rotary oscillations. Then, adding the results of equations (7), (8) and (11), the in-phase and out-of-phase components of the total lift become

$$R.P.\left(\frac{C_L}{\alpha}\right)=C_{L_\alpha}(\lambda)-k\int_o^{\lambda} F_1(\varphi)\sin k\varphi d\varphi+k^2\int_o^{\lambda} F_2(\varphi)\cos k\varphi d\varphi \tag{12a}$$

$\lambda=\infty,\ M_o<1$

$\lambda=\sigma_a,\ M_o>1$

$$I.P.\left(\frac{C_L}{\alpha}\right)=k\left[C_{L_q}(\lambda)-k\int_o^{\lambda} F_2(\varphi)\sin k\varphi d\varphi-\int_o^{\lambda} F_1(\varphi)\cos k\varphi d\varphi\right] \tag{12b}$$

The phase relationships for the rotary oscillation may, of course, also be obtained by directly adding the results given in figures 7 and 8. The result of this addition is shown in figure 9.

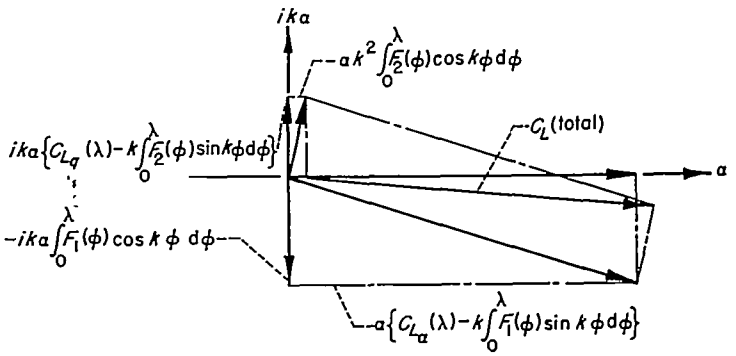

FIGURE 9.—Phase relationships for harmonic rotary oscillation.

It will be noted in figure 9 that the total-lift force can either lag behind or lead the angle of attack, depending on the relative magnitudes of the three terms comprising the out-of-phase lift. The total lift is shown lagging behind the angle of attack in figure 9, which situation, for axis positions ahead of the point of concentration of the total lift, gives rise to the possibility of the development of divergent rotary oscillations.

Again, the complete frequency-dependent equations for the total lift of a wing in supersonic flow due to the rotary oscillation (eqs. (12), $\lambda=\sigma_a$) may be reduced to first order in k for the low-frequency case in the same manner as was described in the two previous examples to give

$$\left.\begin{aligned} R.P.\left(\frac{C_L}{\alpha}\right)&=C_{L_\alpha}(\sigma_a)\\ I.P.\left(\frac{C_L}{\alpha}\right)&=k\left[C_{L_q}(\sigma_a)-\int_o^{\sigma_a} F_1(\varphi)d\varphi\right]\end{aligned}\right\} \tag{13}$$

For all three examples, the same procedure may, of course, be used to obtain the pitching-moment coefficient. Only the pitching-moment equations for the rotary oscillation are presented below, since the correspondence between the lift and moment equations is obvious. For the rotary oscillation case, then,

$$\left.\begin{aligned} R.P.\left(\frac{C_m}{\alpha}\right)&=C_{m_\alpha}(\lambda)-k\int_o^{\lambda} F_3(\varphi)\sin k\varphi d\varphi+\\ &\qquad k^2\int_o^{\lambda} F_4(\varphi)\cos k\varphi d\varphi \qquad \lambda=\infty,\ M_o<1\\ &\qquad\qquad\qquad\qquad\qquad\qquad \lambda=\sigma_a,\ M_o>1\\ I.P.\left(\frac{C_m}{\alpha}\right)&=k\left[C_{m_q}(\lambda)-k\int_o^{\lambda} F_4(\varphi)\sin k\varphi d\varphi-\right.\\ &\qquad \left.\int_o^{\lambda} F_3(\varphi)\cos k\varphi d\varphi\right]\end{aligned}\right\} \tag{14}$$

where, as previously,

$$F_3(\varphi)=C_{m_\alpha}(\lambda)-C_{m_\alpha}(\varphi)$$

and

$$F_4(\varphi)=C_{m_q}(\lambda)-C_{m_q}(\varphi)$$

Again, reducing equations (14) for supersonic speeds ($\lambda=\sigma_a$) to first order in frequency, there results

$$\left.\begin{aligned} R.P.\left(\frac{C_m}{\alpha}\right)&=C_{m_\alpha}(\sigma_a)\\ I.P.\left(\frac{C_m}{\alpha}\right)&=k\left[C_{m_q}(\sigma_a)-\int_o^{\sigma_a}F_3(\varphi)\,d\varphi\right]\end{aligned}\right\} \tag{15}$$

The complete frequency-dependent equations for the lift and pitching-moment coefficients for the rotary-oscillation case (eqs. (12) and (14)) describe completely the aerodynamic forces and moments resulting from the single-degree-of-freedom pitching mode. For the purposes of the present discussion, however, it is sufficient to limit consideration to the simpler first order in frequency results of equations (13) and (15). The significance of the effect of the higher order terms on the out-of-phase pitching moment will be examined in a later section of this report.

With regard to the first-order results for the supersonic lift and pitching-moment coefficients, it is instructive to note that the quantities $\int_o^{\sigma_a}F_1(\varphi)d\varphi$ and $\int_o^{\sigma_a}F_3(\varphi)d\varphi$ in equations (13) and (15) are represented geometrically by the areas of the shaded portions of figure 10.

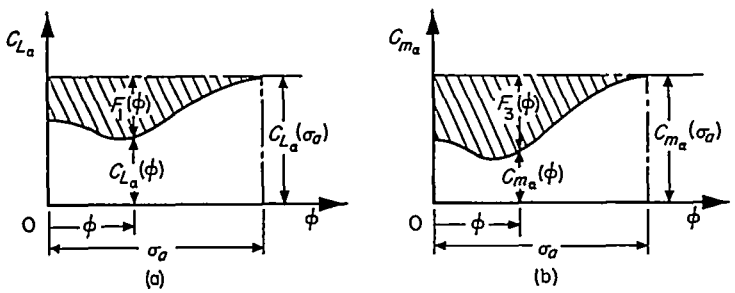

FIGURE 10.—Geometric representation of the functions $\int_o^{\phi_a}F_1(\phi)d\phi$ and $\int_o^{\phi_a}F_3(\phi)d\phi$.

The manner in which these areas are affected by variations in Mach number, aspect ratio, plan-form shape, and frequency will be used as a guide in later sections of this report to determine the significance of these parameters.

In the foregoing discussion, no mention has been made of reducing the complete equations for the lift and moment coefficients at subsonic speed (eqs. (12) and (14), $\lambda=\infty$) to first order in frequency as was done for the equations noted as applying at supersonic speed. It is evident that if the same procedure had been applied for subsonic speeds, the area corresponding to the term $\int_o^{\infty}F_1(\varphi)d\varphi$ can either be finite or can become infinitely large, depending on the manner in which the indicial lift function $C_{L_\alpha}(\varphi)$ approaches its steady-state asymptote as $\varphi\to\infty$. In the latter case, there exists the interesting anamoly of an infinite out-of-phase lift force as the frequency approaches zero. As can be seen from the results of reference 4, such will be the case for the two-dimensional wing. This result as the frequency approaches zero is not peculiar to the indicial analysis alone, but has been pointed out by a number of authors using different approaches. As indicated by Miles in reference 10, however, the anamolous result can be considered to be a consequence of assuming a two-dimensional flow, and there is reason to believe that the difficulty as the frequency approaches zero will not exist for finite-span wings.

As has been mentioned previously, the use of the characteristic areas $\int_o^{\sigma_a}F_1(\varphi)d\varphi$ and $\int_o^{\sigma_a}F_3(\varphi)d\varphi$ will be shown to be of considerable value in estimating the damping-in-pitch characteristics of wings at supersonic speeds. For the two-dimensional wing at subsonic speeds, the singularity as $k\to0$ prevents the use of such a simplified approach without further study. However, rather than return to the use of the full frequency-dependent equations ((12) and (14)), the reduction of the equations for the out-of-phase lift and moment to first order in frequency will be made in such a manner as to preserve the significance of these areas. To accomplish this end, equation (12b) is reconsidered. It is evident that the first integral in equation (12b) may be discarded, since its contribution to the out-of-phase lift is of third order in frequency. The second integral is divided into two parts:

$$\int_o^{\infty}F_1(\varphi)\cos k\varphi d\varphi=\int_o^{\varphi_1}F_1(\varphi)\cos k\varphi d\varphi+\int_{\varphi_1}^{\infty}F_1(\varphi)\cos k\varphi d\varphi \tag{16}$$

where φ_1 is chosen such that $F_1(\varphi_1)$ is close to zero. The first integral in equation (16), being bounded, then causes no difficulty. Expanding the trigonometric term and retaining only the first term in the expansion, there results $\int_o^{\varphi_1}F_1(\varphi)d\varphi$, which is the characteristic area out to the point φ_1. Now for large values of φ, $F_1(\varphi)$ is approximated in reference 4 by

$$F_1(\varphi)=\mu\left[\frac{1}{a+\varphi}+\frac{b}{(a+\varphi)^2}\right]$$

where the values of μ, a, and b are dependent on Mach number, and are given for $M_o=0$, 0.5, and 0.8 in reference 4. Inserting this quantity in the second integral in equation (16), we have

$$\int_{\varphi_1}^{\infty}F_1(\varphi)\cos k\varphi d\varphi=\mu\int_{\varphi_1}^{\infty}\frac{\cos k\varphi d\varphi}{a+\varphi}+\mu b\int_{\varphi_1}^{\infty}\frac{\cos k\varphi d\varphi}{(a+\varphi)^2} \tag{17}$$

Performing the indicated integrations in equation (17), there is obtained a term, $\mu b/a+\varphi_1$, from the second integral, and a term, $-\mu Ci[k(a+\varphi_1)]$ from the first integral. For small values of the argument, the cosine integral is approximated by (see ref. 11),

$$Ci[k(a+\varphi_1)]\approx ln[\gamma k(a+\varphi_1)]$$

$$k(a+\varphi_1)\to0$$

where γ is Euler's constant, 1.78107. Then, through the first order in frequency,

$$I.P.\left(\frac{C_L}{\alpha}\right)=k\left[C_{L_q}(\infty)-\int_o^{\varphi_1}F_1(\varphi)d\varphi+G(\varphi_1,k)\right] \tag{18a}$$

where

$$G(\varphi_1, k)=\left\{\mu ln[\gamma k(a+\varphi_1)]-\frac{\mu b}{a+\varphi_1}\right\}$$

The out-of-phase moment for pitching about the leading edge follows from the above development, with the added result of reference 4 that for large values of φ,

$$F_3(\varphi)\approx-\frac{F_1(\varphi)}{4}$$

Then, through the first order,

$$I.P.\left(\frac{C_m}{\alpha}\right)=k\left[C_{m_q}(\infty)-\int_o^{\varphi_1}F_3(\varphi)\,d\varphi-\frac{1}{4}G(\varphi_1,k)\right] \quad (18b)$$

Thus, after fixing φ_1, choosing a (small) value of k, and computing $G(\varphi_1, k)$, the finite areas corresponding to the terms $-\int_o^{\varphi_1}F_1(\varphi)\,d\varphi$ and $-\int_o^{\varphi_1}F_3(\varphi)\,d\varphi$ can be assessed in the same manner as will be done for the supersonic case. The advantages of such a procedure will be evident later.

CORRESPONDENCE BETWEEN INDICIAL LIFT AND MOMENT ANALYSIS AND OTHER METHODS

Before proceeding further with applications of the indicial response method, it is appropriate to discuss the relationship of this approach to other widely used methods.

Following the fundamental papers of Bryan and Routh, which introduced the basic differential equations of motion of rigid bodies and their stability criteria, the historical development of the theory of longitudinal motions of an aircraft evolved separately in two fields of research: dynamic stability and flutter. Workers in the dynamic stability field soon found that the longitudinal oscillations of a rigid aircraft in flight were generally of small reduced frequency. On this basis, the constants due to the aerodynamic properties of the airframe which appear in the differential equations of motion were considered to be independent of frequency. As a first approach to the problem of obtaining the necessary aerodynamic coefficients analytically, the instantaneous normal velocity distribution at the surface of the airfoil was assumed to be constant with time. The aerodynamic forces and moments arising from the fixed boundary conditions were then calculated using steady-flow theory. Later, this assumption was realized to be an over-simplification for the case of wing-tail combinations and an additional term, essentially correct to the first order in frequency, was added which accounted for the lag in the tail pitching moment caused by the time required for the vorticity discharge from the wing to reach the tail (see ref. (12)). Since at low speeds the pitching moment of the tail far outweighs all other contributions, the results from steady-flow theory together with the term accounting for the vorticity lag satisfactorily predicted the dynamic longitudinal motions of wing-tail combinations, and it was concluded that the major aerodynamic effects had been taken into account. In recent years, however, numerous authors (in particular, Miles; see, e. g., ref. 10) have pointed out that the above-mentioned theory overlooks important contributions to the aerodynamic forces and moments which, though still within the first order in frequency approximation, arise from time-dependent boundary conditions and must be calculated from unsteady-flow theory. It has been shown by these authors that with proper inclusion in the equations of motion of these coefficients, the deterioration of damping in the short-period mode actually occurring for aircraft flying at speeds near the speed of sound can be successfully predicted. The consequences of the assumptions involved in the classical dynamic-stability theory will be more evident from a brief review of the equation of motion and boundary conditions for the single-degree-of-freedom rotary oscillations of a rigid wing flying at constant supersonic speed. At the very outset, the assumption is generally made that the aerodynamic reactions to the motion of the airframe depend only on the angular position and angular velocity and not upon angular accelerations or higher time derivatives. The equation of motion for the change in pitching moment following a displacement from an equilibrium position is then written in the form of a power series in α and $\dot{\alpha}$:

$$\left.\begin{aligned}\frac{I}{q_0S\bar{c}}\ddot{\alpha}=&\left(\frac{\partial C_m}{\partial\alpha}\right)\alpha+\left[\frac{\partial C_m}{\partial\left(\frac{\dot{\alpha}\bar{c}}{2V_o}\right)}\right]\frac{\dot{\alpha}\bar{c}}{2V_o}+\left[\frac{\partial C_m}{\partial\left(\frac{q\bar{c}}{2V_o}\right)}\right]\frac{\dot{\alpha}\bar{c}}{2V_o}+\\&\left(\frac{\partial^2C_m}{\partial^2\alpha}\right)\frac{(\alpha)^2}{2!}+\left[\frac{\partial^2C_m}{\partial^2\left(\frac{\dot{\alpha}\bar{c}}{2V_o}\right)}\right]\frac{(\dot{\alpha}\bar{c}/2V_o)^2}{2!}+\left[\frac{\partial^2C_m}{\partial^2\left(\frac{q\bar{c}}{2V_o}\right)}\right]\frac{(\dot{\alpha}\bar{c}/2V_o)^2}{2!}+\text{cross-derivatives and higher-order terms.}\end{aligned}\right\} \quad (19)$$

It should be remembered that for the rotary-oscillation case, the airfoil is subjected to changes in both angle of attack α and angular velocity q, and that these motions produce normal velocity patterns at the airfoil surface which are different in character. Thus, although for the single-degree-of-freedom case, $\dot{\alpha}$ and q are equal, nevertheless their separate effects must be considered and it is therefore necessary to include both $\frac{\partial C_m}{\partial(q\bar{c}/2V_o)}$ and $\frac{\partial C_m}{\partial(\dot{\alpha}\bar{c}/2V_o)}$ in equation (19). Next, if it is assumed that the moments are linearly dependent on their respective variables, the second and higher-order terms in equation (19) may be discarded and the remaining partial derivatives considered as constants for the given wing. There remains, therefore, a linear second-order system with constant coefficients. In order to calculate the coefficients (termed stability derivatives) theoretically it became necessary, for lack of more refined theoretical methods, to assume that the instantaneous normal velocity of the flow at the surface of the wing was fixed with respect to time. Thus, the partial derivative $\frac{\partial C_m}{\partial(q\bar{c}/2V_o)}$ could be calculated as the pitching moment due to a constant pitching rate, that is, $C_{m_q}(\sigma_a)$, while the derivative $\partial C_m/\partial\alpha$ becomes the pitching moment due to a constant angle of attack, that is,

$C_{m_\alpha}(\sigma_a)$. As a consequence of fixing the normal velocity pattern in time, however, it was necessary to assume that the derivative $\frac{\partial C_m}{\partial(\dot{\alpha}\bar{c}/2V_o)}$ was zero. There was therefore no possibility for this theory to predict the occurrence of dynamic instability for a wing alone, since the only damping term remaining is $C_{m_q}(\sigma_a)$, which is always stabilizing. When the restriction of constant normal velocity with time is lifted, however, the assumption is then made that the stability derivatives in equation (19) may be calculated separately by fixing each of the independent variables α, $\dot{\alpha}$, and q in turn with respect to time. The derivatives $C_{m_q}(\sigma_a)$ and $C_{m_\alpha}(\sigma_a)$ thus remain unchanged, but the derivative $\frac{\partial C_m}{\partial(\dot{\alpha}\bar{c}/2V_o)}$ (or $C_{m_{\dot{\alpha}}}$) can now be included and calculated as the pitching moment due to a constant vertical acceleration, $\dot{\alpha}V_o$. It should be emphasized that while $C_{m_q}(\sigma_a)$ and $C_{m_\alpha}(\sigma_a)$ may be calculated from steady-flow theory by virtue of the assumed invariance with time of the normal velocity pattern, $C_{m_{\dot{\alpha}}}$ must be calculated from unsteady-flow theory since for constant $\dot{\alpha}$ the angle of attack varies linearly with time, as does the normal velocity of the flow at the surface.

It is clear that since the stability derivatives in equation (19) are assumed to be independent of the frequency, the result for the aerodynamic pitching-moment coefficient is thereby limited to one that is correct only to the first order in frequency. For the case of single-degree-of-freedom harmonic rotary oscillations, then, the in-phase and out-of-phase components of the total aerodynamic pitching-moment coefficient, correct to the first order in frequency, become

$$\left.\begin{aligned} R.P.\left(\frac{C_m}{\alpha}\right)&=C_{m_\alpha}(\sigma_a)\\ I.P.\left(\frac{C_m}{\alpha}\right)&=k[C_{m_q}(\sigma_a)+C_{m_{\dot{\alpha}}}(\sigma_a)] \end{aligned}\right\} \qquad (20)$$

By comparison with the first-order in frequency result from the indicial response analysis (eq. (15)), it is evident that the two results are identical if the quantity $-\int_o^{\sigma_a} F_3(\varphi)d\varphi$ can be shown to be equivalent to $C_{m_{\dot{\alpha}}}(\sigma_a)$. To show this equivalence, consider a wing, initially in level steady flight, which is suddenly forced down with constant vertical acceleration $\dot{\alpha}V_o$. As seen in figure 11, the angle-of-attack variation in this case is $\alpha=\dot{\alpha}t'$, where $\dot{\alpha}$ is a constant. Then applying the counterpart of equation (3) for the pitching moment

$$C_m(t')=\frac{d}{dt'}\int_o^{t'} C_{m_\alpha}(\tau)\alpha(t'-\tau)d\tau$$

Inserting $\alpha(t'-\tau)=\dot{\alpha}[t'-\tau]$, and performing the indicated differentiation,

$$C_m(t')=\dot{\alpha}\int_o^{t'} C_{m_\alpha}(\tau)d\tau$$

Now replace $C_{m_\alpha}(\tau)$ by $C_{m_\alpha}(t')-F_3(\tau)$ and let t' be greater than t'_a.
Then

$$C_m(t')=\alpha(t')C_{m_\alpha}(t'_a)-\dot{\alpha}\int_o^{t'_a} F_3(\tau)d\tau$$

and nondimensionalizing, by replacing t' and t'_a by $\bar{c}\varphi/2V_o$ and $\bar{c}\sigma_a/2V_o$, we have,

$$C_m(\varphi)=\alpha(\varphi)C_{m_\alpha}(\sigma_a)-\frac{\dot{\alpha}\bar{c}}{2V_o}\int_o^{\sigma_a} F_3(\varphi)d\varphi \qquad \varphi\geq\sigma_a \qquad (21)$$

Thus, the pitching moment proportional to the constant vertical acceleration parameter $\dot{\alpha}\bar{c}/2V_o$, which is synonymous with the definition of the stability derivative $C_{m_{\dot{\alpha}}}$, is found to be equivalent to the pitching-moment contribution due to $\dot{\alpha}$ for the first order in frequency rotary-oscillation case.[2] Therefore, the results of the indicial response method, when reduced to the first order in frequency for supersonic speeds, are identical to the results from the familiar first-order theory used in dynamic stability work.[3]

Workers in the field of flutter, who were concerned with frequencies many times those encountered in dynamic-stability analyses, required theoretical information showing the behavior of the forces and moments as affected by the frequency of oscillation, and therefore discarded the first-order theory for more precise methods of analysis. One of the most useful of these has been the "oscillating potential" theory, which is based on solutions of the time-dependent linearized equation of compressible potential flow for the case of harmonic motions. The in-phase and out-of-phase lift and moments are thereby determined, generally as functions of powers of the reduced frequency, aspect ratio, Mach number, and position of the axis of rotation. The application of this method, which developed in this country primarily as a result of Theodorsen's work for incompressible flow (ref. 13) has recently produced a number of useful papers covering a wide variety of wings at supersonic speeds (see, e. g., refs. 14 to 18). It has been shown by a number of authors, in particular, Garrick, in reference 7, that through the use of superposition methods the results for the aerodynamic coefficients obtained from the oscillating potential

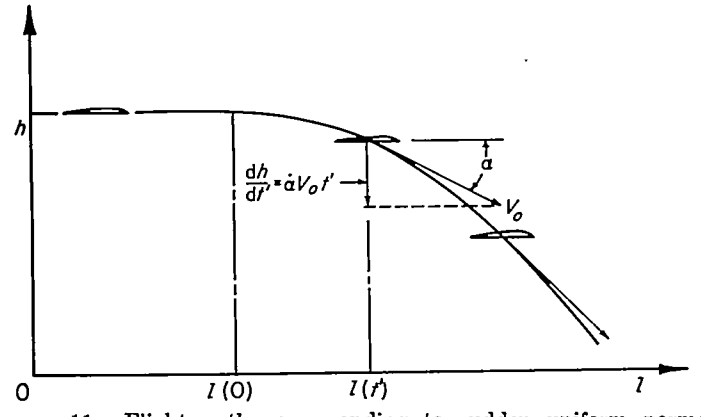

FIGURE 11.—Flight path corresponding to sudden uniform normal acceleration $\dot{\alpha}V_o$.

[2] By the same procedure, the stability derivative $C_{L_{\dot{\alpha}}}(\sigma_a)$ can be shown to be equivalent to the term $-\int_o^{\sigma_a} F_1(\varphi)d\varphi$.

[3] Notice in equation (21) that if σ_a is replaced by infinity, the results apply to subsonic speeds. For the two-dimensional wing, the analogy between $C_{m_{\dot{\alpha}}}$ and $-\int_o^{\infty} F_3(\varphi)d\varphi$ then gives only the previously mentioned singularity at infinity as $k\to 0$. If the area corresponding to $\int_o^{\infty} F_3(\varphi)d\varphi$ were finite, however, the analogy would be equally useful for subsonic as well as supersonic speeds.

theory are wholly compatible with those of the indicial response method applied to harmonic motions (eqs. (12) and (14)).

Thus the indicial response method may be applied with equal validity to problems in both the fields of dynamic stability and flutter. In many cases, however, application of the specialized approaches mentioned above may result in greater economy of effort. The chief virtue of the indicial response method is that it represents a fundamental approach to the problem of unsteady flow, and affords valuable insight into the physical nature of the aerodynamic phenomena taking place.

PHYSICAL CONCEPTS RELATING TO THE INDICIAL LOADING

It has been shown that for even small frequencies, the pitching moment of an airfoil in harmonic rotary motion can lag behind the angle of attack of the airfoil. The magnitude of the lag depends on the character of the indicial response to a step change in angle of attack. It is therefore of interest at this time to re-examine the physical nature of the flow that contributes this lag.

Consider first the lift and moment at the instant the angle of attack changes, assuming that previous to time zero, the wing has been flying a level path at zero angle of attack. At $t'=0$, the wing begins to sink, without pitching, with constant downward velocity αV_o while maintaining its forward velocity. The angle of attack therefore changes discontinuously from zero to a constant α. At the same instant, the step change in angle of attack causes the emission of a compression wave from each point on the lower surface of the wing and expansion waves from points on the upper surface. In the infinitesimal time during which the starting action occurs, each section of the wing experiences the same impulsive force, and by equating the impulse to the momentum transmitted to the mass of fluid affected by the starting waves, the starting lift coefficient can easily be derived as $4\alpha/M_o$ (see ref. 3). During the infinitesimal starting time, the pressure disturbances from the edges of the airfoil, propagated at the speed of sound, travel an insignificant distance and do not influence the remainder of the airfoil. The lift coefficient is therefore independent of the wing plan form. This remarkably simple result for the starting lift coefficient, which is valid for both subsonic and supersonic speeds, is thus dependent solely on the flight Mach number. The starting pitching moment follows directly from the above result, since by virtue of the uniformity of loading the aerodynamic center is located at the wing centroid of area.

For values of time greater than zero, however, the situation differs radically for the supersonic and subsonic speed ranges. Consider first the supersonic case. As time passes, the spherical sound waves emitted at $t'=0$ grow in size with radius $a_o t'$. The wing, however, is moving forward at a faster rate than the rate of growth of the starting sound waves and thus begins to emerge from the influence of these waves. This is shown schematically in figure 12. (Note in fig. 12 that the wing moves away from a coordinate system that is fixed in space at the original position of the wing leading edge.)

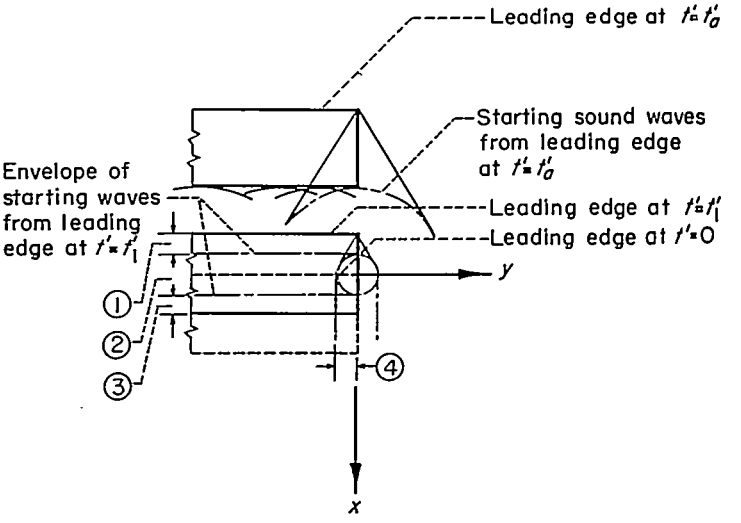

FIGURE 12.—Relation of wing position to starting sound waves for supersonic speed.

At $t'=0$, the starting waves just cover the wing and the loading is uniform as described previously. At $t'=t'_1$, the starting waves have grown in radius and the wing has begun to emerge from their influence. On that portion of the wing which has emerged, region ① in figure 12, the loading has already reached its steady-state value. Notice that in this region the characteristic tip Mach cone has already formed. On the portion of the wing uninfluenced by the starting waves from the edges, region ③ in figure 12, the loading is still uniform as at $t'=0$. In regions ② and ④, the loading is influenced by the starting waves from the leading and side edges, and in these regions is thus different from the loading in either region ① or ③. As time increases still further, the uniform starting load quickly disappears as the sound waves from the leading edge grow in size and as the wing moves forward. Finally, at time t'_a, the envelope of the starting waves from the leading edge is coincident with the trailing edge of the wing, and the steady-state loading corresponding to the new angle of attack α has been completely established over the wing.

The above relationships can be shown more clearly for the entire time interval zero to t'_a for a two-dimensional wing by plotting as a function of time the position of the wing leading and trailing edges and position of the envelopes of the sound waves which emanate from the leading and trailing edges at $t'=0$. Such a plot is shown in figure 13.

It is clear that at $t'=t'_1$ the regions of the wing ①, ②, and ③ correspond to the same regions at $t'=t'_1$ for the wing shown in figure 12. For $t'=0$ and in region ③ the loading is uniform and is given by $4\alpha/M_o$. Note also in figure 13 that disturbances created by the vorticity shed into the airfoil wake at $t'=0$ and all subsequent times cannot influence the flow over the airfoil itself. For $t'>t'_a$ and in region ① the wing has out-stripped the starting waves from the leading edge and has attained its steady-state loading. For $t'<t'_a$ the chordwise loading is composed of combinations of the loading in each of the three regions shown in figure

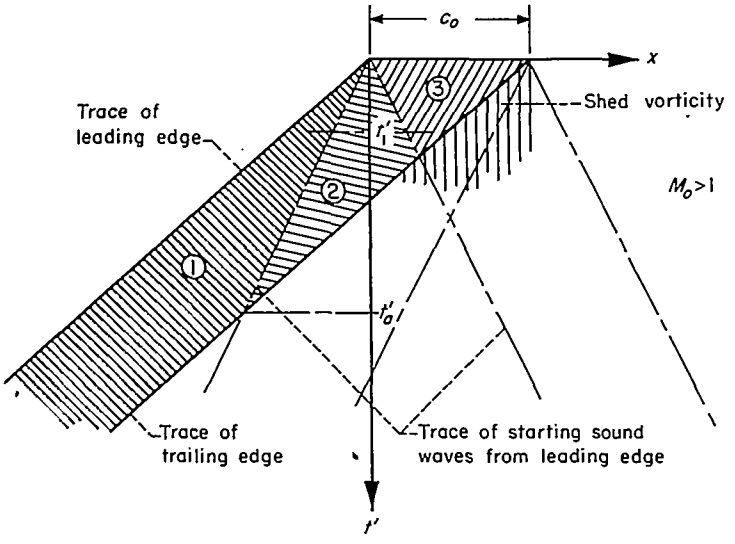

FIGURE 13.—Relation of wing position to starting sound waves for supersonic speed.

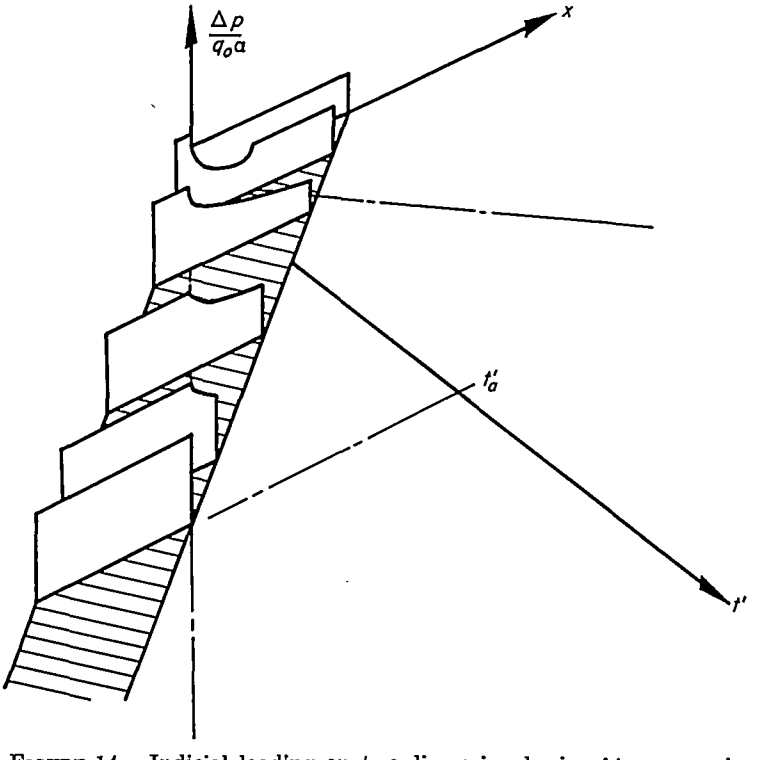

FIGURE 14.—Indicial loading on two-dimensional wing at supersonic speed.

14.[4] Since the loading on the wing attains its final steady-state distribution at precisely the time when the wing has emerged entirely from the influence of the starting sound waves from the leading edge (or apex), the time to reach steady state may be easily calculated for any type of wing by means of the geometric relationships shown in figure 15. It may be easily verified that t_a', the time required for the wing to attain its steady-state loading, is given by either of

[4] The reader will note the similarity between figure 13 and sketches depicting the boundary conditions for three-dimensional wings in steady supersonic flow. Many researchers have pointed out the analogy and it has been used to calculate the pressure over a wing impulsively starting from rest (refs. 3 and 4).

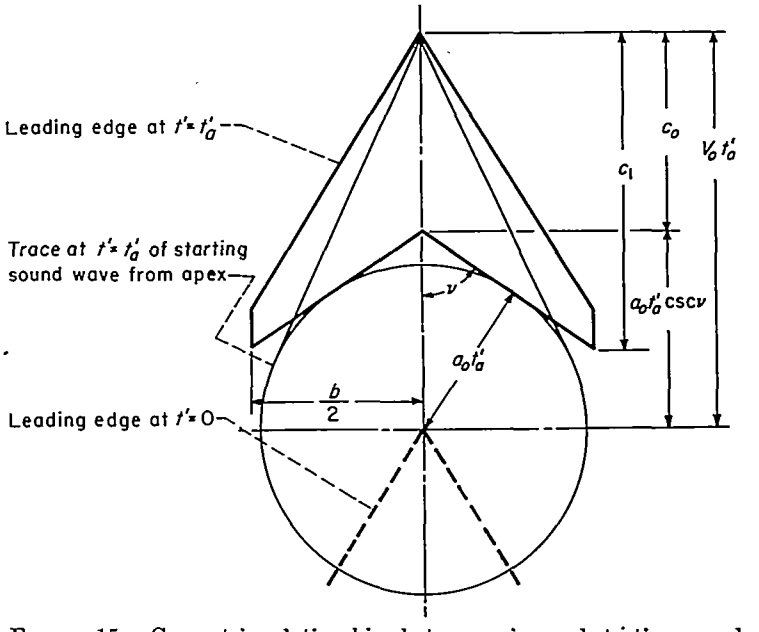

FIGURE 15.—Geometric relationships between wing and starting sound wave at time t_a'.

the following relationships:

$$\left.\begin{aligned} t_a'&=\frac{c_o M_o}{V_o(M_o-\csc\nu)},\ M_o\geq\csc\nu+\frac{2c_o}{b}\cos\nu,\ \nu\leq\frac{\pi}{2}\\ t_a'&=\frac{c_1 M_o}{V_o}\left(\frac{M_o+\sqrt{1-\frac{\beta^2 b^2}{4c_1^2}}}{\beta^2}\right),\ M_o\leq\csc\nu+\frac{2c_o}{b}\cos\nu \end{aligned}\right\} \quad (22)$$

The second of equations (22) applies to that range of Mach numbers for which the trace of the starting sound wave from the apex is not tangent to the trailing edge at $t'=t_a'$. Notice that for wings having straight or sweptforward trailing edges and straight or sweptback leading edges, equation (22) reduces to

$$t_a'=\frac{c_o M_o}{V_o(M_o-1)} \quad (23)$$

In terms of the number of half M. A. C. lengths of travel, it thus appears that for wings having straight or sweptforward trailing edges and straight or sweptback leading edges,

$$\sigma_a=\frac{2V_o}{\bar{c}}t_a'=\frac{2c_o}{\bar{c}}\frac{M_o}{(M_o-1)} \quad (24)$$

whereas for wings having sweptback trailing edges and straight or sweptback leading edges,

$$\left.\begin{aligned} \sigma_a&=\frac{2c_o}{\bar{c}}\frac{M_o}{(M_o-\csc\nu)},\ M_o\geq\csc\nu+\frac{2c_o}{b}\cos\nu,\ \nu\leq\frac{\pi}{2}\\ \sigma_a&=2M_o\frac{c_1}{\bar{c}}\left(\frac{M_o+\sqrt{1-\frac{\beta^2 b^2}{4c_1^2}}}{\beta^2}\right),\ M_o\leq\csc\nu+\frac{2c_o}{b}\cos\nu \end{aligned}\right\} \quad (25)$$

Now consider the subsonic case. Here the situation is more complicated in that, since the starting sound waves travel faster than the wing, the wing never escapes their influence. Furthermore, the vorticity shed by the wing at $t'=0$ can also influence the loading on the wing since the

disturbances created by the shed vorticity travel forward at a faster rate than the wing. For these reasons, the indicial loading at subsonic speeds approaches its steady-state distribution asymptotically with time. The situation for subsonic speeds will be more clearly evident from examination of figure 16, which shows the relationship of the traces versus time of the leading and trailing edges of a two-dimensional wing flying at a subsonic Mach number to the traces of the envelopes of the starting sound waves.

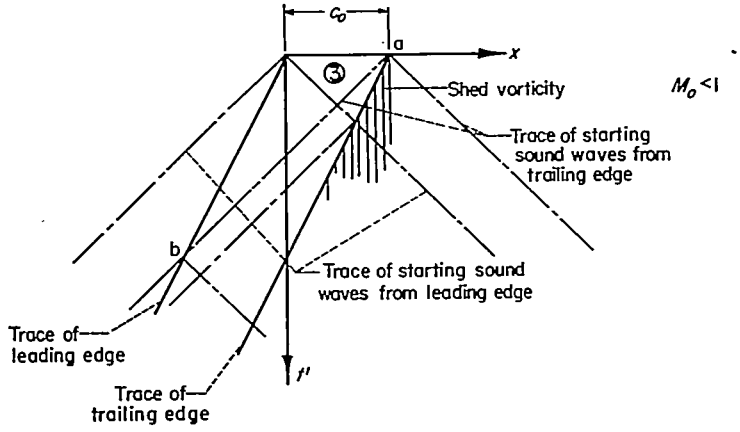

FIGURE 16.—Relation of wing position to starting sound waves for subsonic speed.

Notice in figure 16 that the starting sound waves intersect the edges of the wing and that each intersection causes a new sound wave to be emitted, which in turn will intersect an edge. Furthermore, notice that the vorticity shed from the trailing edge at time zero can influence that portion of the wing behind the sound-wave trace labeled a-b. The influence of each successive sound-wave reflection, however, is weaker than the last, and as the wing moves away from the starting vortices their influence diminishes, so that at $t'=\infty$ the loading on the wing attains its steady-state distribution. The variation of the chordwise loading with time for the two-dimensional wing flying at a subsonic Mach number is shown in figure 17. Notice that for $t'>0$, the chordwise loading is markedly different from the loading at supersonic speeds (fig. 14). However, for $t'=0$ and in the region corresponding to region ③ of figure 16, the loading is uniform and equal to $4\alpha/M_0$, as in the supersonic case.

DAMPING IN PITCH OF LOW-ASPECT-RATIO WINGS

Previously (eq. (20)), it was shown that for single-degree-of-freedom, low-frequency, rotary oscillations of a wing, the principal parameter contributing to the damping of the motion is the damping coefficient $C_{m_q}+C_{m_{\dot{\alpha}}}$. This result, however, is not directly applicable to the case of an aircraft in flight, since generally additional damping is provided by virtue of the fact that the aircraft experiences harmonic vertical translatory oscillations as well as the rotary oscillations. It can be shown, however, that although the effect of the translatory oscillation is usually to increase the total damping, nevertheless, the parameter of primary importance in determining the magnitude and duration of the motion remains the damping-in-pitch coefficient $C_{m_q}+C_{m_{\dot{\alpha}}}$. The remainder of this section is therefore concerned with a study of

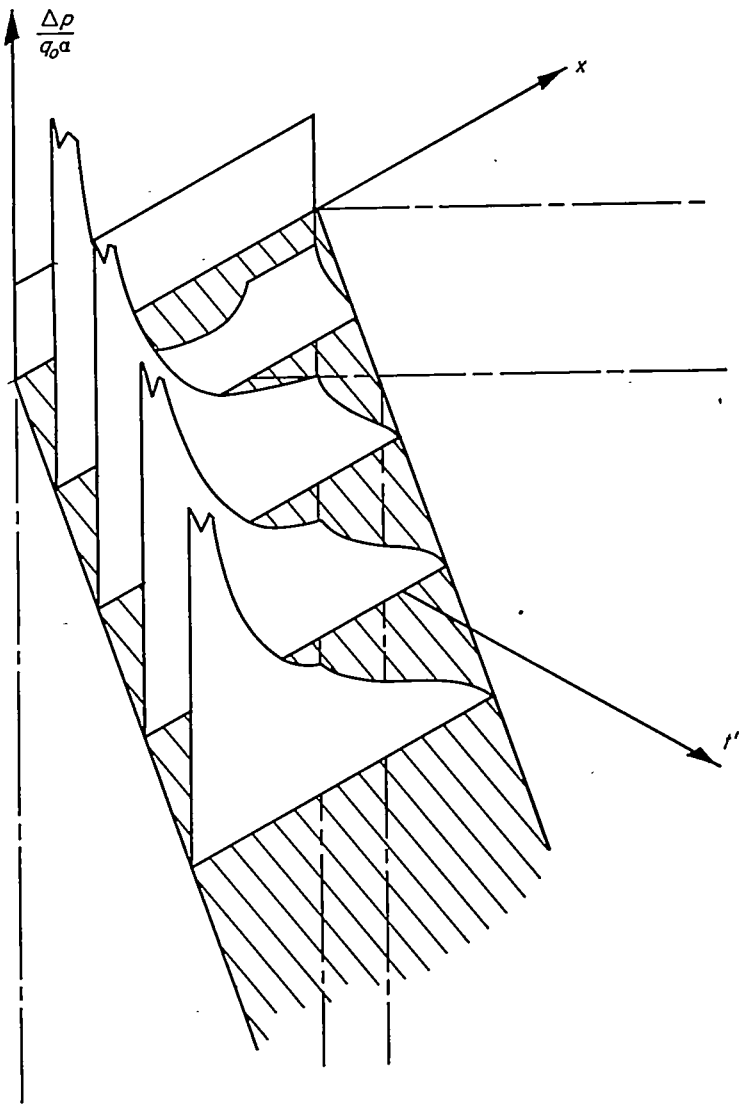

FIGURE 17.—Indicial loading on two-dimensional wing at subsonic speed.

the effect on this parameter of certain important variables. In particular, the effect of the position of the center of gravity, and the effects of Mach number, aspect ratio, planform shape, and frequency will be examined, principally by inspection of the indicial lift and moment responses to a change in angle of attack.

EFFECT OF STATIC MARGIN

From the previous discussion it will be remembered that at supersonic speeds the stability derivatives $C_{L_{\dot{\alpha}}}(\sigma_a)$ and $C_{m_{\dot{\alpha}}}(\sigma_a)$ were shown to be equivalent to the indicial lift and moment expressions, $-\int_0^{\sigma_a} F_1(\varphi)d\varphi$ and $-\int_0^{\sigma_a} F_3(\varphi)d\varphi$. Furthermore, it was shown that these were the contributions which could cause the total lift and moment during the short-period oscillation to lag behind the angle of attack. Hence, by inspection of equation (15), it is evident that since $C_{m_q}(\sigma_a)$ is always stabilizing, when $C_{m_\alpha}(\sigma_a)$ is negative (corresponding to a statically stable condition) the possibility of dynamic instability in the form of divergent rotary oscillations arises when $C_{m_{\dot{\alpha}}}(\sigma_a)$, the shaded area in figure 10 (b), is larger than $C_{m_q}(\sigma_a)$. Now since the normal velocity at the

surface of the wing due to the instantaneous angle of attack is constant over the wing, the lift derivative $C_{L_{\dot{\alpha}}}$ which arises from this boundary condition is independent of the axis position and $C_{m_{\dot{\alpha}}}$ will therefore vary linearly with axis position. This variation is illustrated in figure 18, where Δx_o represents the distance of the center of gravity from the aerodynamic center, measured positive forward of the aerodynamic center.

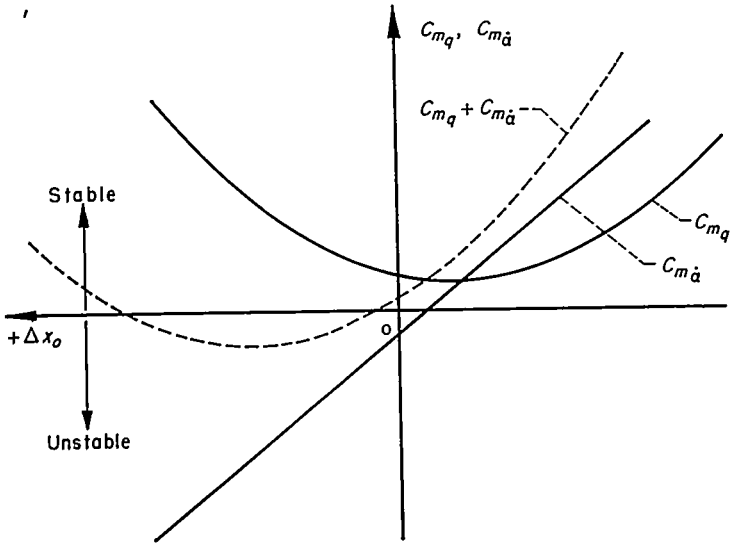

FIGURE 18.—Variation of C_{m_q} and $C_{m_{\dot{\alpha}}}$ with axis position.

The parameter C_{L_q}, on the other hand, is a direct function of the axis position, since it arises from a normal velocity distribution that varies directly as the distance from the axis. The moment coefficient C_{m_q} will therefore vary as the second power of the axis position, and describes the parabolic shape shown also in figure 18. It is evident from figure 18 that the sum of C_{m_q} and $C_{m_{\dot{\alpha}}}$ will be a minimum at some value of the static margin, and that the sign of $C_{m_q}+C_{m_{\dot{\alpha}}}$ at that point determines whether or not a region of axis positions will exist over which the wing can experience negatively damped rotary oscillations. These qualitative statements may be written explicitly by considering the equation for the damping in pitch about an arbitrary axis,

$$C_{m_q}+C_{m_{\dot{\alpha}}}=(C_{m_q})_o+(C_{m_{\dot{\alpha}}})_o-\frac{\Delta x_o}{\bar{c}}[(C_{L_q})_o+C_{L_{\dot{\alpha}}}]-2\left(\frac{\Delta x_o}{\bar{c}}\right)^2 C_{L_\alpha} \tag{26}$$

where again Δx_o refers to the distance of the center of gravity from the aerodynamic center, and the subscripted terms are referred to an axis through the aerodynamic center.

Taking the derivative of equation (26) with respect to $\Delta x_o/\bar{c}$, and setting the result equal to zero, there is obtained the axis location at which the damping in pitch is a minimum

$$\left.\begin{aligned}\frac{d(C_{m_q}+C_{m_{\dot{\alpha}}})}{d(\Delta x_o/\bar{c})}&=-[(C_{L_q})_o+C_{L_{\dot{\alpha}}}]-4\frac{\Delta x_o}{\bar{c}}C_{L_\alpha}=0\\ \frac{\Delta x_o}{\bar{c}}&=-\frac{[(C_{L_q})_o+C_{L_{\dot{\alpha}}}]}{4C_{L_\alpha}}\end{aligned}\right\} \tag{27}$$

When equation (27) is inserted into equation (26), the minimum value of the damping in pitch is given as

$$(C_{m_q}+C_{m_{\dot{\alpha}}})_{min}=[(C_{m_q})_o+(C_{m_{\dot{\alpha}}})_o]+\frac{1}{8C_{L_\alpha}}[(C_{L_q})_o+C_{L_{\dot{\alpha}}}]^2 \tag{28}$$

and hence, a region of instability will exist if

$$[(C_{m_q})_o+(C_{m_{\dot{\alpha}}})_o]+\frac{1}{8C_{L_\alpha}}[(C_{L_q})_o+C_{L_{\dot{\alpha}}}]^2>0 \tag{29}$$

If equation (29) is greater than zero, the boundaries of the region of axis positions over which instability is possible are of course given by setting equation (26) equal to zero and solving for $\Delta x_o/\bar{c}$.

$$\frac{\Delta x_o}{\bar{c}}=-\frac{[(C_{L_q})_o+C_{L_{\dot{\alpha}}}]}{4C_{L_\alpha}}\mp\sqrt{\left[\frac{(C_{L_q})_o+C_{L_{\dot{\alpha}}}}{4C_{L_\alpha}}\right]^2+\left[\frac{(C_{m_q})_o+(C_{m_{\dot{\alpha}}})_o}{2C_{L_\alpha}}\right]} \tag{30}$$

Notice in both figure 18 and equation (30) that for a given Mach number there will be two axis positions at which the damping in pitch vanishes. Then if the above procedure is carried out for a series of Mach numbers, one may trace out a curve as shown in figure 19 which forms the locus of

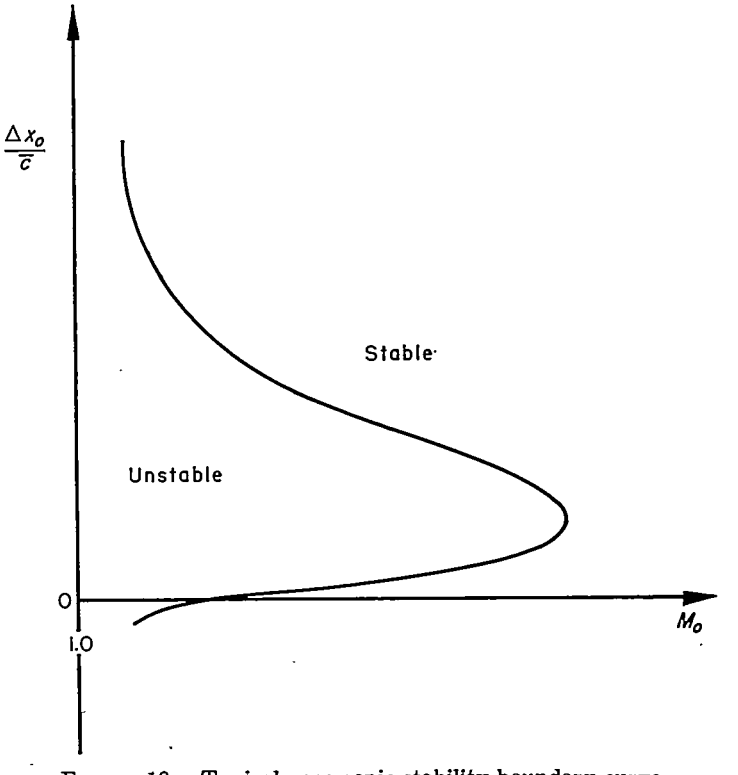

FIGURE 19.—Typical supersonic stability boundary curve.

Mach numbers and axis positions at which the damping in pitch is zero. This locus thus delineates the regions of Mach number and axis position for which dynamic instability is and is not theoretically possible. Such loci, covering a wide variety of wings at supersonic speeds, have been presented by a number of authors. Watkins, for example, presents supersonic boundary curves for rectangular and triangular wings in references 15 and 16. At subsonic speeds, Miles' reduction of Possio's development to first order in frequency (ref. 10) can be used to form a stability boundary curve for the two-dimensional wing for a given (small) reduced frequency. Such a curve is presented for

the entire Mach number range in figure 20, where, here $+x_o$ is the distance of the axis of rotation behind the leading edge and k, the reduced frequency, is 0.011 for subsonic speeds and approaches zero for supersonic speeds. Notice in figure 20 that at both subsonic and supersonic speeds,

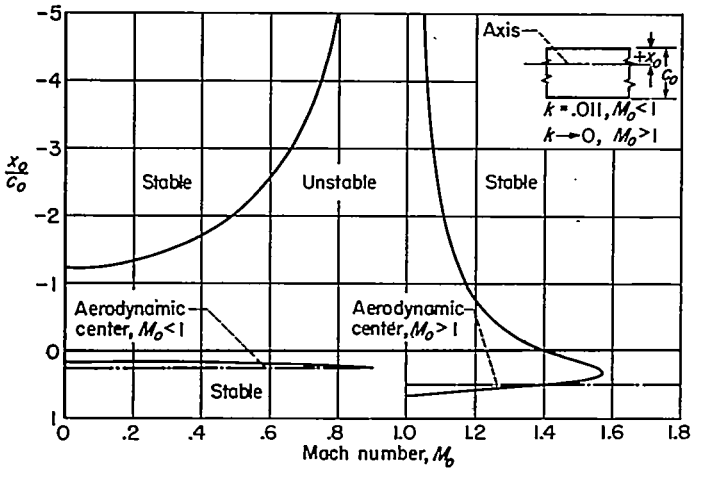

FIGURE 20.—Single-degree-of-freedom short-period pitching stability boundaries for the two-dimensional wing at subsonic and supersonic speeds.

the range of Mach numbers over which dynamic instability is possible is largest for center-of-gravity positions forward of the aerodynamic center. Further, the largest range of axis positions over which dynamic instability is possible occurs near $M_o=1$. Both of these characteristics have been shown to be true as well for three-dimensional wings at supersonic speeds (see, e. g., refs. 15 to 18).

EFFECT OF MACH NUMBER

Next consider the effect of Mach number on the damping in pitch of a two-dimensional wing with axis at the leading edge. The variation with Mach number of the indicial pitching-moment response to a change in α will first be examined, using the information given in the previous sections and the indicial curves given in reference 4. At supersonic speeds, the manner in which $-\int_o^{\sigma_a} F_3(\varphi)d\varphi$, the area corresponding to $C_{m_{\dot{\alpha}}}$, is affected can then be assessed and compared with C_{m_σ} (σ_a). At subsonic speeds, use is made of equation (18b). It is evident in equation (18b) that by fixing k and choosing φ_1, such that the quantity $\frac{1}{4}G(\varphi_1,k)$ is the same at each Mach number, one is free to compare finite areas $-\int_o^{\varphi_1} F_3(\varphi)d\varphi$ on an equivalent basis.

As has been mentioned previously, the starting lift, at any Mach number, is $4\alpha/M_o$ and is concentrated at the midchord. At $M_o=0$, therefore, there is an initial infinite pulse in the pitching moment about an axis coincident with the leading edge after which the indicial curve drops to $\pi/4$ and begins to grow asymptotically toward its steady-state value $\pi/2$. At low subsonic Mach numbers other than zero, the initial pitching moment is less than infinite but very large, being $2/M_o$, and then falls before growing toward the steady value $\pi/2\beta$. As the Mach number increases toward 1.0, the starting pitching moment falls while the asymptotic value grows, until at $M_o=1.0$ the indicial curve becomes unbounded in asymptotic moment.

As seen in figure 21, the effect of increasing the Mach number at subsonic speeds is therefore to increase rapidly the area corresponding to the destabilizing moment contribution, $-\int_o^{\varphi_1} F_3(\varphi)d\varphi$.

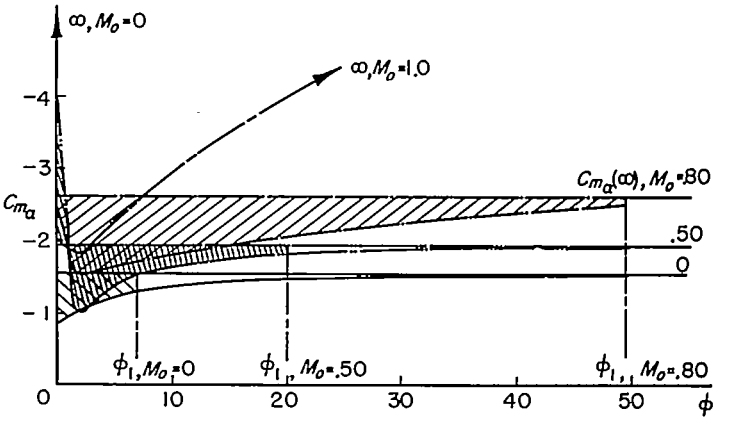

FIGURE 21.—Variation with subsonic Mach number of the indicial pitching-moment response $c_{m_\alpha}(\phi)$ for the two-dimensional wing. Axis at leading edge.

In figure 21, k was chosen to be 0.011 and the values of φ_1 were picked such that $-\frac{1}{4}G(\varphi_1,k)$ was $+4.88$ at each Mach number. In the following discussion, the damping moment $-\int_o^{\varphi_1} F_3(\varphi)d\varphi+4.88$ will be referred to as $C_{m_{\dot{\alpha}}}$ for convenience.

At supersonic speeds, the initial value of the pitching moment $2/M_o$ continues to drop with increasing Mach number, but here the steady-state pitching moment also begins to fall and at a faster rate than the starting moment, being $2/\beta$. Even more important, as the Mach number increases, the number of half-chord lengths traveled to reach steady state decreases rapidly, being 22, for example, at $M_o=1.1$, as compared to 4 at $M_o=2$. As seen in figure 22, the area representing $C_{m_{\dot{\alpha}}}$ therefore shrinks rapidly with increasing supersonic Mach number and becomes relatively unimportant at Mach numbers greater than 2. The trend of $C_{m_{\dot{\alpha}}}$ with Mach number through the range $0<M_o<2$ is more clearly evident in figure 23. It is seen that $C_{m_{\dot{\alpha}}}$ is positive, or destabilizing, throughout the Mach number range and that its effect is most important at Mach numbers near 1.0. Also shown plotted for comparison in figure 23 is the variation of C_{m_q} with Mach number. When the parameters are added, it is evident that the damping moment $C_{m_q}+C_{m_{\dot{\alpha}}}$ for the two-dimensional wing with axis at the leading edge is destabilizing in the Mach number range $0<M_o<1.414$.

EFFECT OF ASPECT RATIO

To illustrate the effect of aspect ratio, it is convenient to compare the supersonic damping-in-pitch characteristics of a group of triangular wings having subsonic leading edges. The wings are of equal area and differ only in aspect ratio. As was done previously, the indicial lift responses to a change in angle of attack will first be examined. The effect of aspect

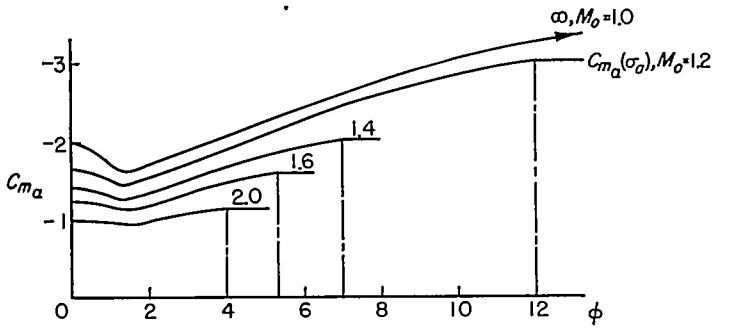

FIGURE 22.—Variation with supersonic Mach number of the indicial pitching-moment response $c_{m_\alpha}(\phi)$ for the two-dimensional wing. Axis at leading edge.

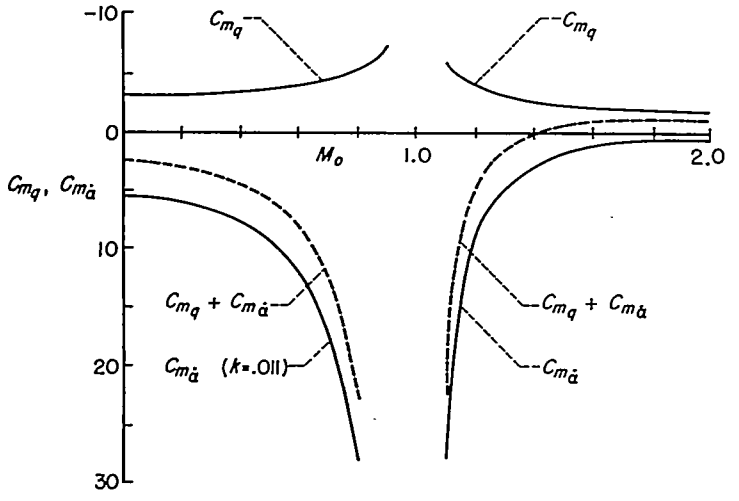

FIGURE 23.—Variation with Mach number of the damping in pitch of the two-dimensional wing. Axis at leading edge.

ratio on the characteristic area representing $C_{L_{\dot\alpha}}$ can then be assessed.

As has been mentioned previously, the starting lift coefficient after a step change in α is independent of aspect ratio and is therefore equal to $4\alpha/M_o$ for each wing. The parameter σ_a, the number of half M. A. C. lengths required to reach steady state, is also the same for each wing, being a function only of Mach number. The steady-state lift coefficient, on the other hand, is a function of aspect ratio

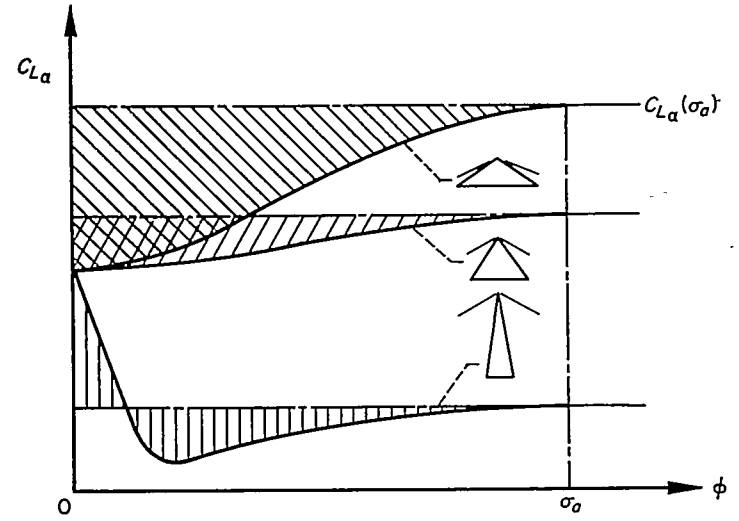

FIGURE 24.—Effect of aspect ratio on the indicial lift response $C_{L_\alpha}(\phi)$ of triangular wings having subsonic leading edges.

and decreases as the aspect ratio is reduced. Thus, as shown schematically in figure 24, as the aspect ratio becomes smaller, the characteristic area representing $C_{L_{\dot\alpha}}$ decreases rapidly.[5] For the wing of smallest aspect ratio, $C_{L_{\dot\alpha}}$ may be positive since the area below the steady-state lift coefficient is more than compensated for by the area above. It is evident, therefore, that a reduction in aspect ratio has a highly stabilizing effect on the damping in pitch, since for positive values of the static margin, the development of a destabilizing damping moment is possible only when $C_{L_{\dot\alpha}}$ is negative. This result is shown in figure 25 where, for an axis of rotation located at 0.25 $\bar{c}$ and M_o=1.2, the damping parameters are presented as functions of aspect ratio. Since for triangular wings the lift due to $\dot\alpha$ is concentrated at 5/8 $\bar{c}$, $C_{m_{\dot\alpha}}$ is equal to $-3/8\ C_{L_{\dot\alpha}}$. The variation of $C_{m_{\dot\alpha}}$ with aspect ratio shown in figure 25 then follows directly from the trend of $C_{L_{\dot\alpha}}$ shown in figure 24. Also plotted in figure 25 is the variation of C_{m_q} with aspect ratio (ref. 19).

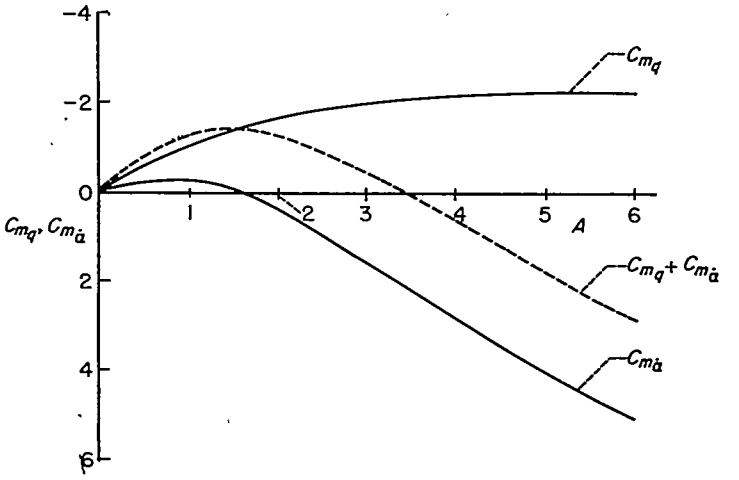

FIGURE 25.—Variation with aspect ratio of the damping-in-pitch coefficients of triangular wings. Axis at 0.25$\bar{c}$ and Mach number 1.2.

It is apparent that although C_{m_q} becomes more stabilizing with increasing aspect ratio, the destabilizing effect of $C_{m_{\dot\alpha}}$ predominates, and the trend of the net damping moment is seen to become highly destabilizing as the aspect ratio is increased.

By the same reasoning, the variation with aspect ratio of the damping moments of other types of wings can be shown to be similar (see, e. g., refs. 10, 20, 21, and 22). A notable exception, however, is the triangular wing with supersonic leading edges, whose damping in pitch has been shown to be independent of aspect ratio (see refs. 17 and 18). This characteristic may be anticipated from a study of the indicial response curves, since not only are the initial pitching moment C_{m_α} (0) and the half M. A. C. lengths traveled to reach steady state (σ_a) independent of aspect ratio, but, unlike the subsonic-edged triangular wing, the steady-state pitching moment $C_{m_\alpha}(\sigma_a)$ is also independent of aspect ratio,

[5] Theoretical indicial curves have not yet been calculated for the triangular wing with subsonic leading edges. The curves drawn in figure 24 are estimates of the true shapes, and are intended only to indicate the trend of the characteristic area with aspect ratio. The exact variation of $C_{L_{\dot\alpha}}$ with aspect ratio can be computed from the results of reference 19.

being $-\frac{4}{\beta}\left(\frac{\Delta x_o}{\bar{c}}\right)$. Inspection of the results of reference 4 then reveals that the indicial variation $C_{m_\alpha}(\varphi)$ between zero and σ_a and the steady-state parameter $C_{m_q}(\sigma_a)$ are likewise independent of aspect ratio.

EFFECT OF PLAN-FORM SHAPE

Next, consider the effect of plan-form shape on the supersonic damping in pitch of a group of wings having the same aspect ratio. For this comparison, three wings of aspect ratio 3 are chosen, having the triangular, swept, and rectangular plan forms shown in figure 26.

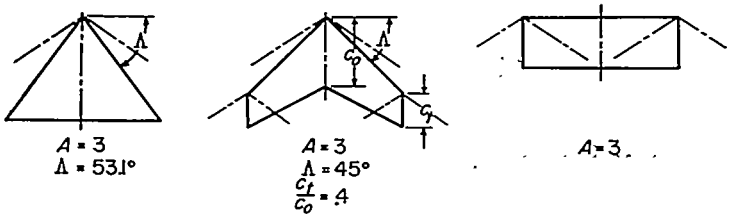

FIGURE 26.—Wings used in study of effect of plan-form shape.

As has been shown in the section entitled "Effect of Static Margin," the tendencies of the wings toward dynamic instability can be compared comprehensively by plotting their stability boundaries. For this comparison, then, use is made of equation (30). The stability derivatives which appear in equation (30) were computed from the theoretical results of references 10, 19, 21, and 22. Results of these calculations are shown in figure 27 wherein the stability boundaries for the three wings are shown as a function of axis position and Mach number. (Note that the axis position for each wing is measured as the distance from the leading edge of the M. A. C. of the wing, and that the dimensions are nondimensionalized on an equivalent basis by referring them to the M. A. C. of the triangular wing.) It is clear from inspection of figure 27 that at any Mach number the triangular wing has the smallest range of axis positions over which dynamic instability is possible and the rectangular wing, the largest.

The differences in the damping characteristics of the triangular and rectangular wings will be more clearly understood by a qualitative study of their indicial lift response for a Mach number of 1.2, and an examination of the distribution of loading due to $\dot{\alpha}$ for the two wings. Consider first the indicial lift responses.

Again, the starting lift coefficient is independent of plan-form shape and is $4\alpha/M_o$ for each wing. For the rectangular wing, the lift drops abruptly after time zero due to the loss in lift in the regions of the wing influenced by the formation of the tip Mach cones and the starting waves from the side edges (see fig. 12). Then, as the wing begins to emerge from the influence of the starting waves, the lift begins to recover, rises toward its steady-state value (given by eq. 6.3–2 of ref. 10), and attains this value after 12 half-chord lengths of travel (eq. (24)). The variation is shown in reference 4 and is redrawn in figure 28. As mentioned previously, theoretical indicial lift results have not yet been developed for triangular wings having subsonic leading edges. However, the variation shown in figure 28 is considered to be a reasonable esti-

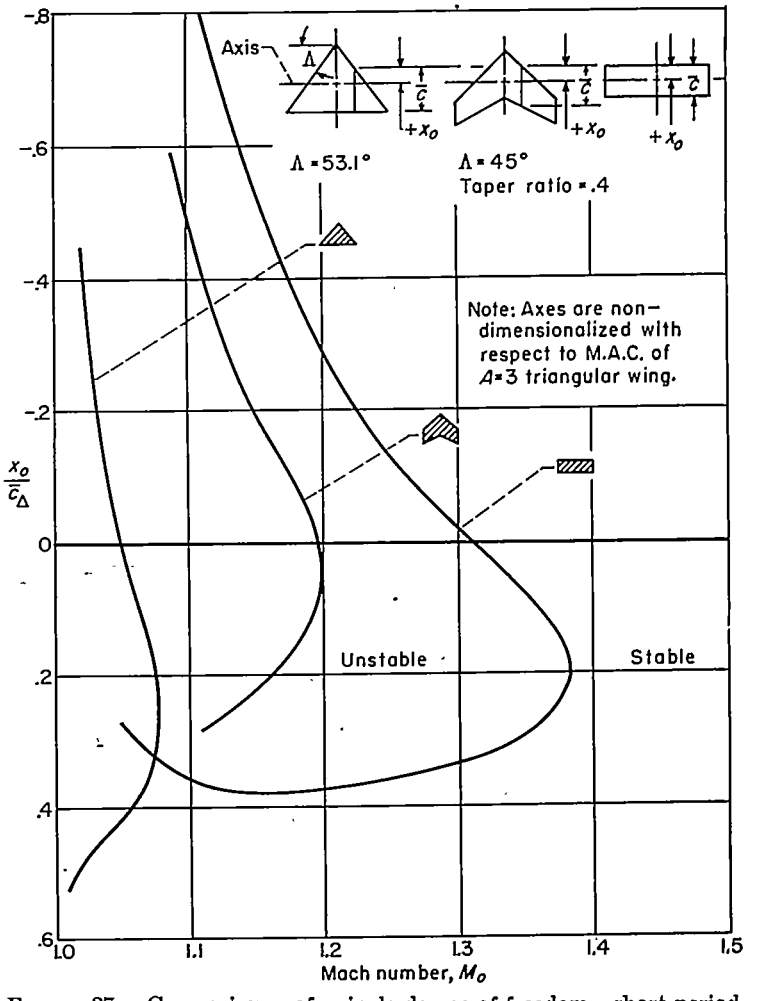

FIGURE 27.—Comparison of single-degree-of-freedom short-period pitching stability boundaries at supersonic speeds for three wings of aspect ratio 3, having triangular, swept, and rectangular planforms.

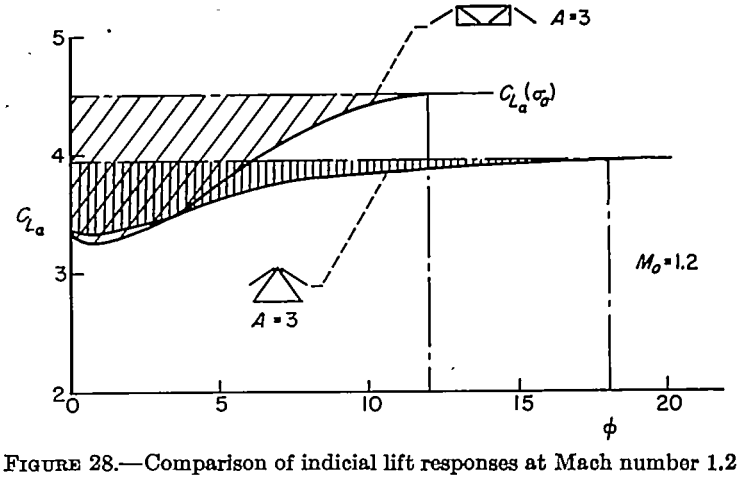

FIGURE 28.—Comparison of indicial lift responses at Mach number 1.2 of rectangular and triangular wings of aspect ratio 3.

mate of the true shape, being based on knowledge of the steady-state lift (ref. 19), the time to reach steady state (eq. (24)), and the assumption that the shape of the variation would be similar to that of the wide triangular wing (ref. 4). The curve was adjusted within the known end points until the area corresponding to $C_{L_{\dot{\alpha}}}$ agreed with that given for this parameter in reference 19. It is evident from examination of figure 28 that because of the initial loss in lift and the

larger steady-state lift for the rectangular wing, $C_{L_{\dot{\alpha}}}$ for this wing is significantly more negative than that for the triangular wing. Next, it is shown in references 10 and 20 that with the exception of regions influenced by tip Mach cones, the loading due to $\dot{\alpha}$ (for $\varphi > \sigma_a$) for wings having sweptback leading edges increases linearly from zero along rays from the apex; whereas for rectangular wings the loading due to $\dot{\alpha}$ increases linearly from zero along chord lines. These characteristics place the center of loading due to $\dot{\alpha}$ at ¾ c_o for the triangular wing and approximately ⅝ c_o for the rectangular wing.[6] Then for an axis of rotation passing through the aerodynamic centers of the wings, the moment arm for the lift due to $\dot{\alpha}$ for the triangular wing is ½ c_o or ⅛ $\bar{c}$; whereas for the rectangular wing it is approximately ⅛ c_o.[7] Thus, not only is the negative out-of-phase lift contribution $C_{L_{\dot{\alpha}}}$ for the rectangular wing significantly larger than that for the triangular wing, but the destabilizing damping moment $-\frac{x}{\bar{c}}C_{L_{\dot{\alpha}}}$ is larger yet, due to the larger moment arm. Calculations for the steady pitching parameter C_{m_q} for an axis through the aerodynamic center (refs. 10 and 19) then reveal that C_{m_q} for the triangular wing is more negative than for the rectangular wing. The net result is therefore a considerably larger damping moment for the triangular wing than for the rectangular wing. The result of this comparison, however, should not be interpreted as a recommendation that the triangular rather than the rectangular wing be used on aircraft from a dynamic stability standpoint. To obtain adequate static stability, the rectangular wing would generally be employed in combination with a tail surface; whereas the triangular plan form may be sufficiently airworthy without the use of a tail. The addition of a tail surface in effect reduces the aspect ratio of the rectangular wing, which reduction, as noted previously, has a highly stabilizing effect on the damping in pitch. The tailless triangular wing may therefore experience more difficulty at Mach numbers near 1.0 than a rectangular wing-tail combination.

EFFECT OF FREQUENCY

The previous discussion has been restricted to the analysis of a harmonic motion that is of vanishingly small frequency. This limitation arose as a consequence of discarding all but first order in frequency terms in the expansions of equations (12) and (14). The question arises: When the frequency can no longer be considered small, what effect has the frequency on the damping in pitch?

Previously, the trigonometric terms in equation (14) were expanded and, assuming k to be very small, terms of order k^2 and higher were eliminated. It was then found that the loss in damping from that provided by the steady damping parameter $C_{m_q}(\sigma_a)$ was associated with the destabilizing moment contribution corresponding to the term $-\int_0^{\sigma_a} F_3(\varphi)d\varphi$. Now, however, we discard the restriction of small k and perform graphically the integrations evident in equation (14) for supersonic speeds for several values of k. The procedure is indicated in figure 29. It is apparent from figure 29 that the effect of increasing k is to reduce the area corresponding to the destabilizing moment contribution $-\int_0^{\sigma_a} F_3(\varphi)\cos k\varphi d\varphi$. There appears another

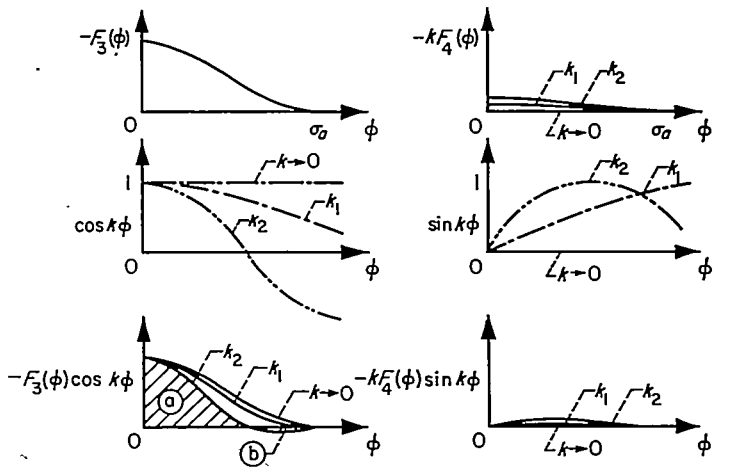

FIGURE 29.—Illustration of graphical integration procedure for finding effect of frequency at supersonic speed.

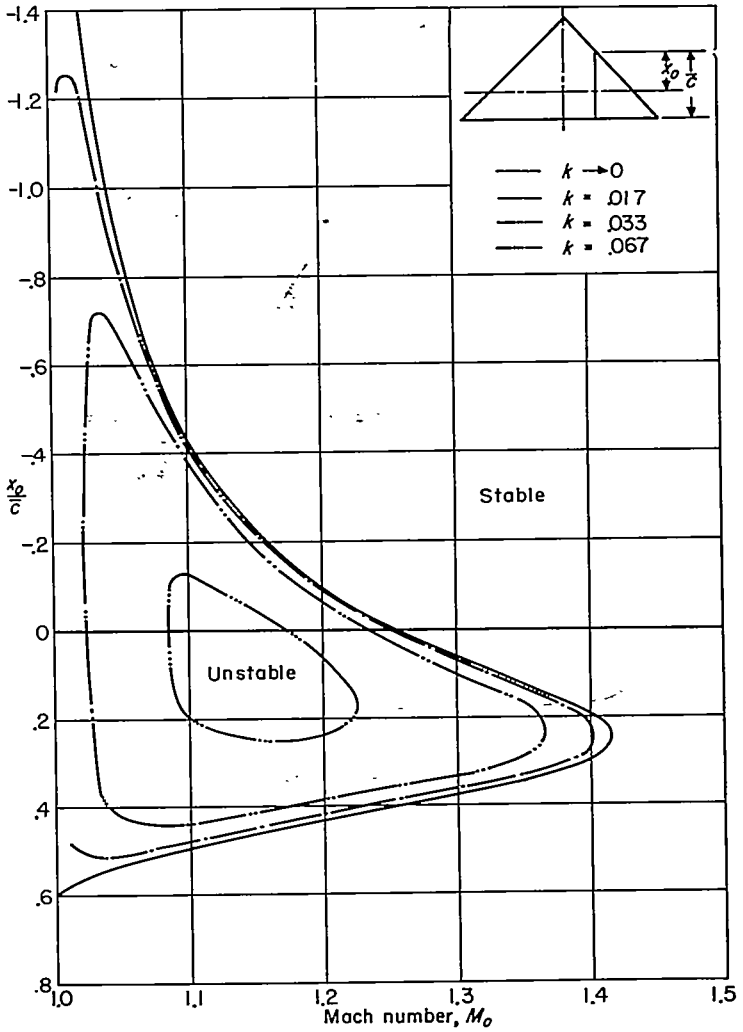

FIGURE 30.—Effect of frequency on the single-degree-of-freedom short-period pitching stability boundaries at supersonic speeds for a triangular wing of aspect ratio 4.

[6] Due to the influence of the tip Mach cones, the center of loading due to $\dot{\alpha}$ is shifted forward somewhat from the position it has for the two-dimensional wing. Calculations for the $A=3$ rectangular wing at $M_o=1.2$ show that the center of loading is at $0.605c_o$.

[7] Again, due to the influence of tip Mach cones, the aerodynamic center is shifted forward from ½ c_o to $0.443\,c_o$. The moment arm is therefore $0.162\,c_o$.

destabilizing contribution, $-k\int_0^{\sigma_a} F_4(\varphi)\sin k\varphi d\varphi$, but quite evidently its effect is small compared to the reduction in the term $-\int_0^{\sigma_a} F_3(\varphi)\cos k\varphi d\varphi$. Notice further in figure 29 that the effect of increasing k becomes of marked importance when the half-period of oscillation is the same order of magnitude as the time for the indicial response to reach steady state. As shown in figure 29 for the frequency k_2, the area b then begins to subtract from a, so that the destabilizing contribution $-\int_0^{\sigma_a} F_3(\varphi)\cos k\varphi d\varphi$ can be very

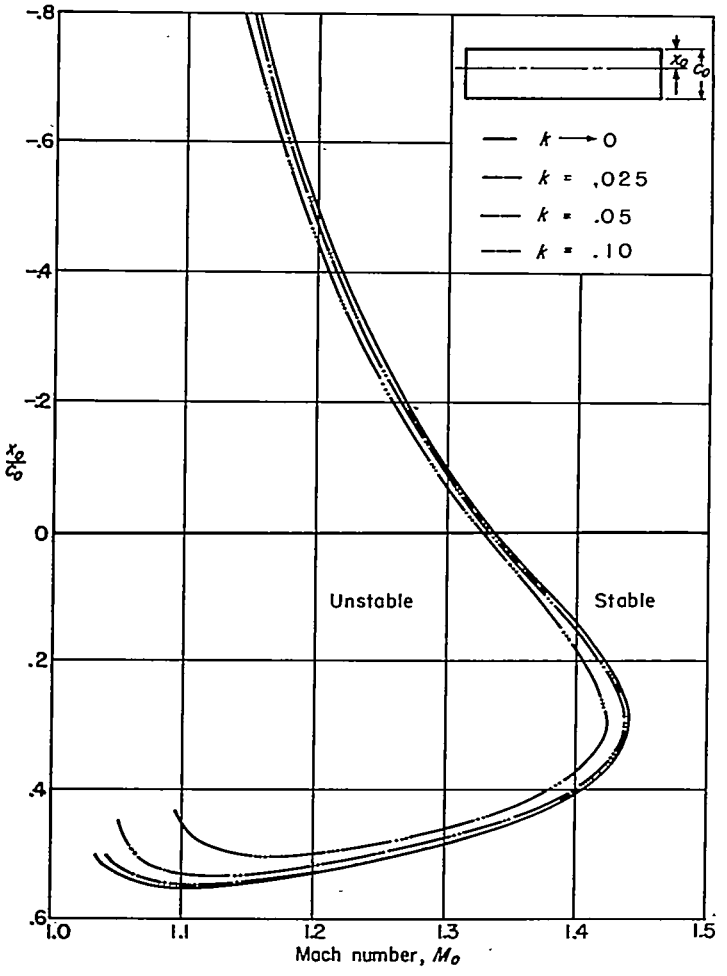

FIGURE 31.—Effect of frequency on the single-degree-of-freedom short-period pitching stability boundaries at supersonic speeds for a rectangular wing of aspect ratio 4.

small. We may therefore expect that increasing the frequency of oscillation has a stabilizing effect on the damping in pitch. This conjecture is substantiated in figures 30 and 31, where the supersonic stability boundary curves for aspect-ratio-4 triangular and rectangular wings are shown plotted for various reduced frequencies. These curves were obtained from calculations based on the results of references 15 and 16. Notice that for both wings the region of possible instability is diminished as the frequency is increased.

From the results of the analysis for supersonic speeds, we may further expect that the stabilizing effect of increasing the frequency will be of even more importance at subsonic speeds, for here the indicial variation $F_3(\varphi)$ dies out at

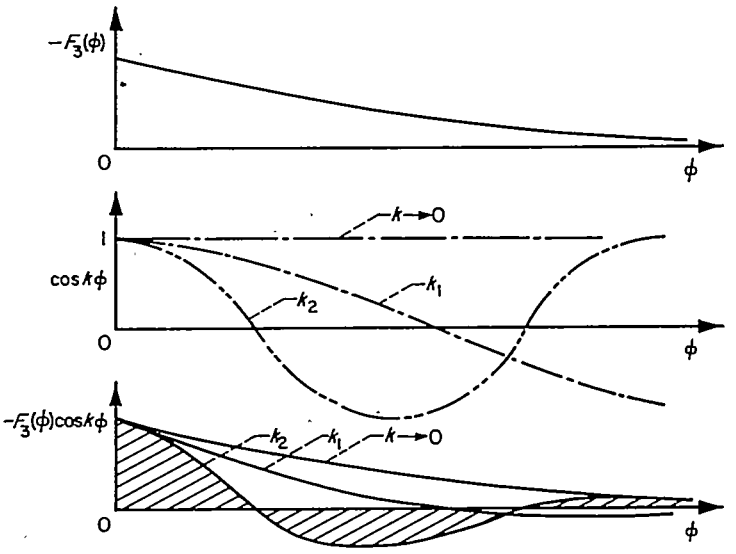

FIGURE 32.—Illustration of graphical integration procedure for finding effect of frequency at subsonic speed.

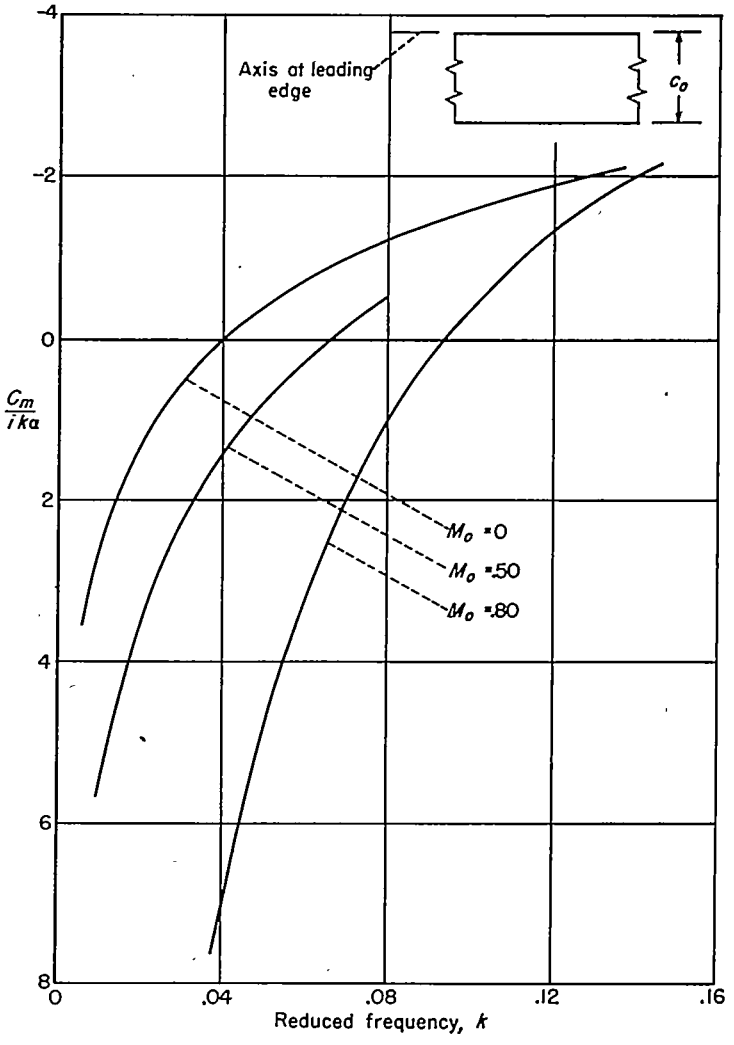

FIGURE 33.—Variation with reduced frequency of the single-degree-of-freedom rotary damping-moment coefficient for the two-dimensional wing at Mach numbers 0, 0.50, and 0.80. Axis at leading edge.

infinity. The half-period of oscillation is therefore always smaller than the time to reach steady state. The situation for the term $-\int_0^{\infty} F_3(\varphi)\cos k\varphi d\varphi$ is shown in figure 32.

It is evident in figure 32 that the destabilizing moment $-\int_0^\infty F_3(\varphi)\cos k\varphi d\varphi$ diminishes rapidly as the frequency is increased. The effect of this reduction on the damping in pitch can be illustrated by plotting the subsonic damping-moment coefficient against reduced frequency for the two-dimensional wing (with axis at the leading edge) for Mach numbers 0, 0.5, and 0.8. The results, which were obtained from reference 4, are shown in figure 33. It is seen in figure 33 that the large destabilizing effects of the moment contributions $-\int_0^\infty F_3(\varphi)\cos k\varphi d\varphi$ and $-k\int_0^\infty F_4(\varphi)\sin k\varphi d\varphi$ are confined to a relatively narrow range of reduced frequencies. Notice further in figure 33 that the range of frequencies for which instability is possible is small at $M_o=0$ $(0<k<0.04)$ and grows with increasing Mach number. This is believed to be the primary reason why unsteady lift effects were found to be unimportant at low speeds but are of great importance at speeds near the sonic speed.

PART II—WING-TAIL COMBINATIONS

In the historical development of the field of dynamic stability, there has been general agreement among researchers that for conventional tail-aft aircraft, the primary source of pitch damping is that provided by the tail. In fact, several early investigators concluded that the tail contribution was the only one of consequence and, hence, that the contributions of the wing and fuselage to the total damping in pitch could be neglected with little error (c. f., ref. (12)). It was also recognized that a major portion of the lift developed by the tail arose from the influence on the tail of the vorticity shed by the forward wing, and, in particular, that a finite time was required for this vorticity to reach the tail, thereby creating a lag in the development of tail lift behind the motion of the aircraft. These considerations led to the formulation of a simple tail damping factor which took into account the time lag in vorticity in terms of the configuration geometry and the effective angle of attack at the tail, and which alone proved to be adequate for predicting the dynamic-stability characteristics of low-speed aircraft.

It has already been shown in previous sections of this report that for higher speeds, the damping moment provided by the wing surface itself (and, analogously, the tail surface) can be highly significant. In subsequent sections the importance of the influence of the vorticity shed by the forward wing on the damping moment provided by the tail is reexamined. Again, the indicial-function concept is used, and proves to be of valuable assistance in illustrating the physical nature of the problem.

GENERAL CONSIDERATIONS

THE FOUR COMPONENTS

For each of the three harmonic motions considered earlier, the full frequency-dependent equations for the lift and moment developed for a single wing and their first-order in frequency counterparts are still applicable for a wing-tail combination, with the following reinterpretation of the indicial functions $C_{L_\alpha}(\varphi)$, $C_{m_\alpha}(\varphi)$, $C_{L_q}(\varphi)$, and $C_{m_q}(\varphi)$: each of the above functions must now be considered to represent the combined responses of the wing and tail plus interference effects between the wing and tail. Obviously, however, since the theory is linear, the combined function is equal to the sum of its components. In the general case, four such components for each of the indicial functions may be enumerated. These are listed below for the indicial function $C_{L_\alpha}(\varphi)$, that is, for the response in lift of the wing-tail combination to a step change in angle of attack of the combination.

(1) The response in lift of the forward wing to a step change in angle of attack of the forward wing, the tail being at zero angle of attack.

(2) The response in lift of the tail to a step change in angle of attack of the tail, the forward wing being at zero angle of attack.

(3) The response in lift of the tail to a step change in angle of attack of the forward wing, the tail being at zero angle of attack.

(4) The response in lift of the forward wing to a step change in angle of attack of the tail, the forward wing being at zero angle of attack.

The situation is entirely analogous for the other three indicial functions. It should be noted, however, that the components of the indicial functions due to pitching velocity, $C_{L_q}(\varphi)$ and $C_{m_q}(\varphi)$, must all be referred to the same axis of rotation. In the following discussion regarding the four components, the use of the indicial lift response to a step change in angle of attack for illustrative purposes is continued. It will be understood that the remarks apply as well to the other indicial functions.

For supersonic speeds, the component (1) is exactly equivalent to the response in lift of an isolated wing, and may be calculated on that basis, utilizing the theoretical results noted previously as applying in the supersonic speed range (refs. 3, 4, 5, and 6). Likewise, component (2) may be computed on the same basis. Furthermore, since at supersonic speeds, the disturbances created by the tail can never overtake the wing, component (4) is zero. There remains to consider, therefore, only component (3), for which there are as yet no theoretical solutions.

For subsonic speeds, as usual, the situation is more complicated. The component (1) is no longer rigorously equivalent to the lift response of an isolated wing, since the disturbances created by the wing by its own motion cause disturbances to be created at the tail which travel forward at the speed of sound, overtake the wing and, in turn, influence the development of lift on the wing. Likewise, the reverse situation exists for component (2), so that the response in lift of the tail is no longer that of an isolated tail. Further, component (4) is not zero, again by virtue of the fact that disturbances propagated at the tail are able to overtake the wing. For subsonic speeds, therefore, all four components require new solutions. It may be expected, however, that the secondary coupling effects between the wing and tail, as exemplified by component (4), are of small magnitude, and may usually be neglected. If it is assumed

that component (4) is zero, it is within the same order of approximation to assume that the coupling effects on components (1) and (2) are also zero, so that the subsonic interference problem is then reduced to the same form as that of the supersonic problem. In the interest of brevity, however, in what follows the subsonic case will not be considered, except to note that the general procedures to be undertaken for obtaining numerical solutions for the two-dimensional supersonic case would be the same for the subsonic case, albeit, considerably more complex.[8]

In the next section, therefore, an heuristic discussion is devoted to the remaining new function, component (3) for supersonic speeds; that is, the response in lift of the tail to a step change in angle of attack of the wing.

BOUNDARY CONDITIONS AT THE TAIL CORRESPONDING TO A STEP CHANGE IN ANGLE OF ATTACK OF THE WING

The boundary conditions corresponding to component (3) may be illustrated clearly by plotting as functions of time the traces of the wing and tail leading and trailing edges, and the traces of the sound waves emitted at the wing leading and trailing edge at the start of the motion. No sound waves are propagated at the tail at $t'=0$ since, under the conditions of the problem, the tail remains at zero angle of attack throughout the motion. The plot is shown in figure 34.[9]

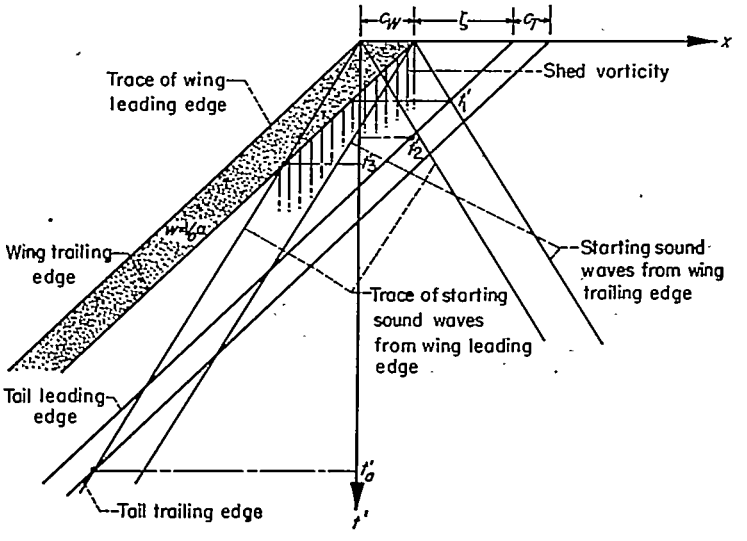

FIGURE 34.—Boundary conditions at tail corresponding to step change in angle of attack of wing.

It is clear from examination of figure 34 that at the start of the motion and until time t_1', the disturbances propagated at the wing as a consequence of the change in angle of attack have not signaled their presence to the tail. During this time interval, obviously no lift is developed by the tail. For time greater than t_1', the tail begins to penetrate the upwash field created by the vorticity shed by the forward wing, and thereby begins to develop positive lift on that portion of its surface which has penetrated the field. As time increases beyond t_2' the tail penetrates the field of shed vorticity itself and experiences combinations of both upwash and downwash on its surface. As the tail penetrates further into the field of vorticity, the region of downwash will predominate, so that it may be expected that the lift developed by the tail will eventually change from positive to negative. At time t_3' the wing has completed its build-up in lift which thereafter remains constant with time. The build-up in lift at the tail, however, continues until t_a', beyond which time the pressures on the tail are no longer influenced by the disturbances created by the wing at the start of the motion. For time greater than t_a', therefore, the lift on the tail remains constant with time and is equal in magnitude to the steady-state interference lift on a tail immersed in the nonuniform but steady downwash field created by the forward wing.

From the above qualitative considerations, one may anticipate that the variation with time of the interference lift of the tail in response to a step change in angle of attack of the wing will resemble the variation shown in figure 35.

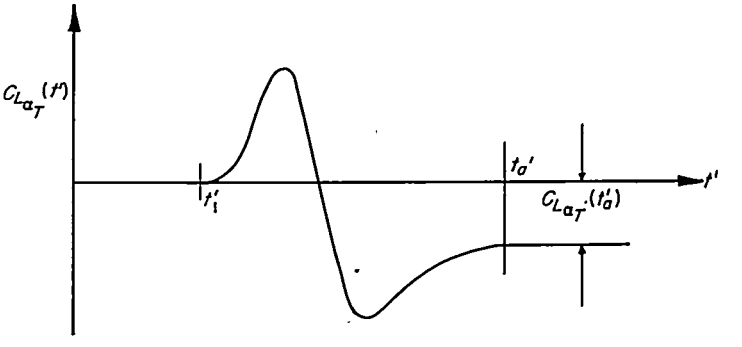

FIGURE 35.—Qualitative prediction of variation with time of tail lift response to step change in angle of attack of wing.

For wings and tails having straight trailing edges, the values of time t_1' and t_a' in figure 35 may be computed exactly from the geometric relationships shown in figure 34. They are,

$$t_1'=\frac{M_o\zeta}{V_o(1+M_o)}$$

$$t_a'=\frac{M_o(c_W+c_T+\zeta)}{V_o(M_o-1)} \tag{31}$$

Furthermore, theoretical solutions exist for the steady-state downwash behind wings of a wide variety of plan forms from which the final value of the interference lift $C_{L_{\alpha_T}}(t_a')$ may be computed. It remains, therefore, to fix with a greater degree of certainty the variation $C_{L_{\alpha_T}}(t')$ between t_1' and t_a'. In view of the paucity of information concerning the nature of this variation, the succeeding six sections of this paper are devoted to the development of theoretical techniques from which results for certain representative cases can be obtained.

THE TWO-DIMENSIONAL CASE

BOUNDARY CONDITIONS

Consider first the problem of calculating the growth in lift at supersonic speed on a tail surface of infinite span in response to a step change in angle of attack of a coplanar

[8] It is to be noted that Jones and Fehlner have treated the incompressible case (ref. 23) by a method very similar to that described in a subsequent section of this report entitled, "Application of Methods of Gust Analysis."

[9] It is implied in figure 34 that the wing and tail are coplanar or nearly coplanar surfaces. This restriction, while not a necessary one, is advisable from the standpoint of simplicity, and will hereinafter presumed to be in force.

forward surface, which is also of infinite span. This problem in two dimensions is chosen as a starting point since, here, use can be made of a valuable theorem; namely, that any unsteady-flow problem involving only two spatial dimensions can be related to and solved as an analogous problem in a supersonic three-dimensional steady flow. The basis for this statement can be made clear by a comparison of the governing linearized perturbation velocity potential equations referred to fixed-space axes for unsteady two-dimensional flow and steady three-dimensional supersonic flow. The former is written as,

$$\Phi_{xx}+\Phi_{zz}=\frac{1}{a_o^2}\Phi_{t't'} \tag{32}$$

and is transformed to the canonical form of the wave equation by the substitution $t=a_o t'$:

$$\Phi_{xx}+\Phi_{zz}=\Phi_{tt} \tag{33}$$

For the steady three-dimensional supersonic case, the potential equation is

$$\Phi_{yy}+\Phi_{zz}=\beta^2\Phi_{xx} \tag{34}$$

It is then apparent that simply by replacing x, y, and β in equation (34) by t, x, and 1, respectively, equation (34) can be made identical to equation (33). Thus, a solution to equation (34) for a Mach number of $\sqrt{2}$ ($\beta=1$) can likewise be taken as a solution to equation (33) with proper reinterpretation of the variables x, y, z. A complete development of this analogy can be found in references 3 and 4 along with several applications to problems of isolated wings. It suffices here simply to state that the theorem may be applied with equal validity to problems of wings in combination. In the light of this result, figure 34, which depicts the boundary conditions for the two-dimensional unsteady flow problem, takes on the following interpretation for the analogous three-dimensional steady-flow problem: the time axis becomes a spatial coordinate alined with the free-stream direction; the x axis becomes the spanwise coordinate, normal to the free-stream direction. The z axis is normal to the xt' plane and again is taken as positive downward. The traces of the wing and tail leading and trailing edges and the projections of their chords on the x axis become in the steady-flow problem the projections onto the xt' plane of the physical outlines of a pair of semi-infinite sweptback wings with tips normal to the free-stream direction. In the unsteady-flow problem the forward wing is caused to attain at $t'=0$ an angle of attack α which remains constant for all time thereafter. This boundary condition is interpreted in the analogous steady-flow problem to mean that a uniform normal velocity of magnitude $V_o\alpha$ exists everywhere over the surface of the forward wing. The traces of the sound waves which are emitted from this wing at $t'=0$ as a consequence of the change in angle of attack become in the steady supersonic problem the characteristic Mach lines which emanate from the foremost extremities of the wing. The rear wing, being at zero angle of attack in the unsteady problem, remains so in the analogous steady problem, and thus no Mach lines appear at the extremities of this wing in the steady-flow analogy. The procedure for calculating the lift at the tail in response to the change in angle of attack of the wing is then theoretically clear. By any of the known methods available in steady three-dimensional supersonic flow theory one computes in the region occupied by the tail the perturbation-velocity field caused by the presence of the forward lifting wing. In the plane of the tail surface, this field contributes a normal-velocity flow component which is canceled by the development of loading at the tail. A "spanwise" integration of the loading over the tail then yields the desired result — tail lift as a function of time.

SIMPLIFIED PROBLEM

The procedure outlined above in principle constitutes a straightforward exercise in the application of the three-dimensional linearized supersonic steady-flow theory. Unfortunately, in practice, the multiple integrations that arise in the course of the computations are exceedingly complex, and have thus far defied solution. These computations were therefore discontinued in favor of a simpler approach which, in itself, retains the essential nature of the problem and has the additional advantage of lending itself readily to extension and further refinement. The simplification consists of replacing the forward wing by a single two-dimensional vortex which, just as the wing, starts impulsively from rest at $t'=0$ and moves forward in the $z=0$ plane with constant supersonic velocity V_o. In addition, in satisfaction of the condition that a vortex cannot end in a fluid, there must be placed at the point of departure of the moving vortex, a stationary or starting vortex of equal and opposite strength.[10] It is well-known that the boundary conditions for a lifting surface may be satisfied by an appropriate distribution of vortices; thus the result to be obtained from this simplification may be viewed as a fundamental one in the sense that the solution to the original problem may in principle be recovered by an appropriate superposition of elementary solutions. A procedure for accomplishing this task is developed in a later section of this paper.

The boundary conditions for the simplified problem are illustrated in figure 36. Here, "true time" t' has been replaced by its spatial analog t, the relationship being $t=a_o t'$. The boundary condition for a closed vortex system is that the

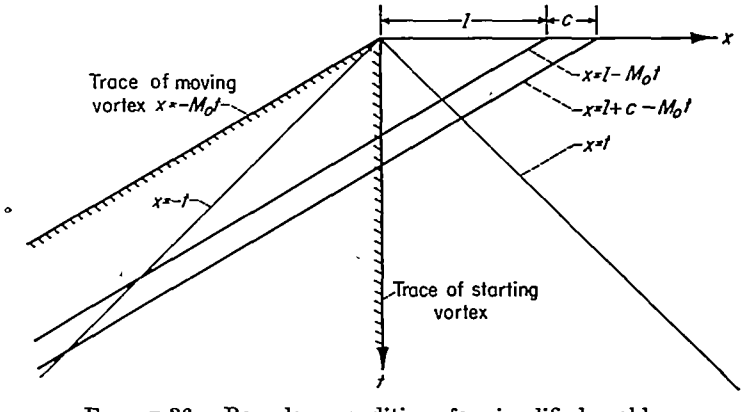

FIGURE 36.—Boundary conditions for simplified problem.

[10] The extremities of the moving and starting vortices must, in general, be connected by two trailing vortices to form the usual closed loop. However, for the two-dimensional problem, it is supposed that the trailing vortices are so far away from the centers of the moving and starting vortices that their effect on the flow there may be neglected.

jump in potential is a constant within the loop formed by the moving, starting, and trailing vortices. For the two-dimensional case this condition translates in figure 36 to the stipulation that the potential difference $\Delta\Phi$ across the $z=0$ plane be a constant within the shaded region bounded by the traces of the moving and starting vortices. The problem of calculating the induced velocity flow field associated with the vortex-pair may now be related to the analogous three-dimensional steady-flow problem; namely, that of calculating the induced flow field due to the presence in a supersonic stream of a yawed triangular wing, one edge of which is parallel to the free stream, the other being swept ahead of the Mach cone from the apex, and whose surface is warped in such a way that the potential difference across it is a constant. This problem has been solved by Lomax, Heaslet, and Fuller in reference 24, wherein it is found that the induced vertical velocity in the $z=0$ plane for supersonic speeds is given by the relation,

$$w(x,t)=M_o\frac{\Delta\Phi}{2\pi}\frac{\sqrt{t^2-x^2}}{x(x+M_o t)},\quad -t\leq x\leq t \tag{35}$$

Thus, the problem of calculating the lift at the tail in response to the step change in angle of attack of the forward wing has now been reduced to one which can be stated in terms of the steady-state analogy as follows: Find the section lift as a function of t on the semi-infinite sweptback plan form shown in figure 36 which rests at zero angle of attack in a supersonic stream and which is subjected to a vertical-flow distribution given by equation (35) on that portion of its surface lying within the region $-t\leq x\leq t$.

METHOD OF SOLUTION

The problem stated above may be solved by any of a number of methods available in steady supersonic flow theory. One that immediately suggests itself, however, by the conical nature of equation (35) is the method of superposition of elementary sectors. If in equation (35) the substitution is made, $a=x/t$, we get,

$$w(a,x)=M_o\frac{\Delta\Phi}{2\pi}\frac{\sqrt{1-a^2}}{x(a+M_o)},\quad -1\leq a\leq 1 \tag{36}$$

The quantity a of course, defines a ray emanating from the origin of the xt coordinate system, and by equation (36) it is seen that along a given ray, the normal velocity varies inversely as x. Then if the normal-velocity distribution is decomposed into infinitesimal steps of magnitude dw along rays from the origin, it can be specified that within each semi-infinite sector of the tail formed by the tail leading and trailing edges and a ray from the origin, the normal velocity over the sector varies only as $\frac{k}{x}$, where k is a constant for the sector, given by,

$$k=\frac{d}{da}\left[M_o\frac{\Delta\Phi}{2\pi}\frac{\sqrt{1-a^2}}{(a+M_o)}\right]da=\psi'(a)da. \tag{37}$$

It is then a relatively simple problem to solve for the loading on a single sector caused by the normal-velocity distribution $\frac{1}{x}$, and thence by the superposition of elementary solutions, to find the loading and integrated loading caused by the given normal-velocity distribution. This superposition procedure is briefly outlined in the following paragraph.

The boundary conditions for an elementary sector formed by an arbitrary ray a are illustrated in figure 37.

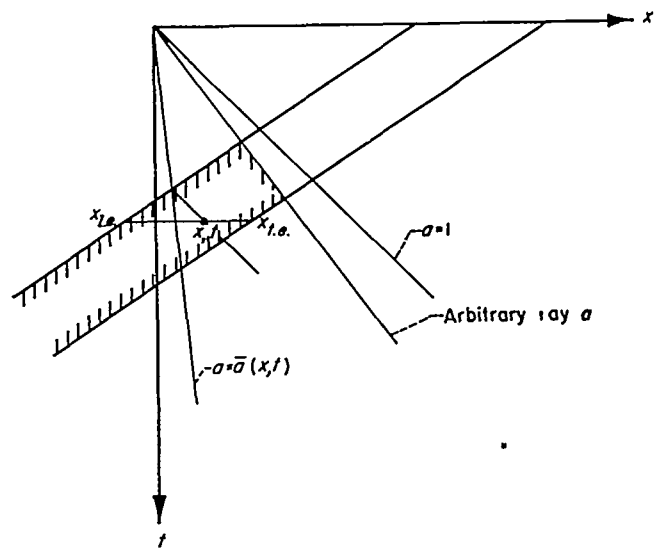

FIGURE 37.—Boundary conditions for elementary sector.

Within the shaded region shown in the figure the normal velocity varies as $\frac{1}{x}$; elsewhere on the plan form it is zero. Presuming now that the loading coefficient $\frac{\Delta p}{q_o}(x,t,a)$ at the point x,t for the elementary sector has been calculated, it is desired to sum the effects of all sectors that influence the loading at the fixed point. A contribution to the loading at the point x,t will be made by each sector within whose zone of influence the point lies. As seen on figure 37 this region extends from the sector defined by the ray $a=1$ to that sector whose trailing Mach line from the apex of the sector passes through the point. On figure 37 this sector is defined by the ray $a=\bar{a}(x,t)$. The total loading at x,t is then expressed by the formula

$$\frac{\Delta p}{q_o}(x,t)=\int_1^{\bar{a}(x,t)}\psi'(a)\frac{\Delta p}{q_o}(x,t,a)\,da+\psi(1)\frac{\Delta p}{q_o}(x,t,1) \tag{38}$$

where $\psi(a)$ is given by equation (37) and $\frac{\Delta p}{q_o}(x,t,a)$ is the loading coefficient at a point on the elementary sector due to a normal-velocity distribution $\frac{1}{x}$. The second term in equation (38) accounts for the effect of a possible jump in w at the ray $a=1$. However, in the present problem, $\psi(1)$ is zero so that this term disappears. The section lift at the station t is then found simply by an integration of the loading in the x direction,

$$c_l(t)=\frac{1}{c}\int_{x_{l.e.}}^{x_{t.e.}}\frac{\Delta p}{q_o}(x,t)\,dx=\frac{1}{c}\int_{x_{l.e.}}^{x_{t.e.}}\int_1^{\bar{a}(x,t)}\psi'(a)\frac{\Delta p}{q_o}(x,t,a)\,da\,dx \tag{39}$$

There remains to discuss the calculation for the sector

loading $\frac{\Delta p}{q_o}(x,t,a)$ at the fixed point x,t. This calculation, however, involving as it does a wing having all supersonic edges, is straightforward and does not require elaboration. An interesting sidelight arising as a result of this work was the discovery that the loading is zero at a point on the sector whose forecone includes only the sector leading edge and intersects the line $x=0$.

The section lift was found to vary in form in each of the five time intervals designated in figure 38.

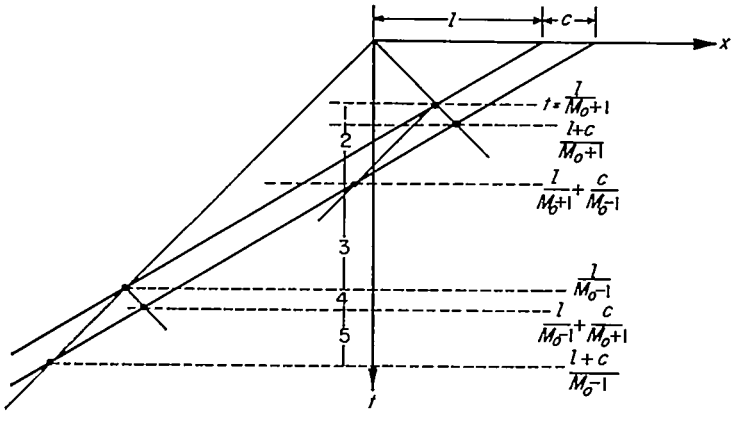

FIGURE 38.—Regions used in analysis of lift response of two-dimensional tail.

Unfortunately, difficulties of integration prevent the presentation of solutions in closed form for the section lift in all but the first time interval. It was always possible, however, to reduce the integrals to single quadratures, so that numerical or graphical methods can be employed to obtain results for specific cases. The results in integral form for the section lift in the intervals 1 to 5 are somewhat lengthy and therefore are presented in Appendix A.

DISCUSSION

In order to illustrate the nature of the result, the variation of section lift at the tail with "time" t has been computed for the following case: a tail of unit chord, tail length l of 3.2 units, and Mach number 1.7. The result is shown on figure 39, together with a sketch of the boundary conditions corresponding to the particular case under study.

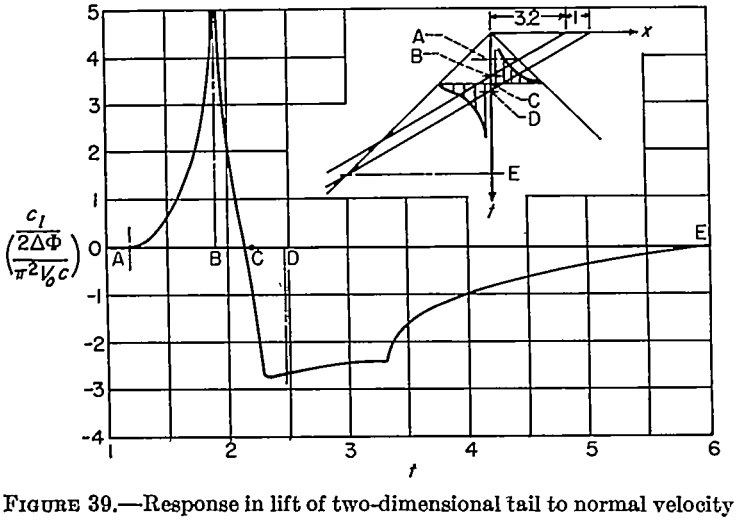

FIGURE 39.—Response in lift of two-dimensional tail to normal velocity of two-dimensional vortex system. $M_o=1.7$.

It is to be noted first in figure 39 that the section lift becomes infinite when the leading edge of the tail reaches the position of the starting vortex ($t=B$ in fig. 39). This is not unexpected, since at the instant before the leading edge penetrates the vortex there exists on the tail an infinity in upwash; whereas just after the penetration the effect of the infinity in upwash is just canceled by an opposite effect caused by the infinity in downwash. It is interesting to observe, however, that a like result does not occur as the tail trailing edge leaves the position of the starting vortex ($t=D$). This can be explained by noting that the sound wave emitted when the leading edge penetrates the starting vortex serves to broadcast the existence of the infinite discontinuity in normal velocity over a finite region of the tail. The distribution of the effect of the discontinuity thereby modifies its influence at any one point. Next, observe that the lift changes sign at $t=C$, which is very closely the time when the tail chord is situated symmetrically with respect to the starting vortex. As can be seen on the figure, the tail chord experiences very nearly equal amounts of upwash and downwash at this time. Finally, note that at $t=E$ the lift on the tail disappears as the tail moves completely beyond the region of disturbances created by the moving vortex at $t=0$. This fact is consistent with the statement made earlier that the final value of the lift on the tail should be that due to the steady-state downwash field of the forward wing, for the downwash behind a moving two-dimensional vortex in steady supersonic flow is zero. It is instructive to remember that the same fact is true for the lifting two-dimensional wing in a steady supersonic flow, so that no inconsistency arises from this source by a superposition of solutions of the type shown in figure 39 as a closer approximation of the response of the tail to a step change in angle of attack of the forward wing. The development of such a procedure will be outlined in a later section of this paper.

APPLICATION OF METHODS OF GUST ANALYSIS

It will no doubt have been noted by the reader that the subject of inquiry in the preceding section, namely, the problem of calculating the growth in lift at the tail caused by its penetration of a region of disturbed flow created by a forward lifting wing, bears in many respects a marked resemblance to another more familiar problem. That problem is the calculation of lift on a wing which penetrates a gust of prescribed spacewise normal velocity distribution. Indeed, the two problems are identical with one exception: in the gust problem it is generally assumed that the normal velocity of the gust at each station in space remains constant with time; whereas in the wing-tail interference problem this is not the case. If it can be shown in the wing-tail problem, however, that at each station in space the variation of normal flow velocity with time can be safely ignored during the time interval required for the tail to pass the station, then the use of a gust-type analysis is valid, and an important advantage accrues. One can then calculate in a relatively simple manner the growth of interference lift on any tail surface for which the response in lift to a sharp-edged gust of uniform intensity is known. The so-called gust-function has been calculated for the two-dimensional case (ref. 3), the rectangular plan form (ref. 6), and the triangular plan form having

supersonic edges (ref. 5). Thus, although it is still necessary to retain the two-dimensional nature of the downwash field created by the forward wing, the gust analysis, if valid, provides a means whereby two important classes of three-dimensional tail surfaces can be treated. The object of this section will therefore be to investigate the validity of the use of a gust-type analysis in place of an exact analysis.

The extent of the approximation involved in the gust-type analysis can be best visualized in the two-dimensional case. Further, since the exact solution for this case has been obtained in the preceding section, a comparison of the two results provides a means of assessing the magnitude of the error introduced by the approximation to the flow. Compare first, then, the boundary conditions at the two-dimensional tail for the exact and approximate cases. On figure 40 these conditions are shown schematically for the Mach number, tail chord c, and tail length l which correspond to the numerical results given in figure 39 of the preceding section. For the exact case, the normal velocity at the tail is seen to vary inversely as x or t along rays from the original position of the moving vortex. For the approximate case, we fix the correct variation of normal flow velocity at the tail leading edge and require that at each station x the normal velocity existing at the leading edge remains the same for all time thereafter. It then is clear from inspection of figure 40 that at least for the particular conditions chosen for study, the differences in normal velocity experienced by the tail for the two cases are not excessive.

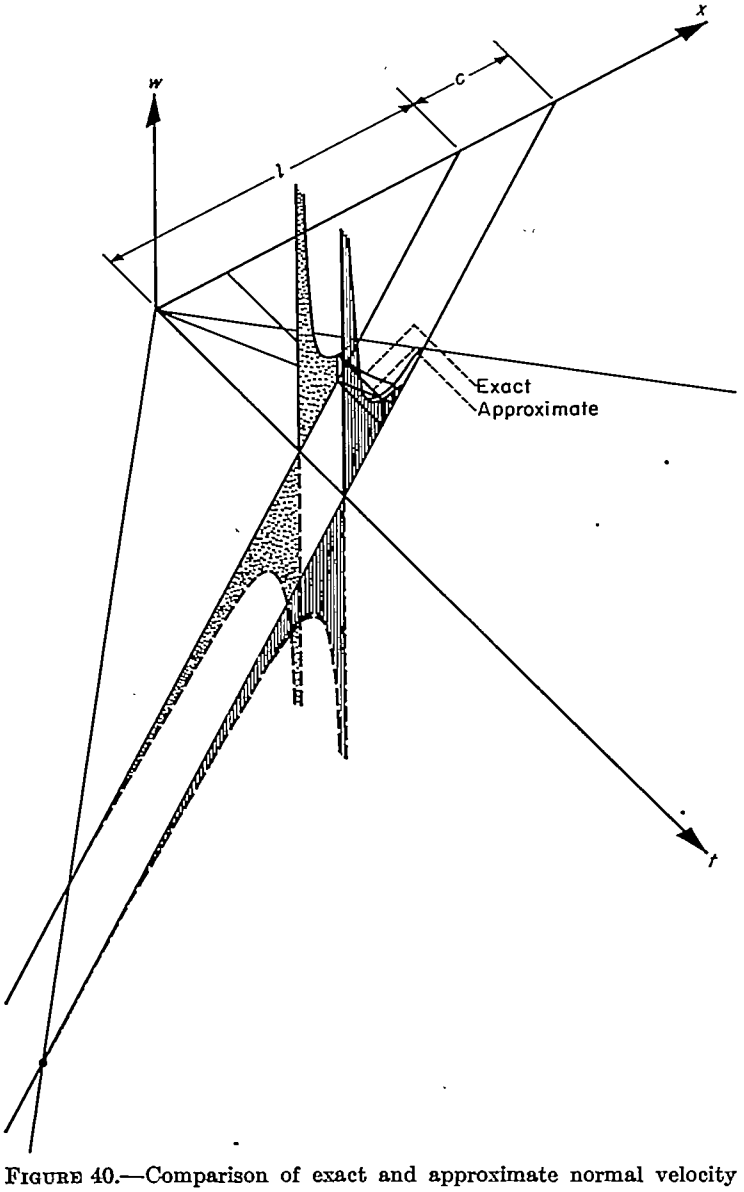

FIGURE 40.—Comparison of exact and approximate normal velocity distributions at the tail location.

By virtue of the approximation, which fixes with respect to time the normal flow velocity at each station in space, the problem of calculating the lift at the tail is reduced simply to a superposition procedure entirely analogous to that already described in the first part of this report for the case of a wing performing arbitrary maneuvers. Here, however, rather than responding to a series of step changes in angle of attack or pitching velocity, the tail responds to a series of sharp-edged gusts, so that the Duhamel integral, expressing lift at the tail as a function of time is written as,

$$C_L(t)=\frac{d}{dt}\int_0^t \frac{C_{L_g}}{1(w/V_o)}(\tau)\,\frac{w}{V_o}(t-\tau)\,d\tau \tag{40}$$

In equation (40) the quantity $\frac{C_{L_g}}{1(w/V_o)}(\tau)$ is the gust function for the two-dimensional surface, given in reference 3, and $w(t)$ is the variation of normal flow velocity experienced by the tail leading edge. Substituting $x=l-M_o t$ in equation (35),

$$w(t)=M_o\,\frac{\Delta\Phi}{2\pi}\,\frac{\sqrt{t^2-(l-M_o t)^2}}{l(l-M_o t)} \tag{41}$$

With the use of equations (40) and (41) and the results of reference 3 the interference lift at the tail may be computed in a straightforward manner. As in the exact problem, however, integration difficulties prevent the presentation of a solution in closed form in all but the first time interval $\frac{l}{M_o+1}\leq t\leq\frac{l+c}{M_o+1}$. The solution in quadrature form is given in Appendix B. These results have been utilized to compute the variation of tail lift with time for the same set of conditions chosen in the preceding section, namely; Mach number 1.7, tail chord of unit length, and tail length of 3.2 units. Results of these computations are compared with the exact results in figure 41.

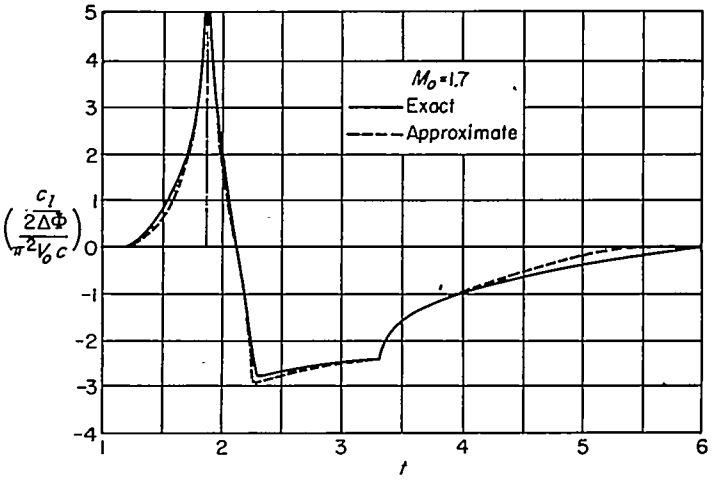

FIGURE 41.—Comparison of exact and approximate tail lift responses. $M_o=1.7$.

It is readily apparent from inspection of figure 41 that at least for the conditions chosen, the gust-type analysis provides an excellent approximation of the variation of tail lift with time over the entire time interval, $\frac{l}{M_o+1} \leq t \leq \frac{l+c}{M_o-1}$. We may therefore proceed to the three-dimensional cases with reasonable expectation that the solutions resulting from the gust approximation will be of acceptable accuracy — again, at least for sets of boundary conditions corresponding to those used above.

The analysis for the rectangular and triangular tail plan forms proceeds exactly as that for the two-dimensional case just discussed. For the rectangular plan form, in fact, the two-dimensional solution constitutes a major part of the total lift, and it is only necessary to add to the results given above the contribution of the tail tip regions. The gust function for the tip regions of the rectangular plan form is presented in reference 6 and is of such simple form that the integration of equation (40) may be done quite easily. Not so for the triangular plan form (ref. 5); for this case graphical or numerical techniques are again necessary to obtain results for specific cases. Solutions for both the tip regions of the rectangular tail and for the triangular tail are given in Appendix B. Numerical results, illustrating the nature of the solutions, are given in figure 42. The boundary conditions for these results have been chosen to be identical to those picked for the two-dimensional results of figures 39 and 41, so that the results of figure 42 for the rectangular tip regions may be directly added to those of figure 41 to give the total lift for the rectangular tail. Note in figure 42 that aspect ratio A appears simply as a multiplying factor, so that these results are applicable for tails of any aspect ratio, subject only to the limiting conditions prescribed in the figure. The condition on the rectangular tail insures that the Mach line from one edge does not intersect the opposite edge; that on the triangular tail insures that the leading edge is supersonic. Note also in figure 42 that unlike the case of the two-dimensional tail, no infinity appears in either the lift contribution of the rectangular tip regions or the lift of the triangular tail when the tail first penetrates the position of the starting vortex. This, of course, is attributable to the fact that the first penetration in either case is made by a surface of infinitesimal span.

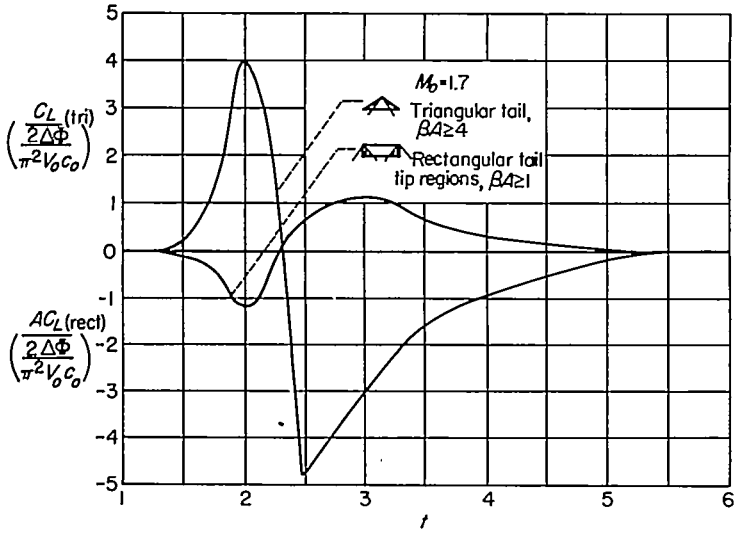

FIGURE 42.—Approximate response in lift of wide triangular tail and tip regions of rectangular tail to normal velocity of two-dimensional vortex system. $M_o=1.7$.

APPLICATION OF STRIP THEORY

In the preceding section it was shown that approximate response functions could be obtained for those three-dimensional tail surfaces for which the indicial gust function was known. There is still another method by which the responses of certain other classes of three-dimensional tail surfaces may be derived, and that is by the use of strip theory.[11] It has been shown by a number of authors (refs. 4, 25, and 26) that the use of strip theory is exact in calculating the lift, pitching moment, and rolling moment of surfaces having all supersonic edges and straight trailing edges normal to the free-stream direction. Further, no restriction need be placed on the generality of the normal-flow-velocity distribution encountered by these plan forms. Thus, for example, in the present connection, the lift on the wide triangular tail in response to either the two-dimensional or three-dimensional vortex field can be computed exactly if the responses of the two-dimensional tail to these fields are known.

When restrictions are placed on the nature of the normal-flow-velocity field, still other types of plan forms may be treated without approximation by the use of strip theory. An obvious example is the response of the apex-rearward wide triangular tail to the two-dimensional vortex field. Clearly, since the loading at no point on the tail can be influenced by disturbances from the edges of the tail, the integrated lift at every section is just the lift on a two-dimensional tail having the same tail length and chord as the section. The same would be true for any tail having supersonic edges and a straight leading edge normal to the stream direction, so long as the normal flow velocity is invariant with the spanwise direction.

As simple examples of the use of strip theory in the present problem, formulas will be developed from which the exact responses in lift of apex-forward and apex-rearward triangular tails to the two-dimensional vortex field may be obtained. Consider first, however, the more general plan form pictured in figure 43, in which the dimension l is defined as the distance between the moving vortex and the foremost point of the tail, and the xy coordinate system is fixed in space.

The use of strip theory (which, it should be cautioned, is not exact for the plan form shown in fig. 43) enables one to formulate immediately the lift on the finite-span tail in terms of the two-dimensional response as follows:

$$C_L(t)=\frac{2}{S}\int_o^{b/2} dy \int_{l.e.(y,t)}^{t.e.(y,t)} \left(\frac{\Delta p}{q_o}\right)_2 (x, t; y)\, dx \qquad (42)$$

where $\left(\frac{\Delta p}{q_o}\right)_2 (x,t\,;y)$ denotes the loading at a point on a two-dimensional tail which is subjected to the same normal flow velocity variation as a section $c(y)$ of the three-dimensional tail. The inner integral in equation (42) is recognized, however, as being just the two-dimensional section lift

[11] The term "strip theory" is used here in its usual sense; that is, the integrated lift at a spanwise station of the three-dimensional surface is assumed to be the same as that on a two-dimensional surface having the same chord length and undergoing the same motion.

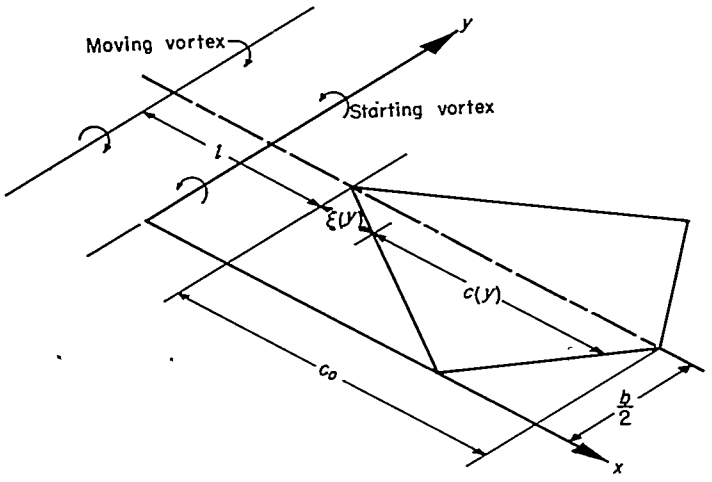

FIGURE 43.—Definition of notation used in strip theory analysis.

coefficient multiplied by the local chord $c(y)$, so that equation (42) becomes,

$$C_L(t)=\frac{2}{S}\int_o^{b/2} c(y)c_l(l+\xi(y),\, c(y),\, t)\,dy \tag{43}$$

where the quantities $l+\xi(y)$, $c(y)$ replace l and c, respectively, in the two-dimensional-tail lift response previously derived. The formulas for the apex-forward and apex-rearward triangular tails are simply special cases of equation (43). For the former case, $c(y)$ is given by $\frac{2c_o}{b}y$, and after a change in variables, $y=\frac{b}{2}\eta$, equation (43) becomes,

$$C_L(t)=2\int_o^1 \eta c_l(l+c_o(1-\eta),\, \eta c_o,\, t)\,d\eta \tag{44}$$

For the apex-rearward triangular tail, $\xi(y)$ is zero, so that,

$$C_L(t)=2\int_o^1 \eta c_l(l,\eta c_o,t)\,d\eta \tag{45}$$

Equations (44) and (45) have been utilized, together with the results for the two-dimensional-tail lift response to compute the responses in lift of apex-forward and -rearward triangular tails to the two-dimensional vortex field. Results in integral form are given in Appendix C, and numerical results for tails of unit chord, tail length 3.2 units, at Mach number 1.7, are shown on figure 44.

The result for the apex-forward triangular tail is compared with the approximate result derived for this wing in the previous section by use of a gust-type analysis. Again, as in the two-dimensional case, it is evident that the gust-type analysis provides an accurate estimate of the tail lift response over the entire time range, $\frac{l}{M_o+1}\leq t\leq\frac{l+c_o}{M_o-1}$.

SUPERPOSITION OF ELEMENTARY SOLUTIONS

It has already been noted in a previous section that the response in tail lift to the normal-velocity field created by a single vortex loop could be viewed as a fundamental result in this sense: The solution can, in principle, be used as the elementary function in a superposition procedure designed to determine the response in lift of the tail to the normal

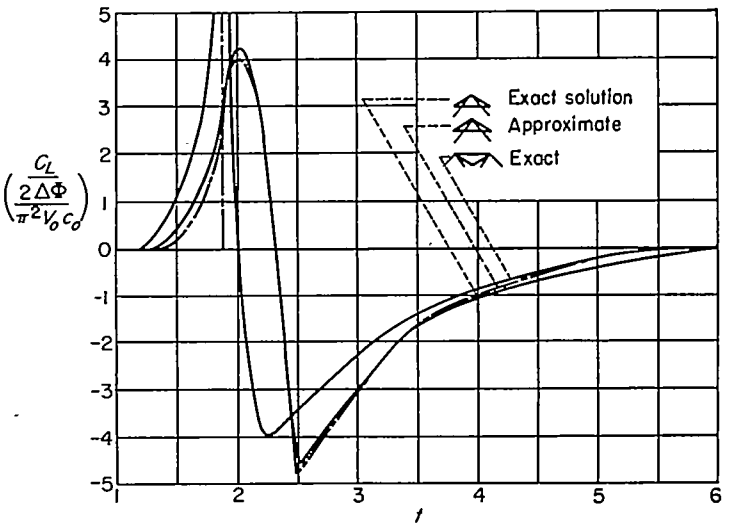

FIGURE 44.—Exact response in lift of apex-forward and apex-rearward wide triangular tail to normal velocity of two-dimensional vortex system. $M_o=1.7$.

velocity field created by a forward wing of finite chord. In this section a procedure for accomplishing this end is developed and the result of the analysis applied to a special case. For the sake of simplicity, the analysis is again restricted to one dealing with two-dimensional forward surfaces, so that the normal-velocity field encountered by the tail is uniform in the spanwise direction. However, no restriction is placed on the span of the tail.

In the previous sections solutions have been obtained for the lift at the tail in response to a single vortex pair. The boundary conditions for the vortex pair are exhibited in the xt plane as a triangular sector having a uniform potential difference $\Delta\Phi$ within the sector (see fig. 36). We wish now to distribute these sectors over the region traced out in the xt plane by the forward wing and its wake in such a way as to build up the variation of $\Delta\Phi$ in these regions corresponding to prescribed normal-velocity patterns over the wing. The sum of the responses in lift of the tail to each of these slabs of $\Delta\Phi$ is then the response to the normal-velocity field created by the wing. It is convenient to treat the effects of the wing and wake separately, and we consider the wing first. Place a vortex pair at an arbitrary chordwise position of the wing with origin at $t=0$. The response in lift at the tail to the single vortex pair is a function of time t and a characteristic distance, chosen to be the distance μ between the moving vortex and the tail leading edge. This of course is the solution derived previously with l replaced by μ. Now place another vortex pair of opposite strength with origin at the same position in space as the first pair, but shifted an incremental time $\Delta\eta$ later. As shown in figure 45 there remains a strip of chord $M_o\Delta\eta$ having unit $\Delta\Phi$ within the strip.

The response in lift at the tail to the remaining strip at a fixed time t is,

$$\Delta C_L(\mu,\, t)=C_L(\mu,\, t)-C_L(\mu-M_o\Delta\eta,\, t-\Delta\eta) \tag{46}$$

Letting the changes in μ and t approach zero, equation (46) may be cast in the form of the directional derivative,

$$\frac{\Delta C_L}{\Delta\eta}(\mu,\, t)=M_o\frac{\partial C_L}{\partial\mu}(\mu,\, t)+\frac{\partial C_L}{\partial t}(\mu,\, t) \tag{47}$$

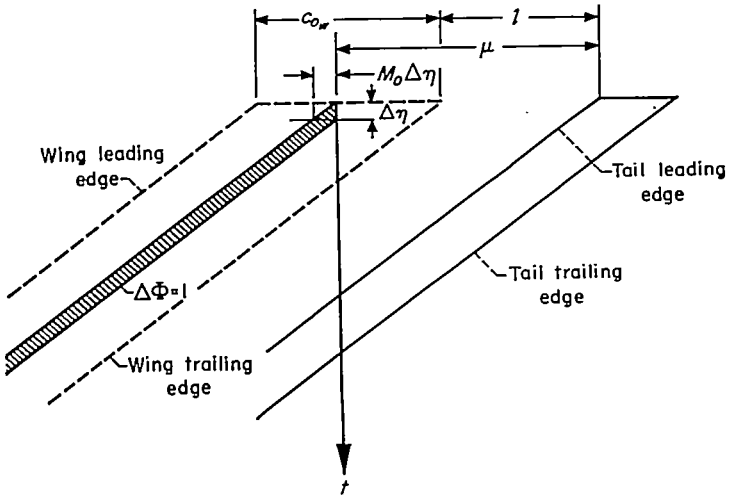

FIGURE 45.—Boundary conditions for response in lift of tail to an elementary strip of unit $\Delta\Phi$.

This is the response in lift to a strip of unit $\Delta\Phi$ situated a distance μ from the tail. The response to any other strip starting at a later time but at the same distance μ from the tail will of course be identical to this result. We may therefore build up the response to an arbitrary variation of $\Delta\Phi$ in the strip simply by use of the Duhamel integral; that is,

$$\frac{\Delta C_L}{\Delta\eta}(\mu, t)=\frac{d}{dt}\int_o^t\left[M_o\frac{\partial C_L}{\partial\mu}(\mu, t-t_1)+\frac{\partial C_L}{\partial(t-t_1)}(\mu, t-t_1)\right]\Delta\Phi(\mu, t_1)\,dt_1 \tag{48}$$

Let $t-t_1=\tau$, and perform the indicated differentiation, noting from physical considerations that $\Delta\Phi(\mu, 0)=C_L(\mu, 0)=0$.

$$\frac{\Delta C_L}{\Delta\eta}(\mu, t)=\int_o^t\left[M_o\frac{\partial C_L}{\partial\mu}(\mu, \tau)+\frac{\partial C_L}{\partial\tau}(\mu, \tau)\right]\Delta\dot{\Phi}(\mu, t-\tau)\,d\tau \tag{49}$$

The influence of the wing on the lift at the tail is then obtained simply by a summation of incremental strips as μ goes from l to $l+c_{o_w}$. Note that the increment $\Delta\mu$ is $M_o\Delta\eta$.

$$C_L(t)_{WING}=\int_l^{l+c_{o_w}}\frac{d\mu}{M_o}\int_o^t\left[M_o\frac{\partial C_L}{\partial\mu}(\mu, \tau)+\frac{\partial C_L}{\partial\tau}(\mu, \tau)\right]\Delta\dot{\Phi}(\mu, t-\tau)\,d\tau \tag{50}$$

Now consider the influence of the wake. The potential difference $\Delta\Phi$ in the wake has the characteristic that at each station in space the $\Delta\Phi$ existing at the trailing edge of the wing remains the same for all time thereafter. The distribution of $\Delta\Phi$ in the wake may therefore be built up by elementary vortex pairs whose origins are placed at the trailing edge of the wing. Since these elementary sectors are all the same distance l from the tail, the response in lift at the tail to each of the sectors is of the same form, and the sum of these responses at a fixed time t may again be found by use of the Duhamel integral,

$$C_L(t)_{WAKE}=\frac{d}{dt}\int_o^t C_L(l, \tau)\Delta\Phi(l, t-\tau)\,d\tau$$

$$=\int_o^t C_L(l, \tau)\Delta\dot{\Phi}(l, t-\tau)\,d\tau \tag{51}$$

The sum of equations (50) and (51) is then the desired response in lift at the tail to a prescribed $\Delta\Phi$ distribution on the forward wing.

$$C_L(t)=\int_l^{l+c_{o_w}}d\mu\int_o^t\left[\frac{\partial C_L}{\partial\mu}(\mu, \tau)+\frac{1}{M_o}\frac{\partial C_L}{\partial\tau}(\mu, \tau)\right]\Delta\dot{\Phi}(\mu, t-\tau)d\tau+$$

$$\int_o^t C_L(l, \tau)\Delta\dot{\Phi}(l, t-\tau)d\tau \tag{52}$$

We consider next a special case for which the form of equation (52) may be simplified considerably. For this case the loading on the forward wing is prescribed to be uniform in the chordwise direction and to remain constant with time. The specified boundary condition may be interpreted either as the exact case for a forward wing which starts to deform at $t=0$ in such a way as to give rise to a uniform loading over its surface, or as an approximation to the response of a flat forward wing to a step change in normal velocity over its surface. It is the latter case which is of real interest here, and of course the approximation introduces some error into the variation of $\Delta\Phi$ on the wing and in the wake. However, as can be seen on figure 46, a comparison of the exact and approximate $\Delta\Phi$ distributions shows that the differences between the two are not great for the case chosen, and would be even smaller for higher Mach numbers. It is expected that the approximation should yield acceptable results for Mach numbers greater than about 1.4.

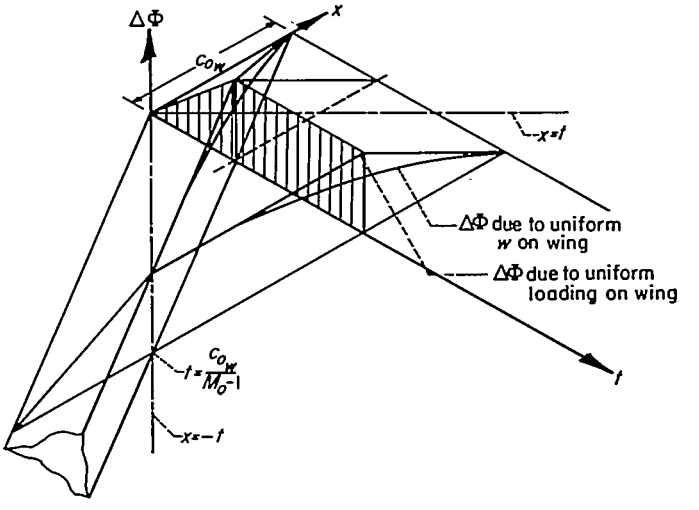

FIGURE 46.—Comparison of distributions of $\Delta\Phi$ for two-dimensional wing and wake due to uniform loading and uniform normal velocity on wing.

The prescription of uniform loading on the forward wing is seen on figure 46 to amount to the following conditions on $\Delta\Phi$ on the wing:

$$\begin{aligned}\Delta\Phi(\mu,t)&=kt \qquad 0\le t\le\bar{t}\\ &=k\bar{t} \qquad t\ge\bar{t}\end{aligned} \tag{53}$$

where

$$\bar{t}=\frac{l+c_{o_w}-\mu}{M_o}.$$

It follows that the condition on $\Delta\Phi$ along the trailing edge of the wing must be,

$$\Delta\Phi(l,t)=kt \qquad 0<t<\frac{c_{o_w}}{M_o}$$

$$=k\frac{c_{o_w}}{M_o} \qquad t\geq\frac{c_{o_w}}{M_o} \tag{54}$$

Performing the required differentation of $\Delta\Phi$ with respect to $(t-\tau)$ and substituting in equation (52), we get

$$C_L(t)=k\int_l^{l+c_{o_w}}d\mu\int_{t-\bar{t}}^{t}\left[\frac{\partial}{\partial\mu}C_L(\mu,\tau)+\frac{1}{M_o}\frac{\partial C_L}{\partial\tau}(\mu,\tau)\right]d\tau+$$
$$k\int_{t-\frac{c_{o_w}}{M_o}}^{t}C_L(l,\tau)d\tau \tag{55}$$

(I_1 and I_2 mark the two integrals)

The inner integral I_2 in equation (55) may be evaluated immediately and gives

$$\frac{1}{M_o}I_2=\frac{1}{M_o}C_L(\mu,t)-\frac{1}{M_o}C_L(\mu,t-\bar{t}) \tag{56}$$

For the inner integral I_1, we make use of the definition for the differentiation of a definite integral, that is,

$$\int_{t-\bar{t}}^{t}\frac{\partial}{\partial\mu}C_L(\mu,\tau)d\tau=\frac{\partial}{\partial\mu}\int_{t-\bar{t}}^{t}C_L(\mu,\tau)d\tau-C_L(\mu,t)0+\frac{1}{M_o}C_L(\mu,t-\bar{t}) \tag{57}$$

Substituting equations (56) and (57) in equation (55) we have,

$$C_L(t)=k\int_l^{l+c_{o_w}}d\mu\left[\frac{\partial}{\partial\mu}\int_{t-\bar{t}}^{t}C_L(\mu,\tau)d\tau+\frac{1}{M_o}C_L(\mu,t)\right]+k\int_{t-\frac{c_{o_w}}{M_o}}^{t}C_L(l,\tau)d\tau \tag{58}$$

Let

$$\int_{t-\bar{t}}^{t}C_L(\mu,\tau)d\tau=F(\mu,t)$$

Then in equation (58)

$$\int_l^{l+c_{o_w}}\frac{\partial}{\partial\mu}F(\mu,t)d\mu=F(\mu,t)\Big|_l^{l+c_{o_w}}=$$
$$\int_t^{t}C_L(l+c_{o_w},\tau)d\tau-\int_{t-\frac{c_{o_w}}{M_o}}^{t}C_L(l,\tau)d\tau \tag{59}$$

Substituting equation (59) in (58) there remains only,

$$C_L(t)=\frac{k}{M_o}\int_l^{l+c_{o_w}}C_L(\mu,t)d\mu \tag{60}$$

This result may be easily verified by interpreting the integral in equation (60) physically. The integral specifies that we sum the effects of elementary sectors, all of the same strength in $\Delta\Phi$, and whose origins are at $t=0$ within the boundaries of the wing leading and trailing edges. A graphical summation of several such sectors will show they do indeed build up the $\Delta\Phi$ distribution over the wing and wake prescribed in figure 46.

Equation (60) has been utilized along with the results of the previous sections for $C_L(\mu,t)$ for the two-dimensional tail and the rectangular tail tip regions to approximate the response of the tail to a step change in angle of attack of a forward surface of finite chord. Results of computations for a wing chord of 2 units, tail chord of 1 unit, tail length l of 3.2 units, and Mach number 1.7 are shown in figure 47.

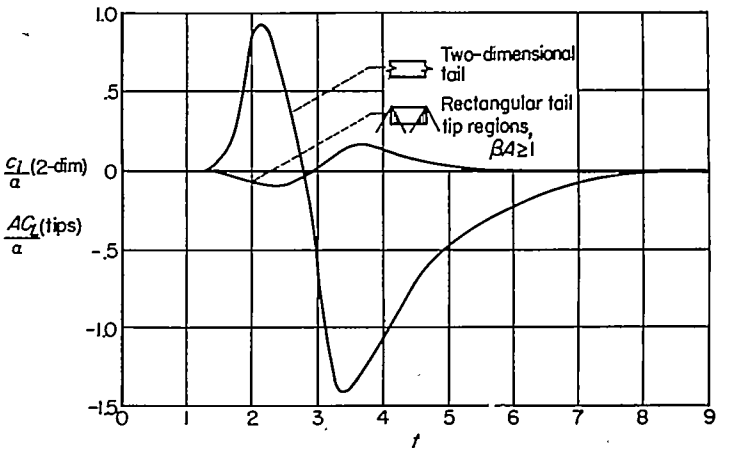

FIGURE 47.—Approximate response in lift of two-dimensional tail and tip regions of rectangular tail to step change in angle of attack of two-dimensional wing. $M_o=1.7$.

Note that the main difference for the two-dimensional result from the result for the response to a single vortex pair is the disappearance of the infinity in lift when the tail penetrates the position of the first starting vortex. Reference to figure 46 will show that this is attributable to the fact that the first vortex penetrated by the tail is of infinitesimal strength. Again, as in the single-vortex example, the response in lift for a finite-span tail satisfying the restriction $\beta A\geq 1$ may be obtained from the results of figure 47 by direct addition of the two variations shown in the figure.

It should perhaps be noted that the form of equation (52) permits of still other simplifications which should yield acceptable results for special cases. For instance, when the chord of the wing is small compared to the tail length, it may be expected that the influence on the build-up in lift at the tail of disturbances on the wing should be minor compared to the influence of disturbances in the wake. It is seen in equation (52) that this condition is equivalent simply to ignoring the first integral in comparison to the second. The simplification, of course, represents a considerable reduction in computational labor, and, in addition, the form of the remaining integral is simple enough so that the exact variation of $\Delta\dot{\Phi}$ at the trailing edge of the wing corresponding to the prescribed normal-velocity distribution on the wing may be used with relative ease. For example, for the case of uniform normal velocity on the wing, the variation of $\Delta\dot{\Phi}(l,t)$ at the wing trailing edge may be derived from the results of reference 3, and is given by

$$\left.\begin{aligned}\Delta\dot{\Phi}(l,t)&=V_o\alpha, \qquad 0\leq t\leq\frac{c_{o_w}}{M_o+1}\\ &=\frac{V_o\alpha}{\pi}\cos^{-1}\left(\frac{M_o t-c_{o_w}}{t}\right), \quad \frac{c_{o_w}}{M_o+1}\leq t\leq\frac{c_{o_w}}{M_o-1}\\ &=0, \qquad \frac{c_{o_w}}{M_o-1}\leq t\end{aligned}\right\} \tag{61}$$

Upon substitution of these expressions in equation (51) and performance of the required integration, the solution yields in any case the exact response of the tail lift to the influence of the wake, and, in cases where the tail length is large compared to the wing chord, a reasonable approximation of the total response in lift of the tail. The response in lift of the tail to, say, indicial pitching motion of the wing, or for that matter, to any indicial motion of the wing for which the variation $\Delta\Phi(l,t)$ is known, can be approximated by the same technique.

CONSIDERATION OF THREE-DIMENSIONAL FLOW EFFECTS

In all of the analysis presented thus far, attention has been focused solely on problems in which the flow field caused by the forward wing is two-dimensional. This effectively limits the results to cases wherein the plan form of the forward wing is essentially rectangular, with span sufficiently large so that the flow from the tips of the wing does not significantly affect conditions in the vicinity of the tail. In order to treat more general cases, including cases wherein the plan forms are of nearly equal span, it becomes necessary to consider in detail the effects on the tail of the remainder of the vortex loop — the trailing vortices. Inevitably, the admittance of spanwise variations of normal velocity into the flow-field picture complicates the analysis considerably, and it appears that exact solutions for the tail lift response will be exceedingly difficult to obtain. However, the change in the physical situation caused by the addition of the trailing vortices can be fully described, and this description will be seen to suggest simplifying approximations which serve, in turn, to make the problem of calculating the tail lift response more tractable.

THE FLOW FIELD

Consider first the flow-field caused by the motion of the complete vortex loop. The boundary condition characteristic of the vortex loop is that within the confines of the moving, starting, and trailing vortices, the jump in potential $\Delta\Phi$ is a constant across the plane containing the vortices, and zero elsewhere in the plane. Thus it is clear that the two-dimensional vortex system considered earlier can be converted to the three-dimensional system by subtracting off regions of constant $\Delta\Phi$ of semi-infinite spanwise extent, as shown in figure 48.

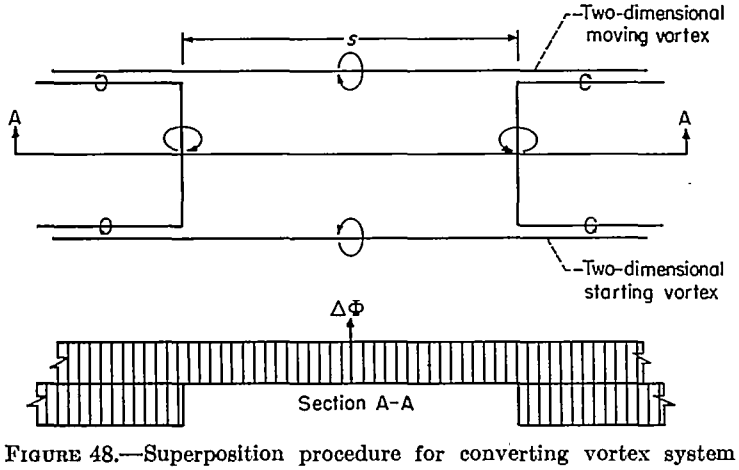

FIGURE 48.—Superposition procedure for converting vortex system from two- to three-dimensions.

Obviously, by reason of symmetry, we need consider the effect of only one of the added trailing-vortex loops, and, further, it is sufficient to consider the effect only within the shaded region of figure 49.

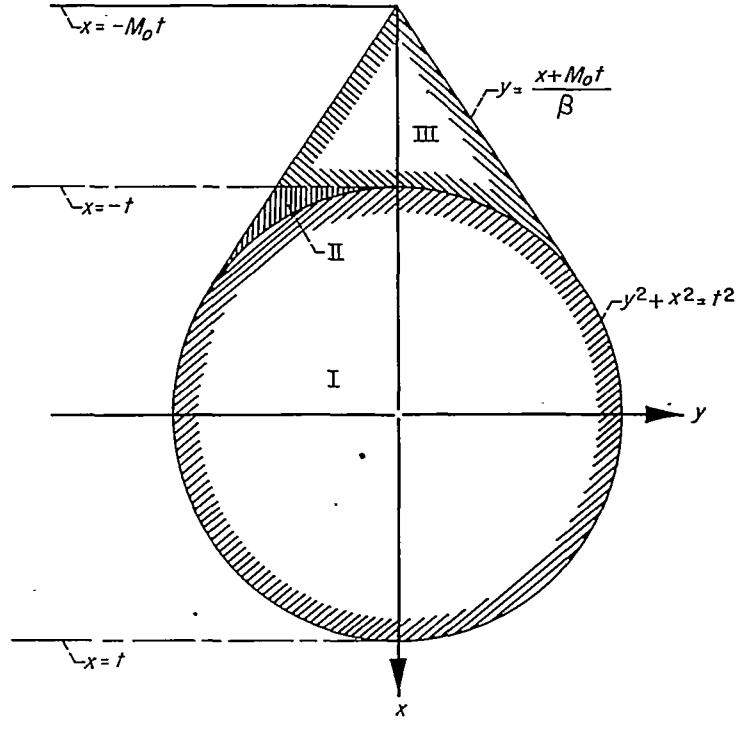

FIGURE 49.—Boundary conditions in the $z=0$ plane for a trailing vortex loop.

In figure 49 the circular region, denoted region I, is the domain in the plane of the vortices within the sound wave emitted at $t=0$ by the motion of the trailing vortex. This region extends from values of x between $+t$ and $-t$, and constitutes the interval within which the flow is both unsteady and three-dimensional. For values of $x<-t$, the flow has reached its steady-state distribution, and is therefore stationary with respect to an observer traveling at the speed of the moving vortex. The lines $y=\mp\left(\frac{x+M_0t}{\beta}\right)$ setting off this steady-flow regime are of course the Mach lines emanating from the juncture of the moving and trailing vortices. All points to the left of the shaded region are clearly unaffected by disturbances from the trailing vortex itself, and hence the flow there is just the mirror image of the two-dimensional flow considered earlier. Points to the right of the shaded region are completely unaffected by the action of the trailing-vortex loop, and there the fluid is undisturbed by the addition of the loop.

The problem of calculating the potential and velocity field associated with the trailing-vortex loop has already been considered for the subsonic speed range by Lomax, Heaslet, and Fuller in reference 24. It is a relatively simple matter to extend these results to the supersonic range, and since the procedure for doing so is plainly developed in reference 24, only the final results that are of interest here will be given. Thus, for the regions marked I, II, III in figure 49, the normal velocity w induced in the plane of the vortices by the

addition of the trailing vortex-loop is given by:

$$\left.\begin{aligned}
y\geq 0;-w(\mathrm{I})&=\frac{\Delta\Phi}{4\pi}\left[\frac{M_o\sqrt{t^2-x^2}}{x(x+M_ot)}-\frac{\sqrt{(x+M_ot)^2-\beta^2y^2}}{y(x+M_ot)}+\frac{\sqrt{x^2+y^2}}{xy}\right]\\
-w(\mathrm{III})&=-\frac{\Delta\Phi}{2\pi}\frac{\sqrt{(x+M_ot)^2-\beta^2y^2}}{y(x+M_ot)}\\
y\leq 0;-w(\mathrm{I})&=+\frac{\Delta\Phi}{2\pi}\frac{M_o\sqrt{t^2-x^2}}{x(x+M_ot)}+\frac{\Delta\Phi}{4\pi}\left[-\frac{M_o\sqrt{t^2-x^2}}{x(x+M_ot)}-\frac{\sqrt{(x+M_ot)^2-\beta^2y^2}}{y(x+M_ot)}+\frac{\sqrt{x^2+y^2}}{xy}\right]\\
-w(\mathrm{II})&=+\frac{\Delta\Phi}{2\pi}\frac{M_o\sqrt{t^2-x^2}}{x(x+M_ot)}-\frac{\Delta\Phi}{2\pi}\frac{\sqrt{(x+M_ot)^2-\beta^2y^2}}{y(x+M_ot)}\\
-w(\mathrm{III})&=-\frac{\Delta\Phi}{2\pi}\frac{\sqrt{(x+M_ot)^2-\beta^2y^2}}{y(x+M_ot)}
\end{aligned}\right\}\quad(62)$$

Several points of interest may be deduced from inspection of equation (62). First note that, as it should, the solution reduces to the two-dimensional normal velocity with just a change in sign along the left-hand boundary $\left(y=-\sqrt{t^2-x^2},\ t>x>-\frac{t}{M_o};\ y=-\left(\frac{x+M_ot}{\beta}\right),\ \frac{-t}{M_o}>x>-M_ot\right)$ and to zero along the right-hand boundary $\left(y=+\sqrt{t^2-x^2},\ t>x>-\frac{t}{M_o};\ y=+\left(\frac{x+M_ot}{\beta}\right),\ \frac{-t}{M_o}>x>-M_ot\right)$.

Second, it appears that the contribution to the normal velocity made by the trailing-vortex loop may be viewed as being composed of two distinct parts: one, a two-dimensional contribution, equal but opposite in sign to the normal velocity contribution of the original two-dimensional system and existing everywhere within the region $y\leq 0$, $-t<x<t$, and second, a three-dimensional contribution that is antisymmetric with respect to the axis $y=0$ and that exists only within the confines of the starting sound wave and Mach line traces, that is, within the shaded region of figure 49. It should be noted that the antisymmetric contribution is zero along both the left-hand and right-hand boundaries, and contains no singularities other than at $y=0$, $x<0$, the path of the trailing vortex itself.

In order to obtain the normal-velocity distribution due to the complete vortex loop, it is now only necessary to combine the results given by equation (62) with the two-dimensional contribution (eq. (35)), and with the contribution of the trailing-vortex loop originating at $y=s$ (see fig. 48). However, we are interested in the effect of this complete loop on the lift at the tail and, inasmuch as the response to the two-dimensional vortex system has already been investigated in previous sections, it is more to the point simply to continue by investigating separately the effect on the tail of only one trailing-vortex loop. The resulting solution for tail lift response can then be doubled to account for the influence of both trailing-vortex loops, and directly added to the result found previously for the response to the two-dimensional vortex system.

RESPONSE IN LIFT OF TAIL TO NORMAL VELOCITY OF TRAILING-VORTEX LOOP

In view of the complicated nature of the flow caused by the trailing-vortex loop, it appears that analyses leading to exact solutions for general tail plan forms will be confronted by formidable difficulties. Thus, for practical purposes, simplifying approximations will no doubt become necessary. There is one type of plan form, however, which can be treated with a minimum of approximation and that is a class of supersonic-edged wings. It has already been mentioned in a previous section that for the supersonic-edged plan form having a straight trailing edge normal to the free-stream direction, the use of strip theory is exact in calculations for the lift due to arbitrary deformations of the surface. Hence, for this type of plan form one can calculate the lift at a given spanwise station as though the station were a two-dimensional surface undergoing the same motion. The reduction of the problem to one involving only two spatial dimensions then opens the way for use of the three-dimensional steady-flow analogy to solve the problem in the same manner as was done previously for the response of the two-dimensional tail to the two-dimensional vortex system.

As an illustration of the use of these principles, we consider two cases involving the response of a tail of triangular plan form; first to a vortex system having a span greater than, and second a span less than the span of the tail.

Case 1; $2mc_o<s$.—

Referring to the notation of figure 50, let us fix attention to a spanwise station y, and examine the normal velocity distribution encountered by chord $c_1(y)$ of the tail as it passes through the region of disturbed flow caused by the left-hand trailing-vortex loop. For the particular chord chosen, the geometry of its experience in time and space is illustrated in figure 51.

As seen on the figure, in virtue of fixing y, the boundaries of the sound wave appear as one branch of a hyperbola. Within the hyperbola, the flow is of the type defined by $w(\mathrm{I})$ of equation (62); whereas to the left of the hyperbola but within the trace $x=\beta y-M_ot$, the flow is constant along lines parallel to the leading edge of the section, being of type III of equation (62). Elsewhere, the flow is zero. Now, in view of the validity of the strip-theory formulation we consider the chord $c_1(y)$ as being the chord of a two-dimensional tail, subjected to the normal-velocity distribution $w(x,\ t;\ y)$, where y is treated as a constant. Then, invoking the three-dimensional steady-state analogy, the problem is to find the steady-state section lift as a function of t (the coordinate t is now the streamwise axis) on the equivalent sweptback tail shown in figure 51, which is subjected within the shaded boundaries to a normal-velocity distribution given by equation (62).

Up to this point, the formulation of the problem has involved no approximations. Now, however, rather than attempt to solve the above problem exactly (which is in truth even now a formidable exercise in integration) we introduce a simplifying approximation based on the nature of the normal-velocity distribution. It has been mentioned that the antisymmetric part of the normal velocity caused by the trailing-vortex loop contains no singularities other

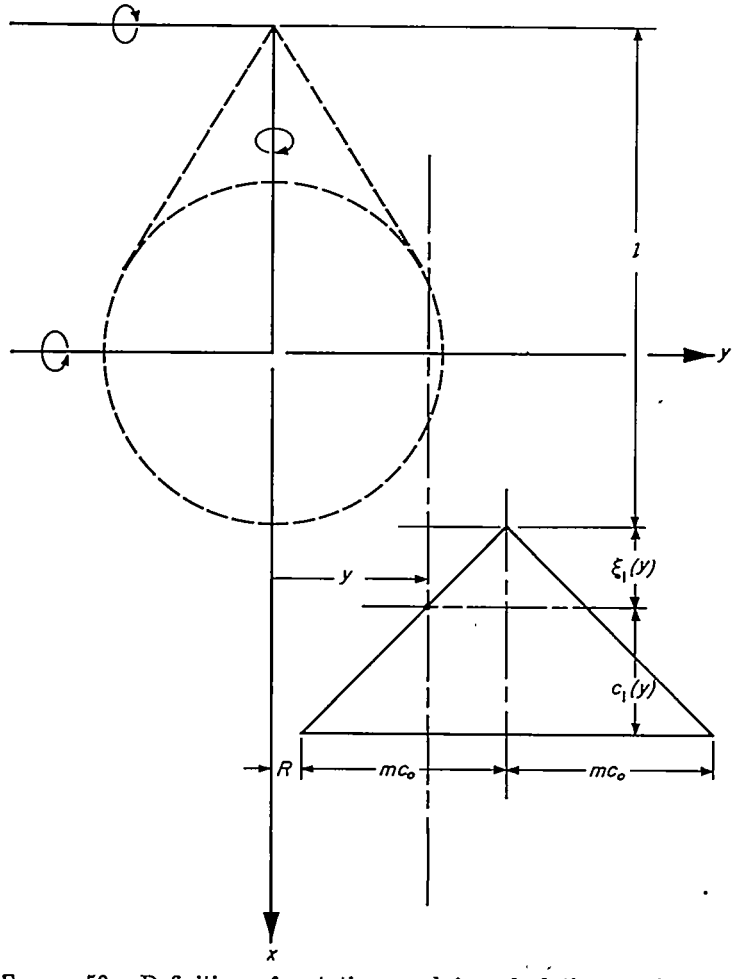

FIGURE 50.—Definition of notation used in calculating section lift response to normal velocity of trailing vortex loop.

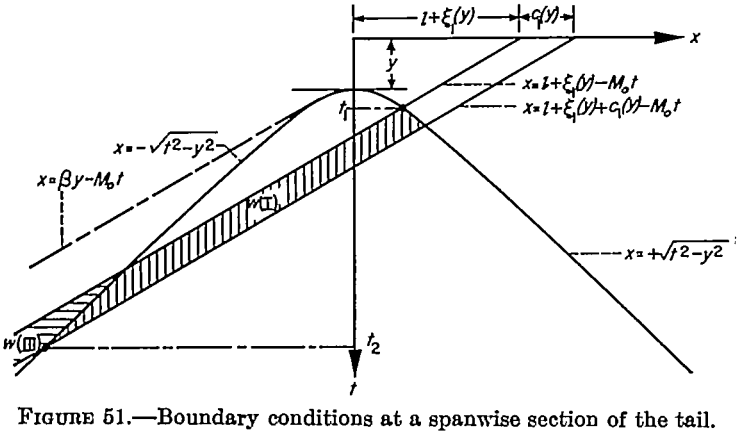

FIGURE 51.—Boundary conditions at a spanwise section of the tail.

than those on the path of the trailing vortex itself. It can also be said that with respect to an observer moving with the chord $c_1(y)$ the magnitude of the antisymmetric flow grows uniformly from zero at one boundary of the sound wave to the steady-state value at the other boundary. These statements are illustrated in figure 52 for the region in x, t, occupied by the tail chord $c_1(y)$ of figure 51.

Thus, from inspection of figure 52 it can also be stated that the response in lift $c_l(l+\xi_1(y), c_1(y), t)$ must start from zero at time $t_1(y)$ (see fig. 51), and also grow uniformly to its steady-state value, which is attained at time $t_2(y)$. Moreover, it can be shown that if w is continuous along lines

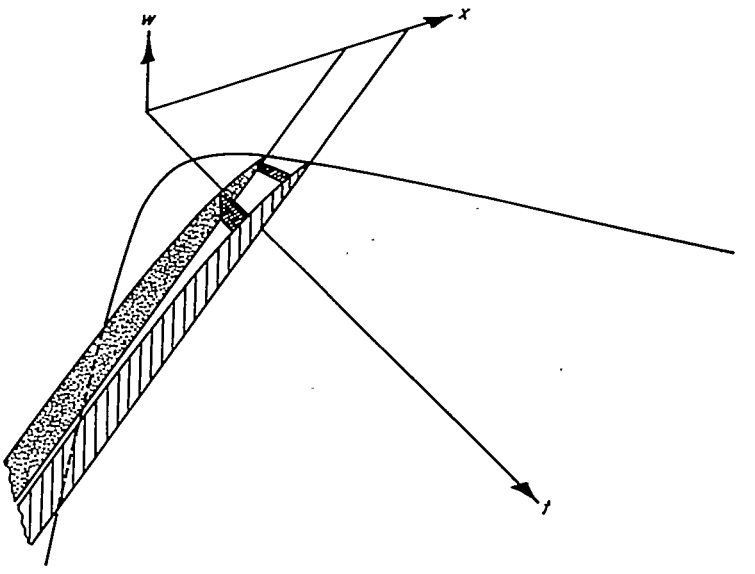

FIGURE 52.—Normal velocity distribution due to trailing vortex loop at a spanwise station of the tail.

parallel to the leading edge the slope of the response curve must be zero at both times t_1 and t_2.

The steady state lift $\bar{c}_l(l+\xi_1(y), c_1(y))$ which is attained at time t_2 can be computed exactly, and the times t_1 and t_2 are obtained easily from the geometry of figure (51). It therefore seems reasonable simply to approximate the response curve by a variation that grows uniformly with time and fits the end conditions correctly in magnitude and slope. One such curve can be written in the form of a cubic equation in t, and gives,

$$c_l(l+\xi_1(y),c_1(y),t)=$$

$$\bar{c}_l(l+\xi_1(y),c_1(y))\left[\frac{t-t_1(y)}{t_2(y)-t_1(y)}\right]^2\left\{3-2\left[\frac{t-t_1(y)}{t_2(y)-t_1(y)}\right]\right\} \quad (63)$$

where, for the conditions of figure (51),

$$t_1(y)=\frac{M_o[l+\xi_1(y)]-\sqrt{[l+\xi_1(y)]^2-\beta^2y^2}}{\beta^2}$$

$$t_2(y)=\frac{M_o(l+c_o)+\sqrt{(l+c_o)^2-\beta^2y^2}}{\beta^2}$$

$$\bar{c}_l(l+\xi_1(y),\, c_1(y))=-\frac{4}{V_o\beta c_1(y)}\frac{\Delta\Phi}{2\pi y}\left\{\sqrt{(l+c_o)^2-\beta^2y^2}-\right.$$

$$\left.\beta y\cos^{-1}\left(\frac{\beta y}{l+c_o}\right)-\sqrt{[l+\xi_1(y)]^2-\beta^2y^2}+\beta y\cos^{-1}\frac{\beta y}{l+\xi_1(y)}\right\}$$

The form of equation (63) can be viewed as being typical of the response of any section $c(y)$ of the tail. However, as y takes on all values from one tip to the other, the equations for t_1, t_2, and $\bar{c}_l$ may change from type to type in different spanwise intervals, depending on the Mach number and configuration geometry under consideration. Referring, for example, to figure 50, it is clear that a section of the tail near the right-hand tip may be completely untouched by the normal velocity caused by the trailing vortex; whereas sections closer inboard may be touched on only a portion of their length. All told, there are five such possible variations

in the boundary conditions and these are listed in Appendix D, together with the corresponding values of t_1, t_2, and $\bar{c}_l$.

Having determined an expression for the response in lift at an arbitrary section of the tail, we may now integrate and find the combined response of all sections of the tail to the given normal-velocity distribution. Thus, in a manner similar to that described previously in connection with calculations for the response to the two-dimensional vortex pattern, we may write, for the response to one trailing vortex,

$$C_L(t)=\frac{1}{S}\left\{\int_R^{mc_o+R} c_1(y)\,c_l(l+\xi_1(y),c_1(y),t)\,dy+\int_{mc_o+R}^{2mc_o+R} c_2(y)\,c_l(l+\xi_2(y),c_2(y),t)\,dy\right\} \quad (64)$$

where the symbols in equation (64) have been defined in figure (50). In order to illustrate the nature of the result for the response in lift to the trailing-vortex loop, calculations based on equations (63) and (64) have been carried out for the triangular tail shown on the side of figure 53. The results account for the effects of both exterior trailing-vortex loops and may be directly added to the response to the two-dimensional vortex system to give the response to the complete loop shown in figure 53. The separate responses and their combination are shown for comparison on figure 53.

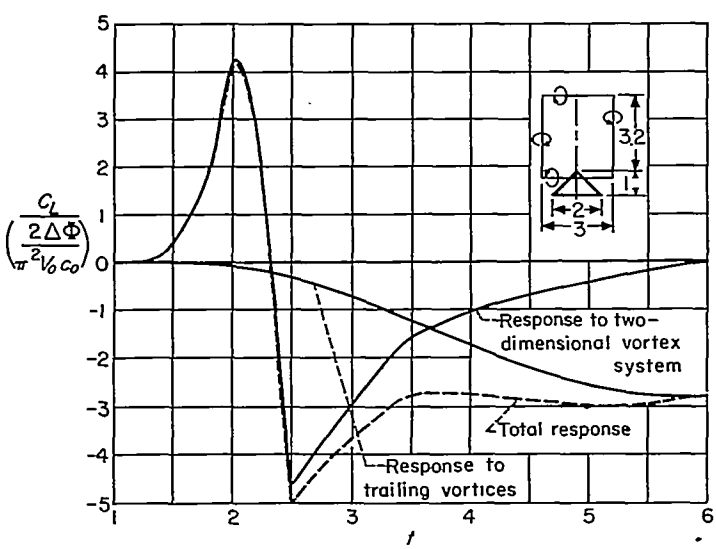

FIGURE 53.—Response in lift of wide triangular tail of aspect ratio 4 to normal velocity of complete vortex loop. $M_o=1.7$.

Case 2: $2mc_o>s$.—

When the span of the trailing vortices is smaller than that of the tail, the development outlined above must be amended slightly. The effect of the antisymmetric part of the normal velocity-distribution may be accounted for, however, by the same technique as described previously, and referring to figure 54 for definition of the notation, the response in lift of the tail to this contribution may be written immediately as,

$$C_L(t)_a=\frac{1}{S}\left\{\int_{-R}^{mc_o-R} c_1(y)\,c_l(l+\xi_1(y),c_1(y),t)\,dy+\int_{mc_o-R}^{2mc_o-R} c_2(y)\,c_l(l+\xi_2(y),c_2(y),t)\,dy\right\} \quad (65)$$

where the variation $c_l(l+\xi(y),\ c(y),t)$ is again given by equation (63).

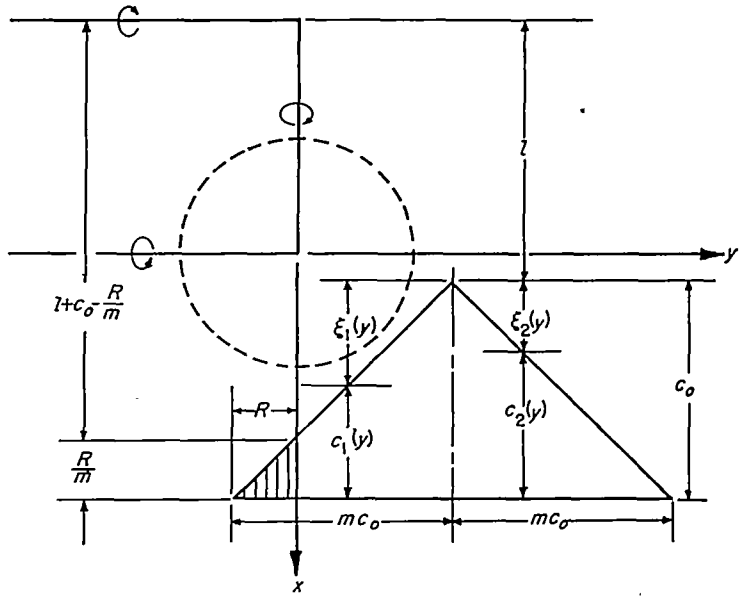

FIGURE 54.—Definition of notation used in calculating section lift response to normal velocity of trailing vortex loop.

Now, it is also necessary to consider the influence of the two-dimensional contribution to the normal velocity which exists in the region $y<0$, $-t<x<+t$. But note, the response in lift of the tail to this contribution is simply equivalent to minus one half the response of a triangular tail of chord $\frac{R}{m}$ and tail length $l+c_o-\frac{R}{m}$ to the two-dimensional vortex pattern, and, inasmuch as the exact result for this case has been obtained in a previous section, it is sufficient to indicate the result in coefficient form as

$$C_L(t)_b=-\frac{1}{2}\frac{R^2}{mS}C_{L_2}\left(l+c_o-\frac{R}{m},\frac{R}{m},t\right) \quad (66)$$

where the subscript 2 indicates that the response to the two-dimensional vortex pattern is to be taken. The sum of equations (65) and (66) then gives the total response of the tail to one trailing-vortex loop. To obtain the response to the complete vortex loop, this result is then doubled and added to the response to the two-dimensional pattern in the same manner as was done for case 1.

SUPERPOSITION OF ELEMENTARY SOLUTIONS

Finally, having obtained a solution for the lift at the tail induced by the normal-velocity distribution of the complete vortex loop, we wish now to use the solution to build up the response to the downwash caused by a three-dimensional forward wing. The analysis for accomplishing this task closely parallels that described previously for the case of the two-dimensional forward wing, and therefore only the final result will be given here. Thus, denoting the elementary solution by $C_L(\mu,s,t)$, where μ is the distance from a moving vortex to the tail leading edge and s is the semispan of the vortex loop, we get, (see figure (55) for definition of notation)

$$C_L(t)=\int_l^{l+c_w}\frac{d\mu}{M_o}\int_0^{\eta(\mu)}ds\int_0^t\left[M_o\frac{\partial^2 C_L}{\partial\mu\partial s}(\mu,s,\tau)+\frac{\partial^2 C_L}{\partial\tau\partial s}(\mu,s,\tau)\right]$$
$$\Delta\dot{\Phi}(\mu,s,t-\tau)d\tau+\int_0^{\eta(l)}ds\int_o^t\frac{\partial C_L}{\partial s}(l,s,\tau)\Delta\dot{\Phi}(l,s,t-\tau)d\tau \quad (67)$$

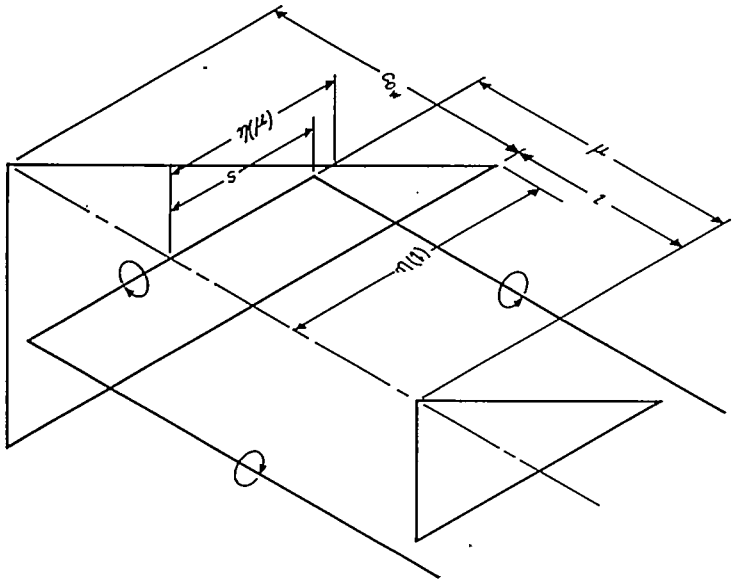

FIGURE 55.—Definition of notation used in calculating response in lift of tail to prescribed $\Delta\Phi$ distribution on three-dimensional forward wing.

As in the two-dimensional case, the first term in equation (67) accounts for the variation of $\Delta\Phi$ on the wing, the second, for the variation in the wake. It is to be noted that in the development leading to equation (67) it is assumed that the trailing edge of the forward wing is straight and normal to the free-stream direction. However, wings having other than straight trailing edges can be treated by the same equation by considering as part of the wing points in the wake between the wing trailing edge and the rearmost spanwise axis passing through the wing.

APPLICATION OF REVERSE FLOW THEOREM

We have devoted several sections to the derivation of methods whereby the tail lift response can be calculated for certain restricted cases. The possibility still exists, however, that these results can be extended to include still other cases which do not lend themselves as readily to analysis. The question may be asked, for instance, whether a relationship exists between the response in lift at the tail to the essentially two-dimensional normal-velocity field shed by a large-span rectangular wing and the analytically more difficult reverse situation; that is, the effect of a small-span forward wing of fairly general plan form (for which the downwash field is far from being two-dimensional) on a large-span rectangular tail. Such a relationship can be sought for the more general case, involving wing-tail configurations of arbitrary size and shape, by application of the reverse-flow theorems for unsteady motion developed in reference 27. It will be the purpose of this section to investigate this possibility.

To begin, we adopt the notation used in reference 27 and also specify that the motion of the wing-tail combination be indicial; that is, the combination is made to start from rest at $t=0$ with uniform velocity V_o in forward and reverse motion, and boundary conditions for the flow over the surfaces are specified only for $t>0$, being zero for $t<0$. After the combination has moved for a time T in both forward and reverse directions, the relationship of the wings and their respective coordinate systems are as shown in figure 56.

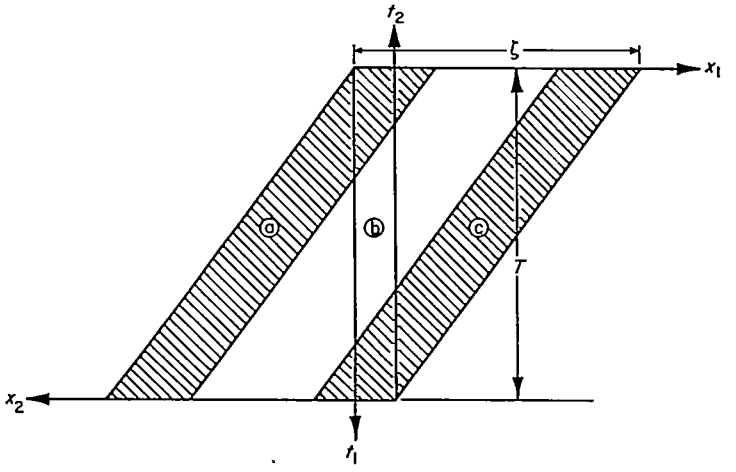

FIGURE 56.—Coordinate systems in forward and reverse motion.

In figure 56, the subscript 1 denotes the axis system in forward motion, the subscript 2, the axis system in reverse motion, and the wing, wake, and tail have been given the symbols a, b, and c, respectively. As may be verified from examination of the figure, the x and t axes are related by the equalities,

$$\left.\begin{aligned}x_2&=-x_1+\zeta-M_oT\\ t_2&=-t_1+T\end{aligned}\right\} \quad (68)$$

and we further specify that $y_2=-y_1$. The general reversal theorem may then be written in the form (see again, ref. 27),

$$\int_0^T dt_1\iint_{P_1(t_1)}[p_{a_1}(x_1,y_1,t_1)\overline{w}_{a_2}(x_1,y_1,t_1)+$$
$$p_{b_1}(x_1,y_1,t_1)\overline{w}_{b_2}(x_1,y_1,t_1)+p_{c_1}(x_1,y_1,t_1)\overline{w}_{c_2}(x_1,y_1,t_1)]\,dx_1dy_1=$$
$$\int_0^T dt_2\iint_{P_2(t_2)}[p_{a_2}(x_2,y_2,t_2)\overline{w}_{a_1}(x_2,y_2,t_2)+$$
$$p_{b_2}(x_2,y_2,t_2)\overline{w}_{b_1}(x_2,y_2,t_2)+p_{c_2}(x_2,y_2,t_2)\overline{w}_{c_1}(x_2,y_2,t_2)]\,dx_2dy_2 \quad (69)$$

where P is the plan form of the combination in the $z=0$ plane. It may be noted the normal-velocity functions, $\overline{w}_{i_1}$, $\overline{w}_{i_2}$ are implicitly dependent on T, the full relationship being,

$$\left.\begin{aligned}\overline{w}_{i_1}(x_2,y_2,t_2)&=w_{i_1}(-x_2+\zeta-M_oT,-y_2,-t_2+T)\\ \overline{w}_{i_2}(x_1,y_1,t_1)&=w_{i_2}(-x_1+\zeta-M_oT,-y_1,-t_1+T)\\ &i=a,b,c\end{aligned}\right\} \quad (70)$$

Notice further that, since the wake cannot sustain a pressure difference, the products $p_{b_1}\overline{w}_{b_2}$ and $p_{b_2}\overline{w}_{b_1}$ in equation (69) may be set to zero. Then taking a derivative with respect to T of both sides of equation (69), we get,

$$\iint_{P_{a_1}(T)} p_{a_1}(x_1,y_1,T)\overline{w}_{a_2}(x_1,y_1,T)dx_1dy_1+\iint_{P_{c_1}(T)} p_{c_1}(x_1,y_1,T)\overline{w}_{c_2}(x_1,y_1,T)dx_1dy_1+\int_0^T dt_1\iint_{P_{a_1}(t_1)} p_{a_1}(x_1,y_1,t_1)\left(-M_o\frac{\partial w_{a_2}}{\partial x_2}+\frac{\partial w_{a_2}}{\partial t_2}\right)dx_1dy_1+\int_0^T dt_1\iint_{P_{c_1}(t_1)} p_{c_1}(x_1,y_1,t_1)\left(-M_o\frac{\partial w_{c_2}}{\partial x_2}+\frac{\partial w_{c_2}}{\partial t_2}\right)dx_1dy_1=\iint_{P_{a_2}(T)} p_{a_2}(x_2,y_2,T)\overline{w}_{a_1}(x_2,y_2,T)dx_2dy_2+\iint_{P_{c_2}(T)} p_{c_2}(x_2,y_2,T)\overline{w}_{c_1}(x_2,y_2,T)dx_2dy_2+\int_0^T dt_2\iint_{P_{a_2}(t_2)} p_{a_2}(x_2,y_2,t_2)\left(-M_o\frac{\partial w_{a_1}}{\partial x_1}+\frac{\partial w_{a_1}}{\partial t_1}\right)dx_2dy_2+\int_0^T dt_2\iint_{P_{c_2}(t_2)} p_{c_2}(x_2,y_2,t_2)\left(-M_o\frac{\partial w_{c_1}}{\partial x_1}+\frac{\partial w_{c_1}}{\partial t_1}\right)dx_2dy_2 \tag{71}$$

It is easily verified that a sufficient condition for the disappearance of the triple integrals in equation (71) is that the normal-velocity distributions on the surfaces be restricted to those defined by the relations,

$$\left.\begin{aligned} w_1(x_1,t_1;\ y_1)&=f(x_1+M_ot_1;\ y_1)\\ w_2(x_2,t_2;\ y_2)&=g(x_2+M_ot_2;\ y_2)\end{aligned}\right\} \tag{72}$$

Another such condition is simply that $w_1=0$, or $w_2=0$. Assuming henceforth that either or both of these conditions are in force, the flow reversal relationship for the wing-tail combination becomes,

$$\left.\begin{aligned}&\iint_{P_{c_1}(T)} p_{a_1}(x_1,y_1,T)\overline{w}_{a_2}(x_1,y_1,T)dx_1dy_1+\\&\iint_{P_{c_1}(T)} p_{c_1}(x_1,y_1,T)\overline{w}_{c_2}(x_1,y_1,T)dx_1dy_1\\&=\iint_{P_{a_2}(T)} p_{a_2}(x_2,y_2,T)\overline{w}_{a_1}(x_2,y_2,T)dx_2dy_2+\\&\iint_{P_{c_2}(T)} p_{c_2}(x_2,y_2,T)\overline{w}_{c_1}(x_2,y_2,T)dx_2dy_2\end{aligned}\right\} \tag{73}$$

Now in the present problem, the boundary conditions for the flow on the wing and tail are simply that in forward motion the normal velocity on the forward wing is uniform while on the tail it is zero, and in reverse flow we specify that the same situation be true. Obviously, these conditions satisfy the restrictions imposed by equation (72), and setting $\overline{w}_{a_1}$ and $\overline{w}_{c_2}$ equal to unity, equation (73) becomes,

$$\iint_{P_{c_1}(T)} p_{c_1}(x_1,y_1,T)dx_1dy_1=\iint_{P_{a_2}(T)} p_{a_2}(x_2,y_2,T)dx_2dy_2 \tag{74}$$

Thus, the response in lift induced on the tail by the indicial change in angle of attack of the wing is exactly the same as the lift response of the wing due to indicial change in angle of attack of the tail in reverse motion. It will be noted that the above result applies for wing-tail combinations flying at either subsonic or supersonic speeds, and that no restriction has been placed on size or shape of the plan forms.

APPLICATION OF RESULTS TO DYNAMIC STABILITY ANALYSIS

The preceding sections have been concerned with the development of methods whereby the variation with time of the lift developed at the tail in reaction to the normal velocity shed by a forward wing could be estimated. Now, having arrived at a fairly rigorous physical understanding of the nature of the variation, we will attempt in this section to assess the significance of its contribution to the over-all dynamic stability of an aircraft. For simplicity, attention is devoted to the single-degree-of-freedom rotary-oscillation case.

It has been noted that the oscillatory lift and moment equations developed previously for a single wing are still applicable for the wing-tail case with proper interpretation of the indicial functions. For supersonic speeds, this redefinition was seen to reduce for each indicial function simply to the sum of the indicial functions of the wing and tail considered as isolated wings and an interference function which accounts for the influence of vorticity shed by the wing on the development of lift at the tail. Then, denoting the interference functions by primed quantities, we conform to the notation used in Part I by letting

$$\left.\begin{aligned} C'_{L_\alpha}(\tau)&=C'_{L_\alpha}(t'_a)-F'_1(\tau)\\ C'_{m_\alpha}(\tau)&=C'_{m_\alpha}(t'_a)-F'_3(\tau)\\ C'_{L_q}(\tau)&=C'_{L_q}(t'_a)-F'_2(\tau)\\ C'_{m_q}(\tau)&=C'_{m_q}(t'_a)-F'_4(\tau)\end{aligned}\right\} \tag{75}$$

Again introduce the parameters,

$\varphi=\dfrac{2V_o}{\bar{c}}\tau$ — number of half M. A. C. lengths traveled in time τ

$k=\dfrac{\omega\bar{c}}{2V_o}$ — reduced frequency

$\sigma'_a=\dfrac{2V_o}{\bar{c}}t'_a$ — number of half M. A. C. lengths for interference function to reach steady-state,

where the characteristic unit of length $\bar{c}$ is taken as the *wing* M. A. C. The in-phase and out-of-phase lift and moment coefficients for the harmonic rotary-oscillation case then follow directly from the form of equations 12 and 14.

$$\left.\begin{aligned}
R.P.\left(\frac{C_L}{\alpha}\right)&=C_{L_{\alpha_w}}(\sigma_{a_w})+C_{L_{\alpha_T}}(\sigma_{a_T})+C'_{L_\alpha}(\sigma'_a)-\\
&\quad k\int_0^{\sigma'_a}[F_{1_w}(\varphi)+F_{1_T}(\varphi)+F'_1(\varphi)]\sin k\varphi d\varphi+\\
&\quad k^2\int_0^{\sigma'_a}[F_{2_w}(\varphi)+F_{2_T}(\varphi)+F'_2(\varphi)]\cos k\varphi d\varphi\\
I.P.\left(\frac{C_L}{\alpha}\right)&=k\Big\{C_{L_{q_w}}(\sigma_{a_w})+C_{L_{a_T}}(\sigma_{a_T})+C'_{L_q}(\sigma'_a)-\\
&\quad k\int_0^{\sigma'_a}[F_{2_w}(\varphi)+F_{2_T}(\varphi)+F'_2(\varphi)]\sin k\varphi d\varphi-\\
&\quad \int_0^{\sigma'_a}[F_{1_w}(\varphi)+F_{1_T}(\varphi)+F'_1(\varphi)]\cos k\varphi d\varphi\Big\}
\end{aligned}\right\}\quad(76)$$

$$\left.\begin{aligned}
R.P.\left(\frac{C_m}{\alpha}\right)&=C_{m_{\alpha_w}}(\sigma_{a_w})+C_{m_{\alpha_T}}(\sigma_{a_T})+C'_{m_\alpha}(\sigma'_a)-\\
&\quad k\int_o^{\sigma'_a}[F_{3_w}(\varphi)+F_{3_T}(\varphi)+F'_3(\varphi)]\sin k\varphi d\varphi+\\
&\quad k^2\int_o^{\sigma'_a}[F_{4_w}(\varphi)+F_{4_T}(\varphi)+F'_4(\varphi)]\cos k\varphi d\varphi\\
I.P.\left(\frac{C_m}{\alpha}\right)&=k\Big\{C_{m_{q_w}}(\sigma_{a_w})+C_{m_{a_T}}(\sigma_{a_T})+C'_{m_q}(\sigma'_a)-\\
&\quad k\int_o^{\sigma'_a}[F_{4_w}(\varphi)+F_{4_T}(\varphi)+F'_4(\varphi)]\sin k\varphi d\varphi-\\
&\quad \int_o^{\sigma'_a}[F_{3_w}(\varphi)+F_{3_T}(\varphi)+F'_3(\varphi)]\cos k\varphi d\varphi\Big\}
\end{aligned}\right\}\quad(77)$$

In the same way, the reduction of the above results for $k\ll 1$ to first-order in frequency follows directly from the form of equations (13) and (15). There results,[12]

$$\left.\begin{aligned}
R.P.\left(\frac{C_L}{\alpha}\right)&=C_{L_{\alpha_w}}(\sigma_{a_w})+C_{L_{\alpha_T}}(\sigma_{a_T})+C'_{L_\alpha}(\sigma'_a)\\
I.P.\left(\frac{C_m}{\alpha}\right)&=k\Big\{C_{L_{q_w}}(\sigma_{a_w})+C_{L_{a_T}}(\sigma_{a_T})+C'_{L_q}(\sigma'_a)-\\
&\quad \int_o^{\sigma'_a}[F_{1_w}(\varphi)+F_{1_T}(\varphi)+F'_1(\varphi)]\,d\varphi\Big\}
\end{aligned}\right\}\quad(78)$$

$$\left.\begin{aligned}
R.P.\left(\frac{C_m}{\alpha}\right)&=C_{m_{\alpha_w}}(\sigma_{a_w})+C_{m_{\alpha_T}}(\sigma_{a_T})+C'_{m_\alpha}(\sigma'_a)\\
I.P.\left(\frac{C_m}{\alpha}\right)&=k\Big\{C_{m_{q_w}}(\sigma_{a_w})+C_{m_{a_T}}(\sigma_{a_T})+C'_{m_q}(\sigma'_a)-\\
&\quad \int_o^{\sigma'_a}[F_{3_w}(\varphi)+F_{3_T}(\varphi)+F'_3(\varphi)]\,d\varphi\Big\}
\end{aligned}\right\}\quad(79)$$

With the aid of the first order in frequency results (eq. (79)) it is possible to assess the importance of interference effects on the damping moment of a wing-tail combination. Inspection of equation (79) for the out-of-phase pitching moment reveals that the interference effects are contained in the term $C'_{m_q}(\sigma'_a)$ and the integral, $-\int_o^{\sigma'_a}F'_3(\varphi)\,d\varphi$. The term $C'_{m_q}(\sigma'_a)$ is generally relatively small, and may be approximated by replacing the steady nonuniform downwash at the tail caused by the pitching velocity of the wing by an appropriately averaged effective angle of attack at the tail. The term $C'_{m_q}(\sigma'_a)$ may then be related to $C_{m_{a_T}}(\sigma_{a_T})$ by the expression,

$$C'_{m_q}(\sigma'_a)\approx C_{m_{a_T}}(\sigma_{a_T})\,\frac{2\overline{w}_q}{q\bar{c}}\qquad(80)$$

The downwash function $\frac{\overline{w}_q}{q\bar{c}}$ has been plotted for certain cases in reference 28. For other cases, Ribner indicates in reference 29 that a generally suitable expression in terms of the more fully investigated quantity $\frac{\overline{w}_\alpha}{\alpha V_o}$ is

$$2\,\frac{\overline{w}_q}{q\bar{c}}\approx\frac{C_{L_{q_w}}(\sigma_{a_w})}{C_{L_{\alpha_w}}(\sigma_{a_w})}\,\frac{\overline{w}_\alpha}{\alpha V_o}\qquad(81)$$

Thus, combining equations (80) and (81),

$$C'_{m_q}(\sigma'_a)\approx C_{m_{a_T}}(\sigma_{a_T})\left[\frac{C_{L_{q_w}}(\sigma_{a_w})}{C_{L_{\alpha_w}}(\sigma_{a_w})}\right]\frac{\overline{w}_\alpha}{\alpha V_o}\qquad(82)$$

For pitching in the positive sense the effective angle of attack at the tail will in most cases be increased, so that equation (82) represents a small but stabilizing damping moment.

Consider now the term $-\int_o^{\sigma'_a}F'_3(\varphi)\,d\varphi$. For axes of rotation well ahead of the tail, the form of the pitching moment variation $C'_{m_\alpha}(\varphi)$ will vary closely as $-\frac{l_T}{\bar{c}}\,C'_{L_\alpha}(\varphi)$, where l_T may be taken as the distance from the steady-state center of pressure of the tail to the axis of rotation. Then, recalling the general nature of the curves found for tail lift in previous sections, a typical variation $C'_{m_\alpha}(\varphi)$ can be drawn as shown in figure (57).

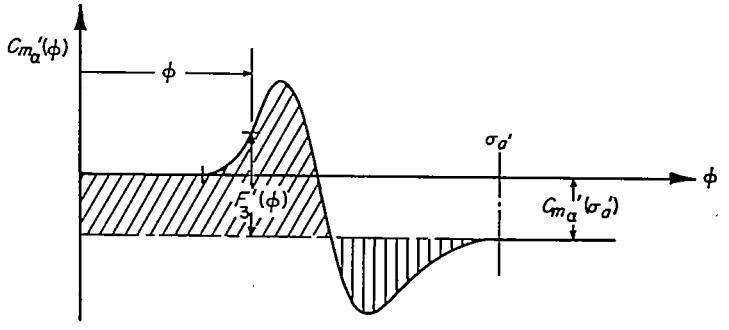

FIGURE 57.—Typical response in pitching moment of tail to step change in angle of attack of wing.

The term $-\int_o^{\sigma'_a}F'_3(\varphi)d\varphi$ is then seen to be equivalent to the net shaded area in figure (57). Plainly, it can be of significant magnitude, and since the steady-state ordinate $C'_{m_\alpha}(\sigma'_a)$ will most generally be positive, it represents a potentially large stabilizing damping moment.

It is interesting to compare the interference damping moment given by other theories in terms of the result given

[12] It is presumed in equations (75) to (79) that all of the coefficients have been nondimensionalized with respect to the same characteristic area and length.

by the integral $\int_0^{\sigma_a'} F_3'(\varphi)d\varphi$. Most of these theories (c. f., refs. 12, 28, and 10) are similar in that they recognize that an out-of-phase lift at the tail is caused by the fact that a finite time is required for the normal velocity shed by the wing to reach the tail. The normal velocity at the tail, which is usually taken to be the normal velocity in steady flow, is then usually averaged to form an effective angle of attack, and the damping moment cast in a form which may be represented in the present notation as $-\frac{2l'}{\bar{c}}\frac{\bar{w}_\alpha}{\alpha V_o}C_{m_{\alpha_T}}(\sigma_{a_T})$. Now this result may also be interpreted as an area, being in fact the area of a rectangle having as ordinate the quantity $-\frac{\bar{w}_\alpha}{\alpha V_o}C_{m_{\alpha_T}}(\sigma_{a_T})$. But note that this ordinate is equal to the ordinate $C_{m_\alpha}'(\sigma_a')$ in figure 57. Thus, it can be said that the classical "lag in downwash factor" is essentially correct but depends for its accuracy almost entirely on the proper choice of the effective tail length $\frac{2l'}{\bar{c}}$. In reference 12, the length l' is chosen to be the mean distance between the tail and the wing. Thus, for rectangular plan forms, and in the notation of figure 34, the effective length $\frac{2l'}{\bar{c}}$ is $\frac{c_W+c_T+2\zeta}{\bar{c}}$. The damping moment is then equal to $-\frac{\bar{w}_\alpha}{\alpha V_o}C_{m_{\alpha_T}}\left(\frac{c_W+c_T+2\zeta}{\bar{c}}\right)$, and its equivalent area is compared with the area $\int_0^{\sigma_a'} F_3'(\varphi)d\varphi$ in figure 58.

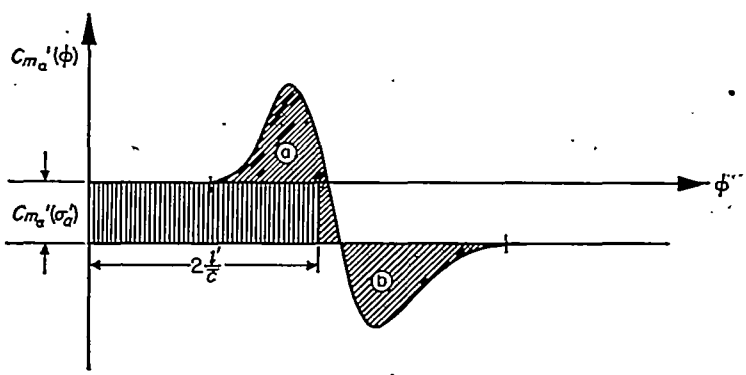

FIGURE 58.—Comparison of area $\int_0^{\sigma_a'} F_3'(\phi)d\phi$ with classical lag-in-downwash factor.

It can be seen from examination of figure 58 that the simple representation of the tail length is in this case surprisingly accurate, since the length $\frac{2l'}{\bar{c}}$ is so situated that the area marked a representing a stabilizing contribution is in large part canceled by the destabilizing contribution, area b. Further, it may be argued that this will be true for a large number of cases. The reasoning is as follows: Referring to figure 58, we see that the use of the simple tail length will be essentially correct so long as the number of half-chord lengths $\frac{2l'}{\bar{c}}$ is close to the value of φ at which the pitching-moment variation changes sign, for then the areas a and b tend to cancel. But the pitching moment will be near zero when the tail is so situated in the normal velocity field from the wing that it experiences equal amounts of upwash and downwash over its surface. Reference to figure 59 shows that this will occur when the tail is approximately midway between the starting vortices from the wing leading and trailing edges.

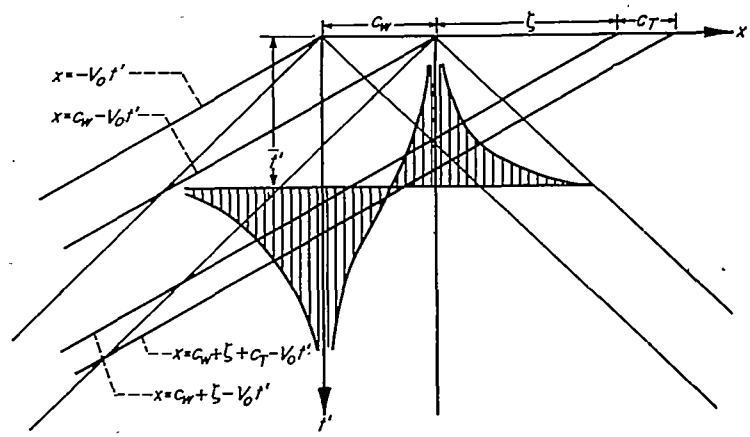

FIGURE 59.—Sketch showing time at which tail experiences approximately equal amounts of upwash and downwash.

The time $\bar{t}'$ when this occurs may be calculated to be $\bar{t}'\approx\frac{1}{V_o}\left(\zeta+\frac{c_W}{2}+\frac{c_T}{2}\right)$, and, after converting to half-chords of travel, we get $\varphi\approx\left(\frac{2\zeta+c_W+c_T}{\bar{c}}\right)$, which is just the value of the effective tail length, $\frac{2l'}{\bar{c}}$.

It should be remarked that the above conclusion regarding the validity of the "lag-in-downwash" factor differs somewhat from that of Martin, Diederich, and Bobbitt (ref. 28). These authors treat several wing-tail cases by direct consideration of the effect on the lift at the tail of the downwash shed by a forward wing which is plunging downward with uniform acceleration $\dot{\alpha}V_o$. For values of $\varphi\geq\sigma_a'$, their results for $C_{L_{\dot{\alpha}_T}}$ and $C_{m_{\dot{\alpha}_T}}$ due to interference should therefore be equivalent to those of this report for the areas $-\int_0^{\sigma_a'} F_1'(\varphi)d\varphi$ and $-\int_0^{\sigma_a'} F_3'(\varphi)d\varphi$. It is found in reference 28 on comparison of some of the results with those derived from the simpler lag-in-downwash theory that the latter theory generally gives accurate results when the axis of rotation is near the wing centroid of area. On examination of the equations used for the simplified theory in reference 28, however, it is noted that the effective tail length (denoted l' in this paper) is taken to be the distance between the tail center of pressure and the axis of rotation, which we have called l_T. With this representation, the out-of-phase tail lift and moment coefficients due to interference may be written (in the notation of this paper) as,

$$\left.\begin{aligned}(C_{L_{\dot{\alpha}_T}})_{int}&\approx-2\frac{l_T}{\bar{c}}\frac{\bar{w}_\alpha}{\alpha V_o}C_{L_{\alpha_T}}\\(C_{m_{\dot{\alpha}_T}})_{int}&\approx 2\left(\frac{l_T}{\bar{c}}\right)^2\frac{\bar{w}_\alpha}{\alpha V_o}C_{L_{\alpha_T}}\end{aligned}\right\}\qquad(83)$$

whereas, by the results of the present analysis, they are,

$$\left.\begin{aligned}\left(C_{L_{\dot{\alpha}_T}}\right)_{int} &\approx -2\frac{l'}{\bar{c}}\frac{\overline{w}_\alpha}{\alpha V_o}C_{L_{\alpha_T}}\\ \left(C_{m_{\dot{\alpha}_T}}\right)_{int} &\approx 2\frac{l'}{\bar{c}}\frac{l_T}{\bar{c}}\frac{\overline{w}}{\alpha V_o}C_{L_{\alpha_T}}\end{aligned}\right\} \quad (84)$$

The two sets of expressions agree when l' and l_T are equal, and, as noted in reference 28, the simple theory gives good results for just the conditions corresponding to this case. For other cases, however, it is believed that equations (84) are more representative of the physical situation, and should extend the range of validity of the simple theory beyond that indicated in reference 28.

Another case is pointed out in reference 28 for which the simple theory breaks down, that is, when the forward wing is two-dimensional, or of large span. The results of this analysis tend to confirm this conclusion, since for the large-span wing, the downwash in steady flow is near zero. Correspondingly, the steady-state interference lift of the tail is near zero, which means that the relative magnitudes of the peaks of the detailed indicial response curve (which are ignored in the simple theory) play a prominent role in determining the magnitude of the area $\int_0^{\sigma_a'} F_3'(\varphi)\,d\varphi$.

PART III

EFFECT OF NONLINEARITIES

In this final section we depart from discussion of the use of the indicial-function concept in dynamic-stability analyses to consider a problem which may have pertinence to performance characteristics under certain nonlinear flow conditions. The problem is: given a flight condition in which the variation of the airfoil's static restoring moment is nonlinear with respect to the angle of attack, what effect has the nonlinearity on the rotary damping-moment coefficient? The question is of especial pertinence to dynamic-stability problems of aircraft operating under separated-flow conditions, since it is well known that one effect of flow separation is often to cause significant departures from linearity of the static-restoring-moment curve. A common type of nonlinear pitching-moment variation is that shown by the family of curves in figure 60, and it is this type which will be considered here.

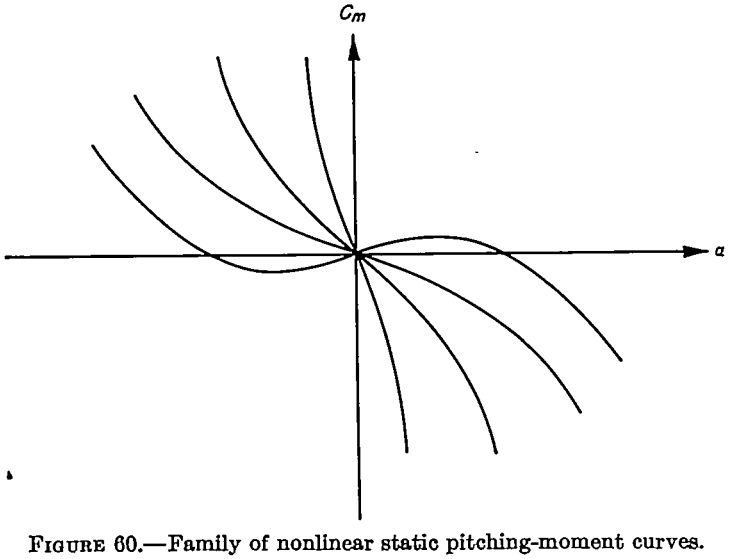

FIGURE 60.—Family of nonlinear static pitching-moment curves.

In order to attack the problem, we again require that the plunging velocity of the aircraft center of gravity be zero and, furthermore, assume that the nonlinear restoring moment is a function only of the *instantaneous* angle of attack. The characteristic differential equation governing the motion may then be written as,

$$I\ddot{\alpha}+\zeta(\alpha,\dot{\alpha})\dot{\alpha}+\kappa(\alpha)\alpha=0 \quad (85)$$

where I is the moment of inertia, $\zeta(\alpha,\dot{\alpha})$ represents the damping coefficient as a nonlinear function of angle of attack and angular velocity, and $\kappa(\alpha)$ is the restoring-moment coefficient as a nonlinear function of angle of attack.

Next, we contend that the departures from linearity of the restoring moment curves $\kappa(\alpha)$ are caused primarily by flow separation, so that in the absence of separation the curves would be nearly linear. In any case, however, a given restoring-moment variation can be broken into two parts; one linear, and given, say, by the results of linearized-flow theory, the other, a nonlinear variation of such magnitude as to combine with the linear variation to give the observed curve. These statements are illustrated in figure 61.

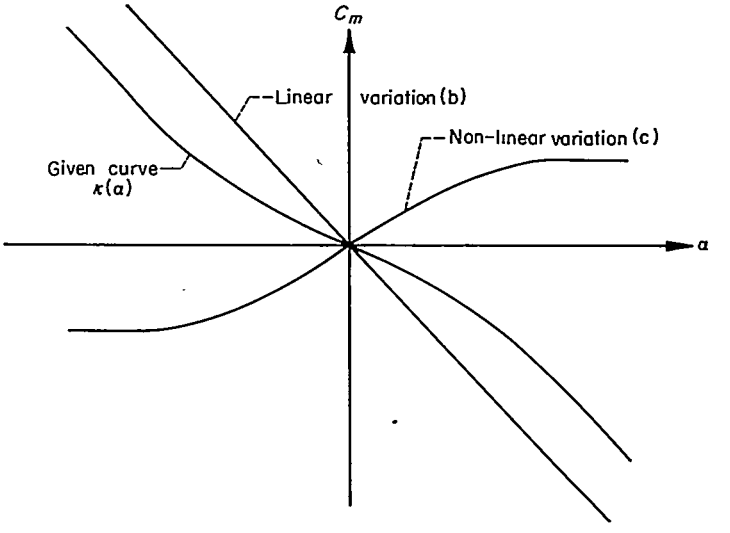

FIGURE 61.—Breakdown of pitching-moment curve into linear and nonlinear components.

It must be noted that the restoring-moment curves shown in figures 60 and 61 are presumed to be taken from the results of static wind-tunnel measurements, where the angle of attack is simply the angle between the chord-plane of the wing and the free-stream direction. When the wing is oscillating, however, each point ξ measured from the axis of rotation experiences an additional angle of attack $\frac{\dot{\alpha}\xi}{V_o}$, due to the angular velocity. Then if the steady-state pitching-moment variation presumed to be caused by flow separation (curve

(c) in figure 61) is approximated in the operating angle-of-attack range by,

$$C_m(\alpha)=a\alpha-b\alpha^3$$

in the unsteady case it is

$$C_m\left(\alpha+\frac{\dot{\alpha}\xi}{V_o}\right)=a\left(\alpha+\frac{\dot{\alpha}\xi}{V_o}\right)-b\left(\alpha+\frac{\dot{\alpha}\xi}{V_o}\right)^3 \tag{86}$$

where now ξ is assumed to be the distance from the axis to the point at which the additional lift due to separation is concentrated. Now, since for slow frequencies, $\frac{\dot{\alpha}\xi}{V_o}$ is much smaller than α, all but first-order terms in $\dot{\alpha}$ are neglected, so that equation (86) becomes

$$C_m=\alpha(a-b\alpha^2)+\frac{\dot{\alpha}\xi}{V_0}(a-3b\alpha^2) \tag{87}$$

The characteristic equation of motion then becomes

$$I\ddot{\alpha}-\frac{\dot{\alpha}c}{2V_0}\left[(C_{m_q}+C_{m_{\dot{\alpha}}})+\frac{2\xi}{\bar{c}}(a-3b\alpha^2)\right]-\alpha[C_{m_\alpha}+(a-b\alpha^2)]=0 \tag{88}$$

where $(C_{m_q}+C_{m_{\dot{\alpha}}})$ and (C_{m_α}) are the (constant) stability derivatives which would be present alone in the absence of separation. Thus it appears that even if the nonlinearity in the static restoring moment is of small magnitude, nevertheless the possibility still remains that the damping moment can be profoundly affected in the event that $(C_{m_q}+C_{m_{\dot{\alpha}}})$ is sufficiently small. Notice that when $(C_{m_q}+C_{m_{\dot{\alpha}}})+\frac{2\xi a}{\bar{c}}$ is greater than zero, and if the nonlinear term in the restoring moment can be ignored in equation (88), that equation then takes on the form,

$$\ddot{\alpha}-2\delta\dot{\alpha}(1-\mu\alpha^2)+K^2\alpha=0 \tag{89}$$

Equation (89) is then recognized as being the well-known Van Der Pol equation of nonlinear mechanics. It is evident that for small values of α the damping term is negative, leading to a divergent oscillation, whereas for larger α the damping term is positive. A stable regime therefore will exist near $\alpha=\frac{1}{\sqrt{\mu}}$, and oscillations of either large or small amplitude will converge to that regime.

Hence, the result of this analysis would appear to indicate that nonlinearities in the variation of restoring moment with angle of attack of the type shown in figure 60 may have the effect of promoting self-sustained rotary oscillations of small amplitude in cases where the damping moment existing under unseparated flow conditions is small.

AMES AERONAUTICAL LABORATORY
NATIONAL ADVISORY COMMITTEE FOR AERONAUTICS
MOFFETT FIELD, CALIF., *Aug. 16, 1954*

APPENDIX A

RESPONSE IN LIFT OF TWO-DIMENSIONAL TAIL TO TWO-DIMENSIONAL VORTEX SYSTEM

The results for the section lift response to the two-dimensional vortex field are listed below, together with the limits of the intervals of "time" t within which the results are applicable. The intervals have been illustrated graphically in figure 38 of the text.

Interval 1, $\dfrac{l}{M_o+1} \leq t \leq \dfrac{l+c}{M_o+1}$

$$\frac{c_{l_1}}{\sigma}(l, t) = \pi\left\{-\frac{1}{M_o}\log\left[\frac{t+\sqrt{t^2-(l-M_o t)^2}}{|l-M_o t|}\right]-\frac{\beta}{M_o}\cos^{-1}\left(M_o-\frac{\beta^2 t}{l}\right)+\cos^{-1}\left(\frac{l-M_o t}{t}\right)\right\}$$

Interval 2, $\dfrac{l+c}{M_o+1} \leq t \leq \dfrac{l}{M_o+1}+\dfrac{c}{M_o-1}$

$$\frac{c_{l_2}}{\sigma}(l, c, t) = c_{l_1}\frac{(l, t)}{\sigma}-\int_1^{\kappa}\Pi_1\, da-\int_1^{\kappa}\Pi_2\, da$$

Interval 3, $\dfrac{l}{M_o+1}+\dfrac{c}{M_o-1} \leq t \leq \dfrac{l}{M_o-1}$

$$\frac{c_{l_3}}{\sigma}(l, c, t) = \frac{c_{l_1}}{\sigma}(l, t)+\pi\left[\frac{1}{M_o}\log\left(\frac{1+\sqrt{1-\kappa_1^2}}{|\kappa_1|}\right)+\frac{\beta}{M_o}\cos^{-1}\left(\frac{1+\kappa_1 M_o}{\kappa_1+M_o}\right)-\cos^{-1}(\kappa_1)\right]-\int_{\kappa_1}^{\kappa}\Pi_1 da-\int_{\kappa_1}^{\kappa}\Pi_2 da$$

Interval 4, $\dfrac{l}{M_o-1} \leq t \leq \dfrac{l}{M_o-1}+\dfrac{c}{M_o+1}$

$$\frac{c_{l_4}}{\sigma}(l, c, t) = \pi^2\left(1-\frac{\beta}{M_o}\right)+\pi\left[\frac{1}{M_o}\log\left(\frac{1+\sqrt{1-\kappa_1^2}}{|\kappa_1|}\right)+\frac{\beta}{M_o}\cos^{-1}\left(\frac{1+\kappa_1 M_o}{\kappa_1+M_o}\right)-\cos^{-1}(\kappa_1)\right]-\int_{\kappa_1}^{\kappa}\Pi_1 da-\int_{\kappa_1}^{\kappa}\Pi_2 da$$

Interval 5, $\dfrac{l}{M_o-1}+\dfrac{c}{M_o+1} \leq t \leq \dfrac{l+c}{M_o-1}$

$$\frac{c_{l_5}}{\sigma}(l, c, t) = \pi^2\left(1-\frac{\beta}{M_o}\right)+\pi\left\{\frac{1}{M_o}\log\left(\frac{1+\sqrt{1-\kappa_1^2}}{|\kappa_1|}\right)+\frac{\beta}{M_o}\cos^{-1}\left(\frac{1+M_o\kappa_1}{\kappa_1+M_o}\right)-\cos^{-1}(\kappa_1)\right\}-\int_{\kappa_1}^{-1}\Pi_1 da-\int_{\kappa_1}^{-1}\Pi_2 da$$

where

$$\Pi_1 = \frac{\sqrt{1-a^2}}{a(a+M_o)}\cos^{-1}(-\epsilon_1)$$

$$\Pi_2 = \frac{1}{(a+M_o)}\log\left(\frac{1+a\epsilon_1+\sqrt{1-a^2}\sqrt{1-\epsilon_1^2}}{|a+\epsilon_1|}\right)$$

$$\epsilon_1 = \frac{(a+M_o)(M_o t-c)-M_o l}{(a+M_o)t-l}$$

$$\kappa = \frac{(1+M_o)(l-M_o t)+M_o c}{t(1+M_o)-c}$$

$$\kappa_1 = \frac{(1-M_o)(l-M_o t)-M_o c}{t(1-M_o)+c}$$

and

$$\sigma = -\frac{2\Delta\Phi}{\pi^2 V_o c}$$

These results may be transformed in terms of either true time t' or number of half-chord lengths of travel φ by the substitutions $t = a_o t'$ or $t = \dfrac{c\varphi}{2M_o}$, respectively.

APPENDIX B

RESPONSE IN LIFT OF TWO-DIMENSIONAL, RECTANGULAR, AND WIDE TRIANGULAR TAILS TO TWO-DIMENSIONAL VORTEX SYSTEM—GUST ANALYSIS

Approximate solutions for the responses of two-dimensional, rectangular, and wide triangular tails are listed below. Solutions were obtained by means of a gust type analysis, explained in the text. The indicial gust functions used in the analysis are those obtained from references 3, 5, and 6.

TWO-DIMENSIONAL TAIL

Interval 1, $\frac{l}{M_o+1} \leq t \leq \frac{l+c}{M_o+1}$

$$\frac{c_{l_1}}{\sigma}(l,t)=\kappa(l,t)$$

Interval 2, $\frac{l+c}{M_o+1} \leq t \leq \frac{l}{M_o+1}+\frac{c}{M_o-1}$

$$\frac{c_{l_2}}{\sigma}(l,c,t)=\kappa(l,t)-\kappa(l,\tau)-$$

$$\frac{M_o}{l}\int_{\frac{c}{M_o+1}}^{t-\frac{l}{M_o+1}} \cos^{-1}\left(\frac{M_o t_1-c}{t_1}\right)\frac{\sqrt{(t-t_1)^2-[l-M_o(t-t_1)]^2}}{l-M_o(t-t_1)}\,dt_1$$

Interval 3, $\frac{l}{M_o+1}+\frac{c}{M_o-1} \leq t$

$$\frac{c_{l_3}}{\sigma}(l,c,t)=\kappa(l,t)-\kappa(l,\tau)-$$

$$\frac{M_o}{l}\int_{\frac{c}{M_o+1}}^{\frac{c}{M_o-1}} \cos^{-1}\left(\frac{M_o t_1-c}{t_1}\right)\frac{\sqrt{(t-t_1)^2-[l-M_o(t-t_1)]^2}}{l-M_o(t-t_1)}\,dt_1$$

where

$$\kappa(l,t)=\pi\left\{\frac{\sqrt{t^2-(l-M_o t)^2}}{l}-\right.$$

$$\left.\frac{1}{M_o}\log\left[\frac{t+\sqrt{t^2-(l-M_o t)^2}}{|l-M_o t|}\right]+\frac{1}{\beta M_o}\cos^{-1}\left(M_o-\frac{\beta^2 t}{l}\right)\right\}$$

and

$$\tau=t-\frac{c}{M_o+1}, \qquad \sigma=-\frac{2\Delta\Phi}{\pi^2 V_o c}$$

RECTANGULAR TIP REGIONS

Interval 1, $\frac{l}{M_o+1} \leq t \leq \frac{l+c}{M_o+1}$

$$\frac{C_{L_1}}{\sigma}(l,t)=\zeta(l,t)$$

Interval 2, $\frac{l+c}{M_o+1} \leq t \leq \frac{l}{M_o+1}+\frac{c}{M_o-1}$

$$\frac{C_{L_2}}{\sigma}(l,c,t)=\zeta(l,t)-\frac{(M_o+1)}{2}\zeta(l,\tau)$$

Interval 3, $\frac{l}{M_o+1}+\frac{c}{M_o-1} \leq t$

$$\frac{C_{L_3}}{\sigma}(l,c,t)=\zeta(l,t)-\left(\frac{M_o+1}{2}\right)\zeta(l,\tau)-\left(\frac{M_o-1}{2}\right)\zeta(l,\tau_1)$$

where,

$$\zeta(l,t)=-\frac{\pi}{Ac}\left\{\left(\frac{l-M_o t}{M_o}\right)\left[\frac{\sqrt{t^2-(l-M_o t)^2}}{l}-\right.\right.$$

$$\left.\frac{1}{M_o}\log\left(\frac{t+\sqrt{t^2-(l-M_o t)^2}}{|l-M_o t|}\right)\right]+$$

$$\left.\frac{1}{2\beta^2}\left[\frac{l}{\beta}\cos^{-1}\left(M_o-\frac{\beta^2 t}{l}\right)-\left(M_o-\frac{\beta^2 t}{l}\right)\sqrt{t^2-(l-M_o t)^2}\right]\right\}$$

and

$$\tau=t-\frac{c}{M_o+1}$$

$$\tau_1=t-\frac{c}{M_o-1}$$

$$\sigma=\frac{2\Delta\Phi}{\pi^2 V_o c}$$

The response for the rectangular tail may be formed by direct addition of the solutions given above.

WIDE TRIANGULAR TAIL

Interval 1, $\frac{l}{M_o+1} \leq t \leq \frac{l+c_o}{M_o+1}$

$$\frac{C_{L_1}}{\sigma}(l,t)=\delta(l,t)$$

Interval 2, $\frac{l+c_o}{M_o+1} \leq t \leq \frac{l}{M_o+1}+\frac{c_o}{M_o-1}$

$$\frac{C_{L_2}}{\sigma}(l,c_o,t)=\delta(l,t)-\delta(l,\tau)+\frac{2M_o^2}{lc_o}\int_{\frac{c_o}{M_o+1}}^{t-\frac{l}{M_o+1}} \Pi\,dt_1$$

Interval 3, $\frac{l}{M_o+1}+\frac{c_o}{M_o-1} \leq t$

$$\frac{C_{L_3}}{\sigma}(l,c_o,t)=\delta(l,t)-\delta(l,\tau)+\frac{2M_o^2}{lc_o}\int_{\frac{c_o}{M_o+1}}^{\frac{c_o}{M_o-1}} \Pi\,dt_1$$

where,

$$\delta(l,t)=\frac{2\pi M_o}{c_o}\left\{\left(\frac{l-M_o t}{M_o}\right)\left[\frac{\sqrt{t^2-(l-M_o t)^2}}{l}-\right.\right.$$

$$\left.\frac{1}{M_o}\log\left(\frac{t+\sqrt{t^2-(l-M_o t)^2}}{|l-M_o t|}\right)\right]+\frac{1}{2\beta^2}\left[\frac{l}{\beta}\cos^{-1}\left(M_o-\frac{\beta^2 t}{l}\right)-\right.$$

$$\left.\left.\left(M_o-\frac{\beta^2 t}{l}\right)\sqrt{t^2-(l-M_o t)^2}\right]\right\}$$

$$\Pi=\left[t_1\cos^{-1}\left(\frac{M_o t_1-c_o}{t_1}\right)+\right.$$

$$\left.(c_o-M_o t_1)\cosh^{-1}\left(\frac{t_1}{|M_o t_1-c_o|}\right)\right]\frac{\sqrt{(t-t_1)^2-[l-M_o(t-t_1)]^2}}{l-M_o(t-t_1)}$$

$$\tau=t-\frac{c_o}{M_o+1}, \qquad \sigma=\frac{2\Delta\Phi}{\pi^2 V_o c_o}$$

APPENDIX C

RESPONSE IN LIFT OF APEX-FORWARD AND APEX-REARWARD WIDE TRIANGULAR TAILS TO TWO-DIMENSIONAL VORTEX SYSTEM

Exact solutions for the responses of apex-forward and apex-rearward wide triangular tails are listed below. Solutions were obtained by the application of strip theory. The section-lift response used in the analysis has already been presented as Appendix A.

APEX-REARWARD TRIANGULAR TAIL

Interval 1, $$\frac{l}{M_o+1}\leq t\leq\frac{l+c_o}{M_o+1}$$

$$\frac{C_{L_1}}{2\sigma}(l,t)=\int_1^{\frac{l-M_o t}{t}}\Pi_a\,da$$

Interval 2, $$\frac{l+c_o}{M_o+1}\leq t\leq\frac{l}{M_o+1}+\frac{c_o}{M_o-1}$$

$$\frac{C_{L_2}}{2\sigma}(l,c_o,t)=\int_1^{\frac{-M_o t}{t}}\Pi_a\,da+\int_1^{\kappa}\Pi_1\,da+\int_1^{\kappa}\Pi_2\,da$$

Interval 3, $$\frac{l}{M_o+1}+\frac{c_o}{M_o-1}\leq t\leq\frac{l}{M_o-1}$$

$$\frac{C_{L_3}}{2\sigma}(l,c_o,t)=\int_{\kappa_1}^{\frac{l-M_o t}{t}}\Pi_a\,da+\int_{\kappa_1}^{\kappa}\Pi_1\,da+\int_{\kappa_1}^{\kappa}\Pi_2\,da$$

Interval 4, $$\frac{l}{M_o-1}\leq t\leq\frac{l}{M_o-1}+\frac{c_o}{M_o+1}$$

$$\frac{C_{L_4}}{2\sigma}(l,c_o,t)=\int_{\kappa_1}^{-1}\Pi_a\,da+\int_{\kappa_1}^{\kappa}\Pi_1\,da+\int_{\kappa_1}^{\kappa}\Pi_2\,da$$

Interval 5, $$\frac{l}{M_o-1}+\frac{c_o}{M_o+1}\leq t\leq\frac{l+c_o}{M_o-1}$$

$$\frac{C_{L_5}}{2\sigma}(l,c_o,t)=\int_{\kappa_1}^{-1}\Pi_a\,da+\int_{\kappa_1}^{-1}\Pi_1\,da+\int_{\kappa_1}^{-1}\Pi_2\,da$$

where

$$\Pi_a=\frac{\pi\sqrt{1-a^2}}{a(a+M_o)}\left[1-\frac{\alpha}{c_o}\right]$$

$$\Pi_1=\frac{\sqrt{1-a^2}}{a(a+M_o)}\frac{\alpha}{c_o}\left[\epsilon_1\cos^{-1}(-\epsilon_1)+\sqrt{1-\epsilon_1^2}\right]$$

$$\Pi_2=\frac{1}{(a+M_o)}\left[\alpha_1\log\left(\frac{1+a\epsilon_1+\sqrt{1-a^2}\sqrt{1-\epsilon_1^2}}{|a+\epsilon_1|}\right)+\frac{\sqrt{1-a^2}}{(a+M_o)}\frac{\alpha}{c_o}\cos^{-1}(-\epsilon_1)\right]$$

and,

$$\epsilon_1=\frac{M_o\alpha-(a+M_o)c_o}{\alpha}$$

$$\alpha=(a+M_o)t-l$$

$$\alpha_1=\alpha-c_o$$

$$\kappa=\frac{(1+M_o)(l-M_o t)+M_o c_o}{(1+M_o)t-c_o}$$

$$\kappa_1=\frac{(1-M_o)(l-M_o t)-M_o c_o}{(1-M_o)t+c_o}$$

$$\sigma=\frac{2\Delta\Phi}{\pi^2 V_o c_o}$$

The integral $\int_{a_1}^{a_2}\Pi_a\,da$ may be evaluated easily, and gives,

$$\int_{a_1}^{a_2}\Pi_a\,da=\frac{\pi}{M_o}\left[-\log\left(\frac{1+\sqrt{1-a^2}}{|a|}\right)-\beta\cos^{-1}\left(\frac{1+aM_o}{a+M_o}\right)+M_o\cos^{-1}(a)\right]\Bigg|_{a_1}^{a_2}\frac{-\pi}{M_o c_o}\left[(l-M_o t)\log\left(\frac{1+\sqrt{1-a^2}}{|a|}\right)+M_o t\sqrt{1-a^2}+\beta l\cos^{-1}\left(\frac{1+aM_o}{a+M_o}\right)-M_o l\cos^{-1}(a)\right]\Bigg|_{a_1}^{a_2}$$

APEX-FORWARD TRIANGULAR TAIL

The form and intervals of the results for the apex-rearward tail also apply to the apex-forward tail. The terms Π_a, Π_1, Π_2, are, of course, different, and these are listed below.

$$\Pi_a=\frac{\pi\sqrt{1-a^2}}{a(a+M_o)}\frac{\alpha}{c_o}$$

$$\Pi_1=-\frac{\sqrt{1-a^2}}{a(a+M_o)}\left[\frac{\alpha}{c_o}\cos^{-1}(-\epsilon_1)+\frac{\alpha_1}{c_o}\frac{(a+M_o)}{\sqrt{1-a^2}}\log\left(\frac{1+a\epsilon_1+\sqrt{1-a^2}\sqrt{1-\epsilon_1^2}}{|a+\epsilon_1|}\right)\right]$$

$$\Pi_2=-\frac{1}{(a+M_o)}\left\{\left[1+\frac{\alpha_1}{c_o}\left(\frac{1+aM_o}{1-a^2}\right)\right]\log\left(\frac{1+a\epsilon_1+\sqrt{1-a^2}\sqrt{1-\epsilon_1^2}}{|a+\epsilon_1|}\right)-\frac{\alpha}{c_o}\frac{\sqrt{1-\epsilon_1^2}}{\sqrt{1-a^2}}\right\}$$

Evaluation of $\int_{a_1}^{a_2}\Pi_a\,da$ gives,

$$\int_{a_1}^{a_2}\Pi_a\,da=\frac{\pi}{M_o c_o}\left[M_o t\sqrt{1-a^2}+(l-M_o t)\log\left(\frac{1+\sqrt{1-a^2}}{|a|}\right)+\beta l\cos^{-1}\left(\frac{1+aM_o}{a+M_o}\right)-M_o l\cos^{-1}(a)\right]\Bigg|_{a_1}^{a_2}$$

APPENDIX D

BOUNDARY CONDITIONS AT THE TAIL DUE TO PENETRATION OF VELOCITY FIELD OF TRAILING-VORTEX SYSTEM

The boundary conditions at a spanwise section of the tail due to the tail's penetration of the normal-velocity field created by a trailing-vortex loop are illustrated below. The five types of conditions are those possible at various sections of the tail due to its shape and its position with respect to the moving and trailing vortices.

Case 1, $y \leq l+\xi(y)$

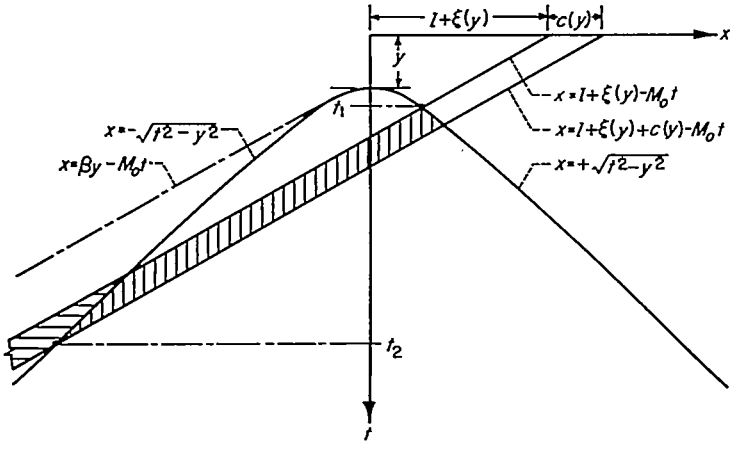

$$t_1=\frac{M_o(l+\xi)-\sqrt{(l+\xi)^2-\beta^2y^2}}{\beta^2}$$

$$t_2=\frac{M_o(l+\xi+c)+\sqrt{(l+\xi+c)^2-\beta^2y^2}}{\beta^2}$$

$$\bar{c}_l(t_2)=-\frac{4}{\beta}\frac{\Delta\Phi}{2\pi V_o c}\frac{1}{y}\left[\sqrt{(l+\xi+c)^2-\beta^2y^2}-\sqrt{(l+\xi)^2-\beta^2y^2}+\beta y\left(\cos^{-1}\frac{\beta y}{l+\xi}-\cos^{-1}\frac{\beta y}{l+\xi+c}\right)\right]$$

Case 2, $\dfrac{l+\xi}{M_o}\leq y\leq\dfrac{l+\xi}{\beta}$

or

$$\frac{l+\xi}{M_o}\leq y\leq\frac{l+\xi+c}{M_o}$$

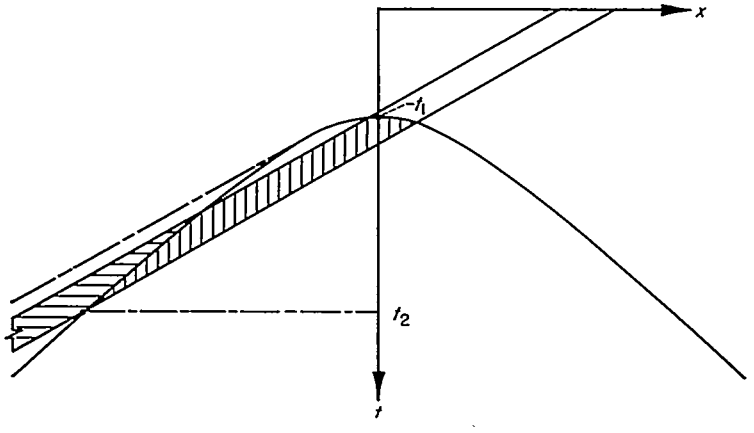

$$t_1=y$$

$$t_2=\frac{M_o(l+\xi+c)+\sqrt{(l+\xi+c)^2-\beta^2y^2}}{\beta^2}$$

$$\bar{c}_l(t_2)=-\frac{4}{\beta}\frac{\Delta\Phi}{2\pi V_o c}\frac{1}{y}\left[\sqrt{(l+\xi+c)^2-\beta^2y^2}-\sqrt{(l+\xi)^2-\beta^2y^2}+\beta y\left(\cos^{-1}\frac{\beta y}{l+\xi}-\cos^{-1}\frac{\beta y}{l+\xi+c}\right)\right]$$

Case 2(a), $\dfrac{l+\xi+c}{M_o}\leq y\leq\dfrac{l+\xi}{\beta}$

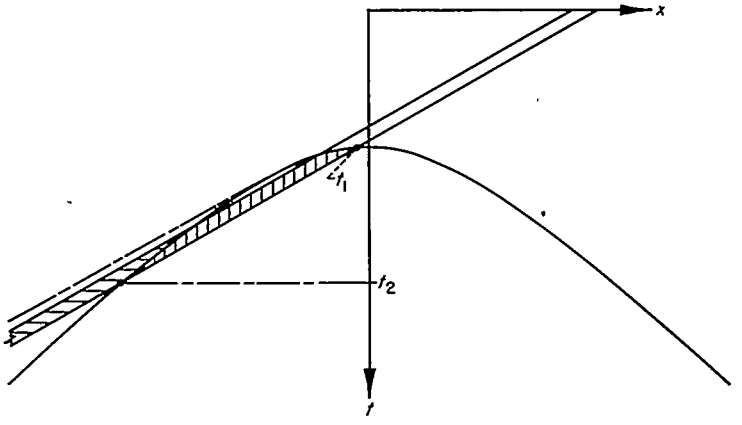

$$t_1=\frac{M_o(l+\xi+c)-\sqrt{(l+\xi+c)^2-\beta^2y^2}}{\beta^2}$$

$$t_2=\frac{M_o(l+\xi+c)+\sqrt{(l+\xi+c)^2-\beta^2y^2}}{\beta^2}$$

$$c_l(t_2)=-\frac{4}{\beta}\frac{\Delta\Phi}{2\pi V_o c}\frac{1}{y}\left[\sqrt{(l+\xi+c)^2-\beta^2y^2}-\sqrt{(l+\xi)^2-\beta^2y^2}+\beta y\left(\cos^{-1}\frac{\beta y}{l+\xi}-\cos^{-1}\frac{\beta y}{l+\xi+c}\right)\right]$$

Case 3, $\dfrac{l+\xi}{\beta}\leq y\leq\dfrac{l+\xi+c}{M_o}$

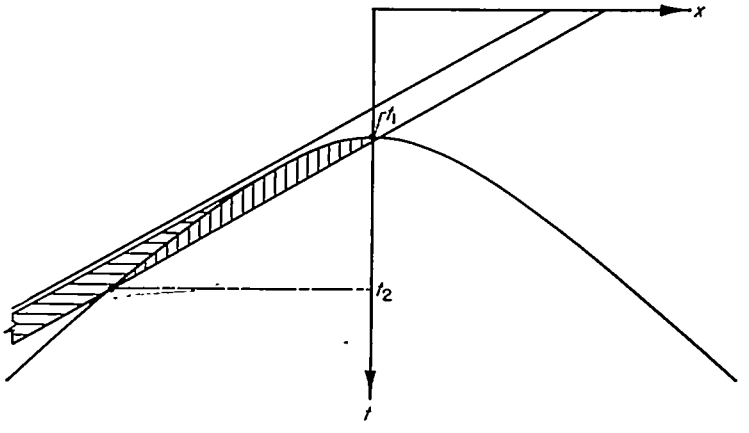

$$t_1=y$$

$$t_2=\frac{M_o(l+\xi+c)+\sqrt{(l+\xi+c)^2-\beta^2y^2}}{\beta^2}$$

$$\bar{c}_l(t_2)=-\frac{4}{\beta}\frac{\Delta\Phi}{2\pi V_o c}\frac{1}{y}\left[\sqrt{(l+\xi+c)^2-\beta^2y^2}-\beta y\cos^{-1}\frac{\beta y}{l+\xi+c}\right]$$

Case 4, $$\frac{l+\xi+c}{M_o}\leq y\leq\frac{l+\xi+c}{\beta}$$

or

$$\frac{l+\xi}{\beta}\leq y\leq\frac{l+\xi+c}{\beta}$$

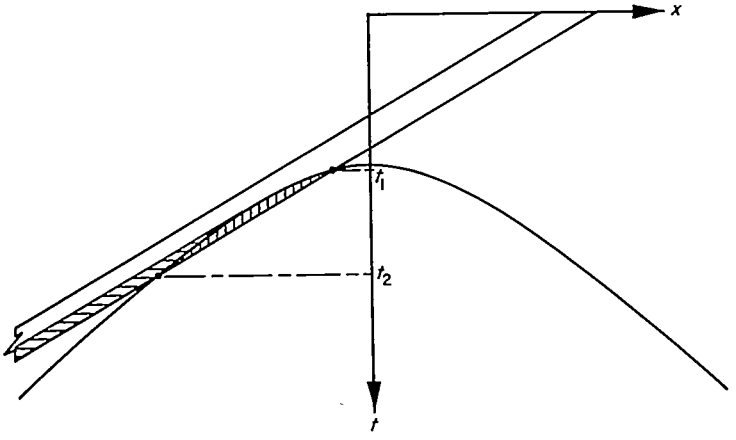

$$t_1=\frac{M_o(l+\xi+c)-\sqrt{(l+\xi+c)^2-\beta^2y^2}}{\beta^2}$$

$$t_2=\frac{M_o(l+\xi+c)+\sqrt{(l+\xi+c)^2-\beta^2y^2}}{\beta^2}$$

$$\bar{c}_l(t_2)=-\frac{4}{\beta}\frac{\Delta\Phi}{2\pi V_o c}\frac{1}{y}\left[\sqrt{(l+\xi+c)^2-\beta^2y^2}-\beta y\cos^{-1}\frac{\beta y}{l+\xi+c}\right]$$

REFERENCES

1. Zimmerman, Charles H.: An Analysis of Longitudinal Stability in Power-Off Flight with Charts for Use in Design. NACA Rep. 521, 1935.
2. Wagner, Herbert: Über die Entstehung des dynamischen Auftriebes von Tragflügeln. z.f.a.M.M. Bd. 5, Heft 1, Feb. 1925, S. 17–35.
3. Heaslet, Max A., and Lomax, Harvard: Two-Dimensional Unsteady Lift Problems in Supersonic Flight. NACA Rep. 945, 1949.
4. Lomax, Harvard, Fuller, Franklyn B., and Sluder, Loma: Two- and Three-Dimensional Unsteady Lift Problems in High-Speed Flight. NACA Rep. 1077, 1952. (Supersedes NACA TNs 2403 and 2387).
5. Miles, John W.: Transient Loading of Wide Delta Airfoils at Supersonic Speeds. NAVORD Rep. 1235, 1950.
6. Miles, John W.: Transient Loading of Supersonic Rectangular Airfoils. Jour. Aero. Sci., vol. 17, no. 10, Oct. 1950, pp. 647–652.
7. Garrick, I. E.: On Some Reciprocal Relations in the Theory of Non-stationary Flows. NACA Rep. 629, 1938.
8. Jones, Robert T.: The Unsteady Lift of a Wing of Finite Aspect Ratio. NACA Rep. 681, 1940.
9. Churchill, R. V.: Modern Operational Mathematics in Engineering. McGraw-Hill Book Company, N. Y., 1944.
10. Miles, John W.: The Application of Unsteady Flow Theory to the Calculation of Dynamic Stability Derivatives. North American Aviation Rep. AL-957, 1950.
11. Jahnke, Eugen, and Emde, Fritz: Tables of Functions with Formulae and Curves. Fourth ed., Dover Pub., N. Y., 1945.
12. Durand, W. F., ed.: Aerodynamic Theory. Vol. V, Julius Springer (Berlin), 1935. (Available as CIT Reprint, 1943).
13. Theodorsen, Theodore: General Theory of Aerodynamic Instability and the Mechanism of Flutter. NACA Rep. 496, 1935.
14. Garrick, I. E., and Rubinow, S. I.: Flutter and Oscillating Air-Force Calculations for an Airfoil in a Two-Dimensional Supersonic Flow. NACA Rep. 846, 1946.
15. Watkins, Charles E.: Effect of Aspect Ratio on the Air Forces and Moments of Harmonically Oscillating Thin Rectangular Wings in Supersonic Potential Flow. NACA TN 2064, 1950.
16. Watkins, Charles E.: Air Forces and Moments on Triangular and Related Wings with Subsonic Leading Edges Oscillating in Supersonic Potential Flow. NACA TN 2457, 1951.
17. Nelson, Herbert C.: Lift and Moment on Oscillating Triangular and Related Wings with Supersonic Edges. NACA TN 2494, 1951.
18. Miles, John W.: On Harmonic Motion of Wide Delta Airfoils at Supersonic Speeds. NAVORD Rep. 1234, 1950.
19. Ribner, Herbert S., and Malvestuto, Frank S., Jr.: Stability Derivatives of Triangular Wings at Supersonic Speeds. NACA Rep. 908, 1948.
20. Malvestuto, Frank S., Jr., and Margolis, Kenneth: Theoretical Stability Derivatives of Thin Sweptback Wings Tapered to a Point with Sweptback or Sweptforward Trailing Edges for a Limited Range of Supersonic Speeds. NACA Rep. 971, 1950. (Supersedes NACA TN 1761).
21. Malvestuto, Frank S., Jr., and Hoover, Dorothy M.: Lift and Pitching Derivatives of Thin Sweptback Tapered Wings with Streamwise Tips and Subsonic Leading Edges at Supersonic Speeds. NACA TN 2294, 1951.
22. Malvestuto, Frank S., Jr., and Hoover, Dorothy M.: Supersonic Lift and Pitching Moment of Thin Sweptback Tapered Wings Produced by Constant Vertical Acceleration. Subsonic Leading Edges and Supersonic Trailing Edges. NACA TN 2315, 1951.
23. Jones, Robert T., and Fehlner, Leo F.: Transient Effects of the Wing Wake on the Horizontal Tail. NACA TN 771, 1940.
24. Lomax, Harvard, Heaslet, Max A., and Fuller, Franklyn B.: Three-Dimensional, Unsteady-Lift Problems in High-Speed Flight-Basic Concepts. NACA TN 2256, 1950.
25. Miles, John W.: Simple Planforms in Supersonic Flow. Jour. Aero. Sci., vol. 17, no. 2, Feb. 1950, p. 127.
26. Walsh, J., Zartarian, G., and Voss, H. M.: Generalized Aerodynamic Forces on the Delta Wing with Supersonic Leading Edges. Jour. Aero. Sci. vol. 21, no. 11, Nov. 1954, pp. 739–748.
27. Heaslet, Max A., and Spreiter, John R.: Reciprocity Relations in Aerodynamics. NACA Rep. 1119, 1953.
28. Martin, John C., Diederich, Margaret S., and Bobbitt, Percy J.: A Theoretical Investigation of the Aerodynamics of Wing-Tail Combinations Performing Time-Dependent Motions at Supersonic Speeds. NACA TN 3072, 1954.
29. Ribner, Herbert S.: Time-Dependent Downwash at the Tail and the Pitching Moment due to Normal Acceleration at Supersonic Speeds. NACA TN 2042, 1950.

368555—56——48